United States
Environmental Protection
Agency

Office of Air Quality
Planning and Standards
Research Triangle Park, NC 27711

EPA-454/R-92-016
October 1992

Air

EPA

DEVELOPMENT AND EVALUATION OF A REVISED AREA SOURCE ALGORITHM FOR THE INDUSTRIAL SOURCE COMPLEX LONG TERM MODEL

EPA-454/R-92-016

DEVELOPMENT AND EVALUATION OF A REVISED AREA SOURCE ALGORITHM FOR THE INDUSTRIAL SOURCE COMPLEX LONG TERM MODEL

Office Of Air Quality Planning And Standards
Office Of Air And Radiation
U. S. Environmental Protection Agency
Research Triangle Park, NC 27711

October 1992

This report has been reviewed by the Office Of Air Quality Planning And Standards, U. S. Environmental Protection Agency, and has been approved for publication. Any mention of trade names or commercial products is not intended to constitute endorsement or recommendation for use.

EPA-454/R-92-016

PREFACE

The ability to accurately estimate pollutant concentration due to atmospheric releases from area sources is important to the modeling community, and is of special concern for Superfund where emissions are typically characterized as area sources. Limitations of the Industrial Source Complex (ISC2) model (dated 92273) algorithms for modeling impacts from area sources, especially for receptors located within and nearby the area, have been documented in earlier studies. An improved algorithm for modeling dispersion from area sources has been developed based on a numerical integration of the point source concentration function. Information on this algorithm is provided in three interrelated reports.

In the first report (EPA-454/R-92-014), an evaluation of the algorithm is presented using wind tunnel data collected in the Fluid Modeling Facility of the U.S. Environmental Protection Agency. In the second report (EPA-454/R-92-015), a sensitivity analysis is presented of the algorithm as implemented in the short-term version of ISC2. In the third report (EPA-454/R-92-016), a sensitivity analysis is presented of the algorithm as implemented in the long-term version of ISC2.

The Environmental Protection Agency must conduct a formal and public review before the Agency can recommend for routine use this new algorithm in regulatory analyses. These reports are being released to establish a basis for reviews of the capabilities of this methodology and of the consequences resulting from use of this methodology in routine dispersion modeling of air pollutant impacts. These reports are one part of a larger set of information on the ISC2 models that must be considered before any formal changes can be adopted.

ACKNOWLEDGEMENTS

This report has been prepared by Pacific Environmental Services, Inc., Research Triangle Park, North Carolina. This effort has been funded by the Environmental Protection Agency under Contract No. 68D00124, with Jawad S. Touma as Work Assignment Manager. Special thanks go to John Irwin of EPA-SRAB and William Petersen of EPA-AREAL, who provided helpful technical guidance and suggestions.

CONTENTS

FIGURES

TABLES

1. INTRODUCTION

Previous model evaluation studies (EPA, 1989) have pointed out the deficiencies of the virtual point source algorithm for modeling area sources used in the Industrial Source Complex (ISC2) Long Term (ISCLT2) model. While it is computationally efficient, the virtual point source algorithm used in the original ISCLT2 model gives physically unrealistic results for receptors located near the edges and corners of the area. Also, the algorithm cannot predict the area source impact for receptors located inside the source itself, and it does not adequately handle effects of complex source-receptor geometry.

This report documents the development and evaluation of a new area source algorithm for the ISCLT2 model, based on the numerical integration algorithm recently developed for the ISC2 Short Term (ISCST2) model. The evaluation of the performance of the new ISCLT2 area source algorithm includes performance tests, statistical analyses, and sensitivity analyses.

For the performance tests, the new ISCLT2 numerical integration area source algorithm is challenged in various ways. First, quality assurance tests are conducted to examine the reasonableness of the results and the efficiency of the algorithm. These quality assurance tests include printing out the intermediate calculation results to perform a line-by-line check of the computer code of the new algorithm. Second, cases with simple area source characteristics (square area source or rectangular area source) and idealized meteorological conditions are used to examine the reliability and accuracy of the algorithm. Third, several tests are conducted to show the concentration distribution for various area source shapes. Fourth, tests are conducted to examine the effects of subdividing the area source and the effects of rotation of the area source on the simulated concentration values. Finally, several cases are examined using realistic meteorological conditions.

In addition to performance tests, a sensitivity analysis is presented comparing design concentrations using the virtual point source algorithm with estimates using the new numerical integration algorithm for a range of source characteristics and meteorological data.

The technical description of the new ISCLT2 area source algorithm is provided in Section 2. The results of the performance tests are presented in Section 3, and the results of the sensitivity analyses involving comparisons with the virtual point source algorithm are given in Section 4. The conclusions of this study are presented in Section 5.

2. THE ISC2 LONG TERM AREA SOURCE ALGORITHM

2.1. The Shortcoming Of The Current ISCLT2 Area Source Algorithm

The algorithm used in ISCLT2 (Version 92062) for modeling area sources is based on the virtual point source approach. As suggested by Turner (1970), the virtual point source algorithm assumes that the plume downwind of an area source can be simulated as a point source. The initial source dimensions are accounted for by placing the point source upwind of the actual area source location, so that the lateral spread of the plume at the area source is comparable to the source width. The emission rate for the replacement source is set equal to the area source emission rate. Therefore, the same form of calculation process used for point sources can be used for area sources.

While it is computationally efficient, the virtual point source algorithm used in the original ISCLT2 model has several inevitable shortcomings (EPA, 1989). First, the algorithm does not accurately account for the impacts for receptors located inside the area source itself. The ISCLT2 model flags receptors located within the area, and sets the concentration value to 0 at those receptors. Second, the virtual point source algorithm is only valid for receptors at a sufficient distance downwind from an area source that the area source impact is well approximated by a point source. Hence, for receptors close to the area source where the source-receptor geometry is crucial, the virtual point source approximation performs poorly. Third, the algorithm performs best for simple square shaped areas. For large area sources with complex shapes, the area must be subdivided into smaller square sources.

2.2. The Implementation Of The Numerical Integration Algorithm

Several factors need to be considered when implementing an area source algorithm in the ISCLT2 model. The first and most important issue is the usage of the STAR (for STability ARray) meteorological data. The ISCLT2 is a climatological model that uses a summary of the wind directions, wind speeds and stability categories encountered throughout a period (e.g., a calendar quarter, a year, or multiple years). Therefore, the meteorological conditions are summarized by using a frequency distribution composed of 16 wind direction sectors, 6 wind speed classes and 6 stability classes. Since all the wind directions within a sector of the STAR data are assumed to be equally likely, the ISCLT2 model calculates sector average concentrations to determine source impacts. In order to account for the abrupt changes that occur in the frequency of occurrence of meteorological conditions at the boundaries between adjacent sectors, an adjustment is made to the concentration distribution. This adjustment is performed in the existing algorithm by a applying a smoothing function that linearly interpolates between the concentration values calculated at the centerline of adjacent sectors.

Since the area source is approximated by a point source in the current ISCLT2 model, and the wind direction is equally likely to occur anywhere within the sector, the impact at a particular distance downwind from the source does not vary by changing the wind direction within the sector. The sector average concentration can therefore be calculated by using a single wind direction corresponding to the centerline of the sector. In the new area source algorithm, the model is treating the source as an area, and the impact at a particular distance downwind from the source does vary by changing the wind direction within the sector. Therefore, the sector average calculation will need to be based on several simulations, each corresponding to a particular wind direction within the sector. Instead of applying a smoothing function to the concentration distribution with the new algorithm, the abrupt changes in concentration at the sector boundaries are smoothed by applying a linear interpretation to calculate the frequency of occurrence corresponding to each wind direction simulated.

Another factor worth considering is that there are certain benefits to maintaining consistency between the ISC2 short term (ISCST2) area source algorithm and the ISCLT2 area source algorithm. These benefits include simplifying future maintenance of the models, keeping compatibility of source input parameters between the two models, and better consistency of results between the two models for the same source characteristics. The new ISCST2 area source algorithm is based on a numerical integration of the point source concentration function over the area, and employs a Romberg integration algorithm (Press, et al, 1986) to improve the efficiency of the computations.

The implementation of the new area source algorithm in the ISCLT2 model is described in more detail in the following sections.

2.2.1. Sector Average Calculation

The STAR meteorological data provides the frequency of occurrence for each of the 16 wind direction sectors. It assumes that, within each sector, all the wind directions are equally likely. However, even for a very simple area source shape, the source-receptor geometry varies with the wind direction. For example, in Figure 2.1, if the wind comes from the north, the distance it travels over the area source is d. If the wind comes from a direction of 5 degrees east from north, the distance it travels over the area source is d'. In this example, d' is larger than d. For a receptor downwind of the area source, different wind directions within the sector result in different impacts to the receptor. Therefore, the sector average of the concentration value cannot be calculated through the use of only one wind direction.

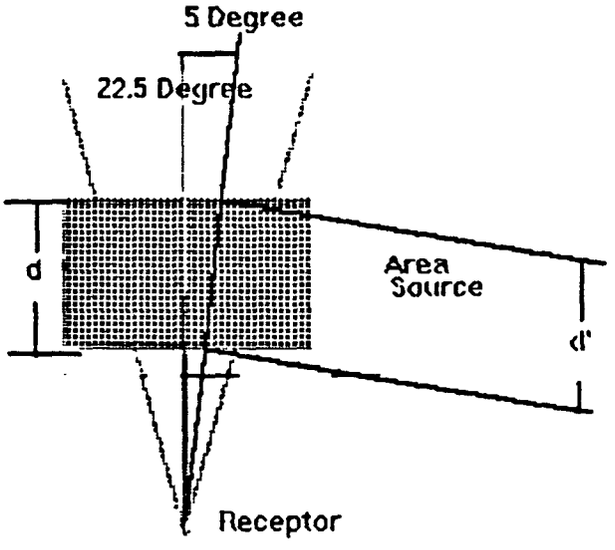

Figure 2.1. Illustration of the computation of the sector average impact.

In order to calculate the sector average concentration, several simulations are needed for a selection of wind directions within the sector. This selection of wind directions can be done as follows. First, the directions corresponding to the boundaries of the sector, together with the direction of the centerline of the sector are selected. The area source impact to the receptor is computed for these three wind directions, and a sector average calculated. Next, two more wind directions are selected, such that they are equally spaced between the central azimuth of the sector and the sector boundaries. The sector average area source impact is computed by trapezoidal integration using the impacts computed for the five wind directions. The trapezoidal integration is used because the directions corresponding to the sector boundaries are also used in calculations for the adjacent sectors, and are therefore weighted by a factor of one half. A test is made to see if the area source impact using five wind directions is significantly different from that obtained using three wind directions. If the estimates differ by more than 2 percent, the sector is further subdivided, until the 2 percent convergence criterion is satisfied. The sector average is calculated using a trapezoidal integration as follows:

$$\overline{\chi_j} = \frac{\int f(\theta) * \chi(\theta)\, d\theta}{S} = \frac{1}{N}\left[\sum_{j=1}^{N-1} f_{ij}\chi(\theta_{ij}) + \frac{(f_{ij}\chi(\theta_{i1}) + f_{iN}\chi(\theta_{iN}))}{2}\right] + \varepsilon(\theta) \quad (2\text{-}1)$$

$$\varepsilon(\theta) = \frac{\overline{\chi_{NEW}} - \overline{\chi_{OLD}}}{\overline{\chi_{mid}}}, \quad \overline{\chi_{mid}} = \frac{\overline{\chi_{NEW}} + \overline{\chi_{OLD}}}{2} \quad (2\text{-}2)$$

where:

- χ_i = the sector average of the concentration value in ith sector.
- S = the sector width.
- f_{ij} = the frequency of occurrence for jth wind direction in ith sector.
- $\varepsilon(\theta)$ = error term. In practice, a criterion of $\varepsilon(\theta) < 2$ percent is used to check for convergence of the algorithm.
- $\chi(\theta_i)$ = the concentration value in ith sector.
- $\chi(\theta_{ij})$ = the concentration value with jth wind direction in ith sector.
- θ_{ij} = the jth wind direction in ith sector, j = 1 and N represent the two boundaries of ith sector.

2.2.2. Smoothing the Frequency Distribution

The application of a smoothing function to the concentration distribution, as done in the current ISCLT2 algorithm, is not applicable to the numerical integration algorithm because, as noted above, the impact at a given distance downwind varies as a function of wind direction within the sector. In order to avoid abrupt changes in the concentrations at the sector boundaries with the new algorithm, a linear interpolation is used to determine the frequency of occurrence of each wind direction used for the individual simulations within a sector, based on the frequencies of occurrence in the adjacent sectors. This "smoothing" of the frequency distribution has a similar effect as the smoothing function used with the current ISCLT2 algorithm. The frequency of occurrence for the jth wind direction between i and i+1 sector can be calculated as:

$$f_{ij} = F_i + (\Theta_{i+1} - \theta_{ij}) (F_{i+1} - F_i) / (\Theta_{i+1} - \Theta_i) \qquad (2\text{-}3)$$

where:

F_i = the frequency of occurrence of wind directions for the ith sector.

F_{i+1} = the frequency of occurrence of wind directions for the i+1th sector.

Θ_i = the central wind direction for the ith sector.

Θ_{i+1} = the central wind direction for the i+1th sector.

θ_{ij} = the wind direction between Θ_i and Θ_{i+1}.

f_{ij} = the frequency of occurrence for the wind direction θ_{ij}.

2.2.3. Convergence Criteria

This section describes the convergence criteria used to determine when the area source calculations for a specific sector are completed. For each combination of wind speed class, stability class and wind direction sector in the STAR data file, at least 5 wind directions are used to approximate the sector average area source impact. The number of wind direction simulations used, N, can be calculated as:

$$N = 2^k + 1 \qquad (2\text{-}4)$$

where k is the referred to as the level number. If k = 1, a total of 3 wind directions are used. This is called level 1. For level 5 (k=5), a total of 33 wind directions are used. These wind directions are equally distributed inside the 22.5 degree sector. For example, in the case of level 5, the wind directions are equally distributed inside the sector with a 0.68 (= 22.5/33) degree interval.

After calculations are completed for each level, the results are compared with results for the previous level. One convergence criterion that the model checks is whether the results for successive levels agree within 2 percent. If the 2 percent convergence criterion is not achieved after level 2, for example, then the model increases one more level, to level 3, which has 9 simulations. Since 5 of these wind directions were used in the previous calculation, the model only performs calculations for the 4 new wind directions. This procedure is computationally efficient.

Although this algorithm is known to converge (to within 2 percent) eventually, the run time may be excessive for some situations. Using the ISCST2 model, one can calculate the annual average by using the hourly meteorological data, which requires only 8760 hourly simulations. This corresponds roughly with the number of simulations needed for level 4 (17*576=9792). If the ISCLT2 model were to routinely employ 10 levels (1,025 simulations for each of the 576 STAR combinations), it would be much more efficient to run the ISCST2 model. For this reason, the algorithm is designed to stop calculating after a certain level is reached. Several tests are needed to determine the optimum level to ensure both reasonable model run times and acceptable accuracy. The results of these tests are presented in Section 3.

In addition to the two convergence criteria discussed above, i.e., the 2 percent comparison between results for successive levels, and the maximum number of computational levels, a third criterion is incorporated into the algorithm in order to further optimize its performance. With numerical schemes of the kind described here, it is often most difficult to achieve convergence for very small concentration values, where truncation errors can be significant. Since these values are also of less concern to the typical user, the model will stop any further calculations for a given STAR combination if the concentration estimate is less than 1.0E-10. This avoids making excessive computations for cases where the algorithm is essentially trying to converge on zero.

3. ISCLT2 AREA SOURCE ALGORITHM PERFORMANCE TEST

3.1. Overview of the Performance Tests

In order to evaluate the performance of the modified ISCLT2 area source algorithm, several tests were designed. These tests can be classified into three categories. The first category is to test the overall accuracy and performance of the algorithm using very idealized meteorological inputs, the second category is to test the reasonableness of the algorithm's performance for various source-receptor geometries, and the third is to examine the algorithm's behavior in more detail using a realistic distribution of meteorological conditions. The latter group includes a series of tests to evaluate the optimum set of convergence criteria for the numerical integration algorithm in order to achieve an appropriate balance between accuracy and model run time. The performance tests include point-to-point comparisons, quality assurance tests, and statistical analyses. Tables and graphs are used to present the analytical results in a comprehensive way.

3.2. Results Of The Performance Tests

3.2.1. Basic Performance Study: Large Area Source and Idealized Meteorological Conditions

The main purpose of this test is to verify that the numerical integration algorithm has been correctly implemented into the ISCLT2 model. The test consists of comparisons of results from the ISCLT2 model with results from the ISCST2 model using the numerical integration algorithm for very idealized meteorological conditions. The meteorological conditions consist of a single wind speed and stability category with a uniform distribution of wind directions in order to force the ISCST2 model to simulate sector averages for comparison with ISCLT2. In this study, a 1000x1000m square source and a 1000x200m rectangular source are used. One polar network of receptors is used, with the origin of the network located at the center of the area source. The polar receptor network has seven distance rings of 250, 500, 750, 1000, 1500, 5000, and 15000 meters, and 36 direction radials (every 10 degrees), for a total of 252 receptors.

To idealize the meteorological conditions, a single wind speed and stability category are used for each test. Three hourly meteorological data files were generated for use by the ISCST2 model, one each for stability category A (unstable), D (Neutral), and F(Stable), respectively. The wind direction was altered 0.5 degrees clockwise for each hour, and a 360 day period was used to approximate sector average annual concentration values from ISCST2. The ISCLT2 model was run using a STAR meteorological data file with frequencies specified to select the same stability category and wind speed as used in the

hourly data files for ISCST2, and a uniform distribution of frequencies for all sectors.

The results of the comparison between ISCST2 and ISCLT2 with the numerical integration area source algorithm and the idealized meteorological conditions, presented in Figures 3.1 to 3.6, are very encouraging. Three figures are provided for each combination of source type (1000x1000m square or 1000x200m rectangle) and stability category (A, D or F). The first figure in each group shows the maximum concentration for both the ISCST2 model and the ISCLT2 model as a function of downwind distance. The results from the two models are virtually indistinguishable on these plots, suggesting that the algorithm has been correctly implemented in the ISCLT2 model. In order to provide a more detailed comparison of the results of the two models, the two additional figures for each case show the "quartiles" of the ratio of ISCLT2/ISCST2 results for all receptors, first as a function of convergence level used in the ISCLT2 model, and second as a function of downwind distance using no limit on the number of convergence levels (full convergence). These quartile plots show the maximum and minimum ratios, together with the ratios that are exceeded 25 percent of the time, 50 percent of the time, and 75 percent of the time.

The series of quartile plots show that the ISCST2 and ISCLT2 models agree within $\pm$ 1 percent in nearly all cases (ratios between 0.99 and 1.01), and that 50 percent of the ratios (between the 25 percent and 75 percent quartiles) fall between 0.9975 and 1.0025, corresponding to differences of less than 0.25 percent. The quartile plots showing ratios as a function of downwind distance show that the closest agreement occurs for the largest concentrations at receptors located within or near the area source. The figures also show that the ISCLT2 converge to relatively stable results by about convergence level 5, corresponding to 33 separate wind direction simulations per 22.5 degree sector.

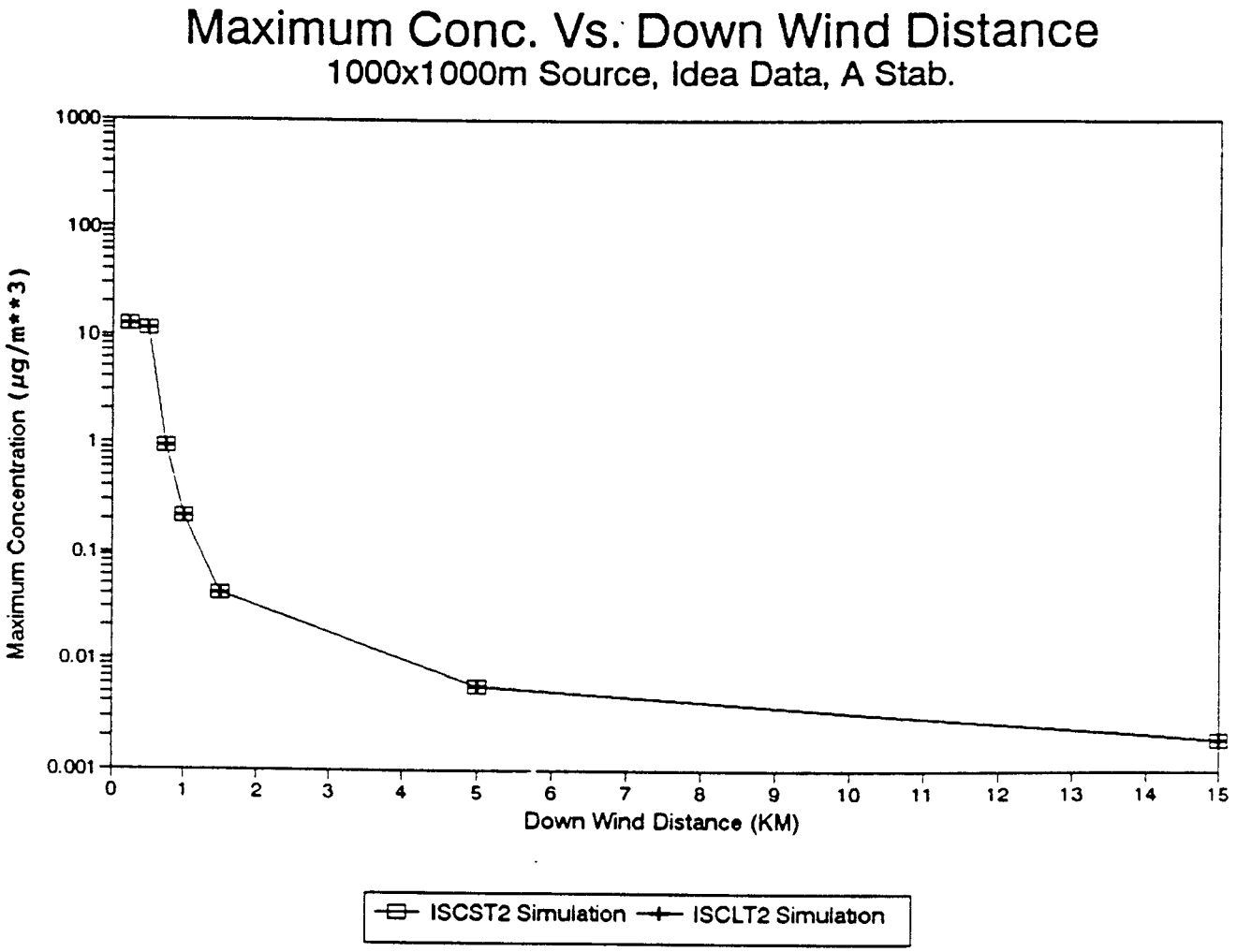

Figure 3.1a. Maximum Concentration Of ISCST Simulation And ISCLT Simulation Plotted With Downwind Distance. 1000x1000m Area Source, A Stability Category

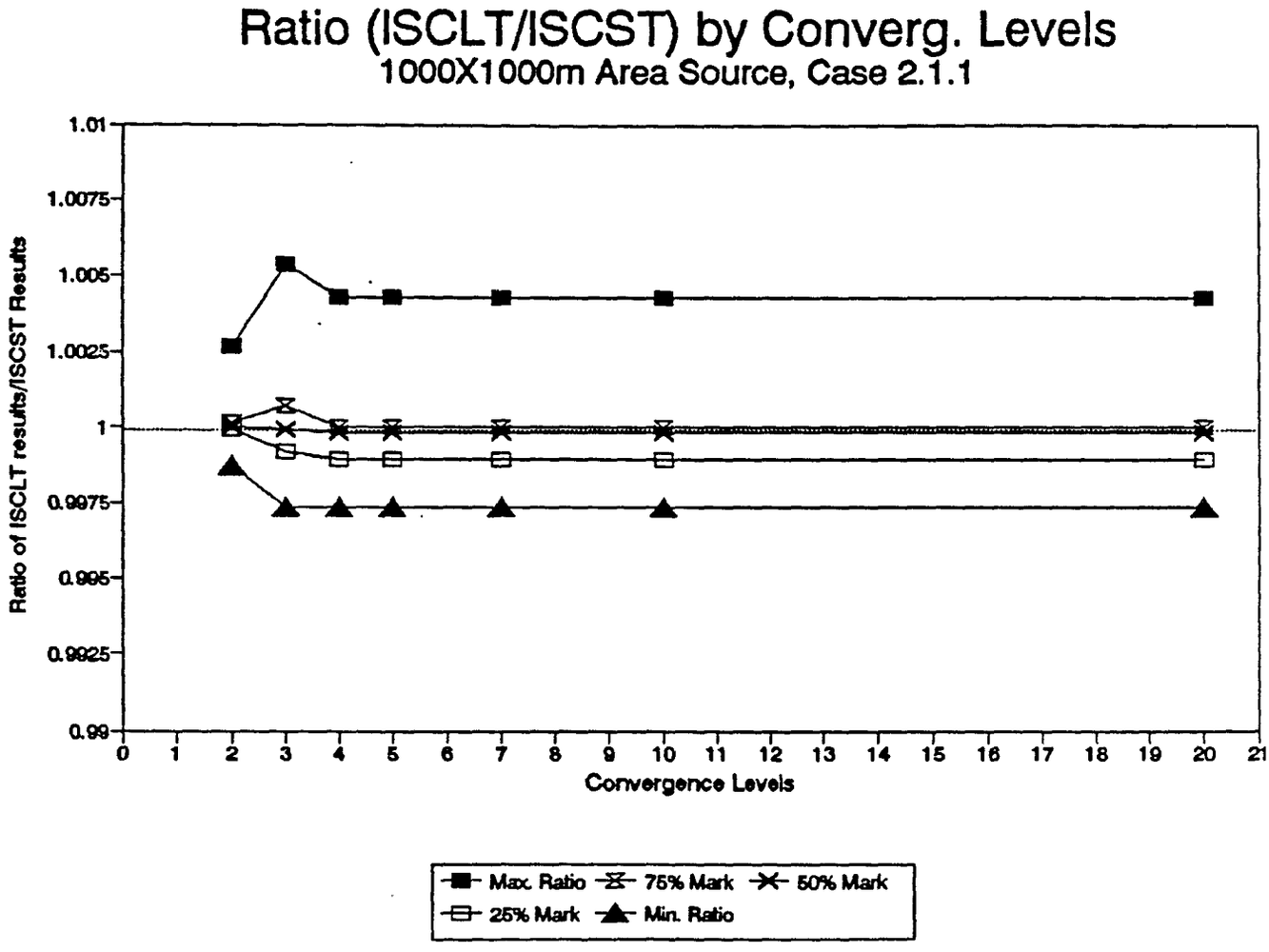

Figure 3.1b. Quartile Plot of Ratios (ISCLT/ISCST) by Convergence Levels For An 1000x1000m Area Source With Idealized Hourly Meteorological Data Set For ISCST Simulation, and the Idealized STAR Data Set For ISCLT Simulation. Stability Category A For All Data.

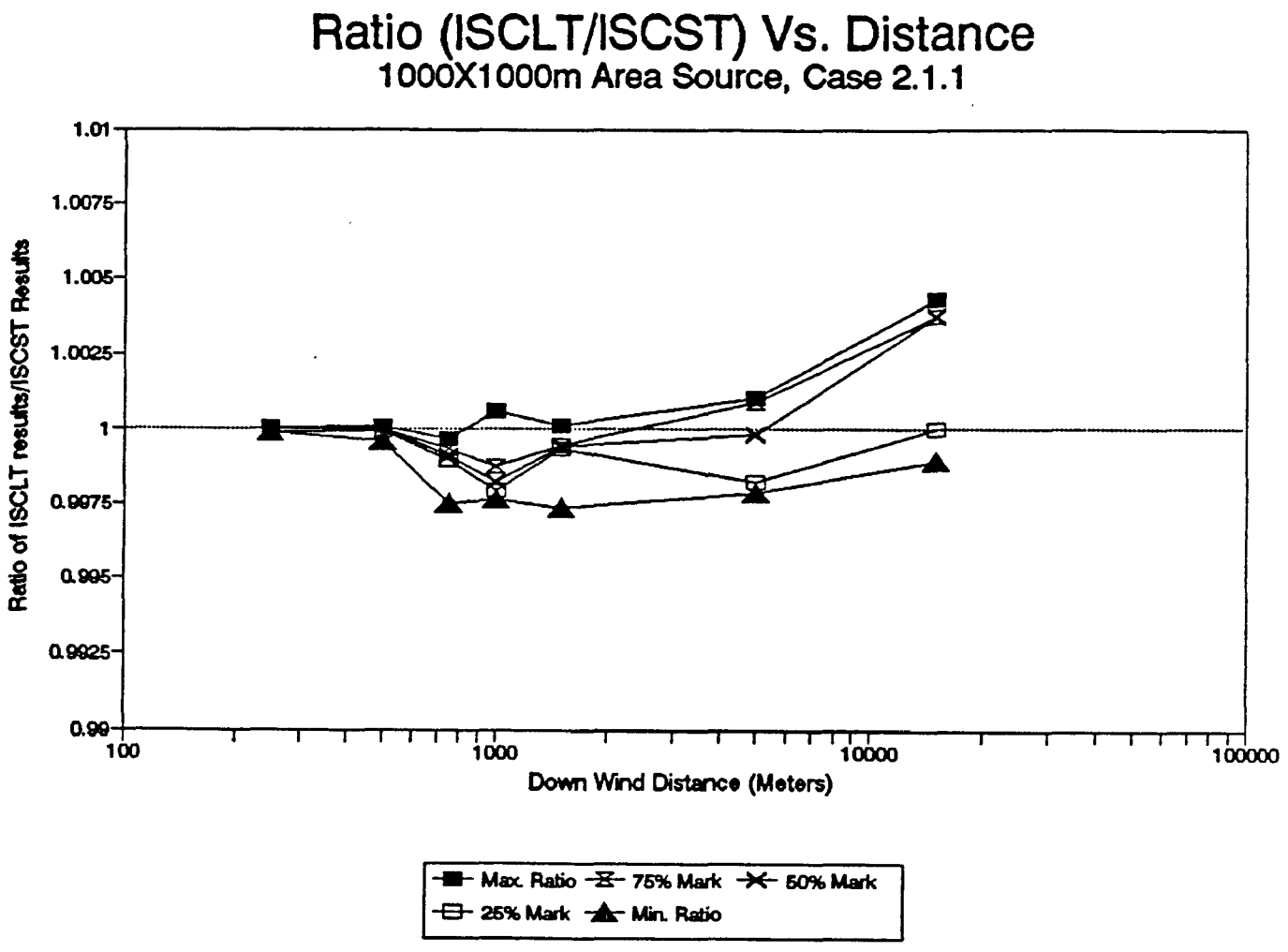

Figure 3.1c. Quartile Plot of Ratios (ISCLT/ISCST) by Downwind Distance For An 1000x1000m Area Source With Idealized Hourly Meteorological Data Set For ISCST Simulation, and the Idealized STAR Data Set For ISCLT Simulation. Stability Category A For All Data. No limit on convergence level limit

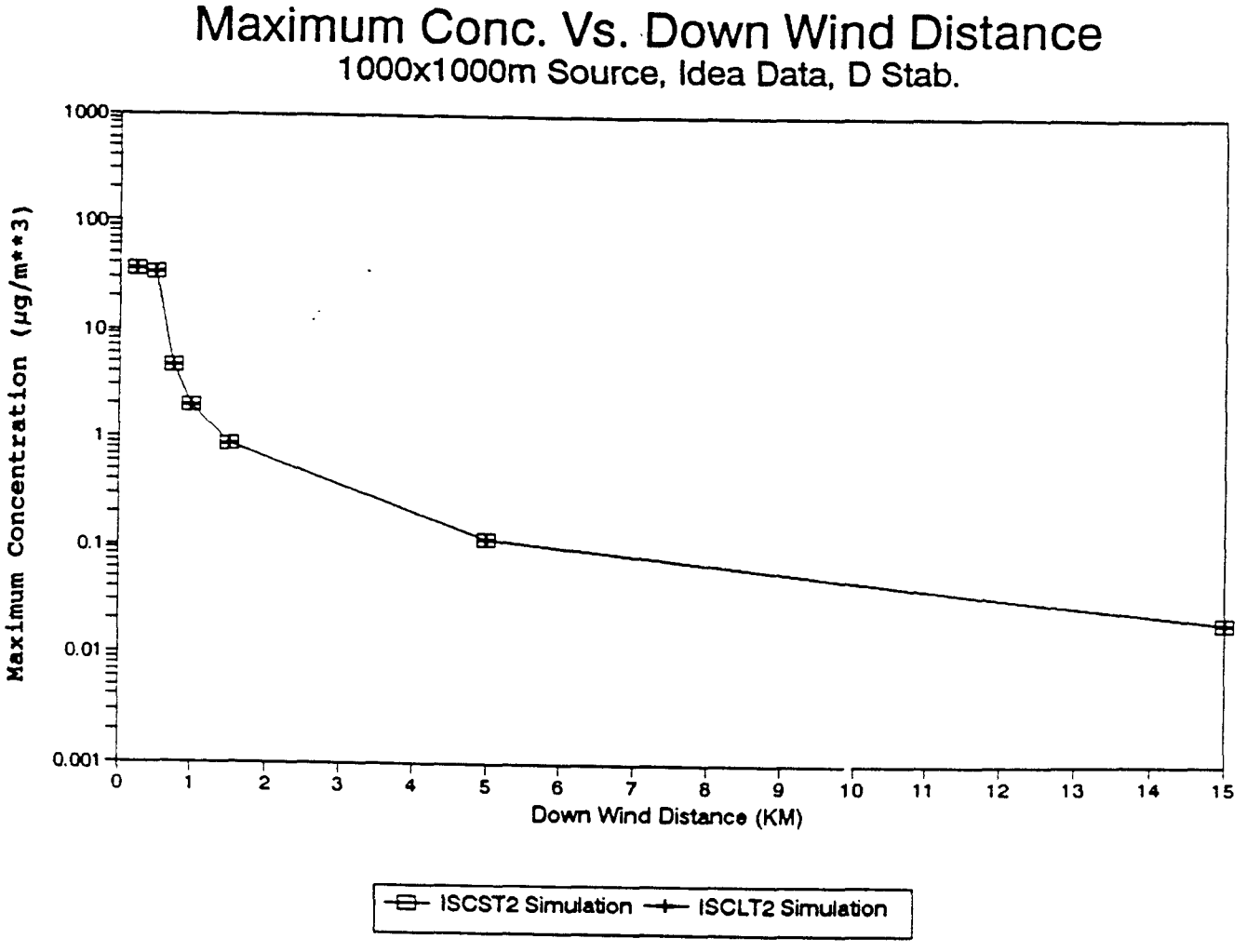

Figure 3.2a. Maximum Concentration Of ISCST Simulation And ISCLT Simulation Plotted With Downwind Distance. 1000x1000m Area Source, D Stability Category

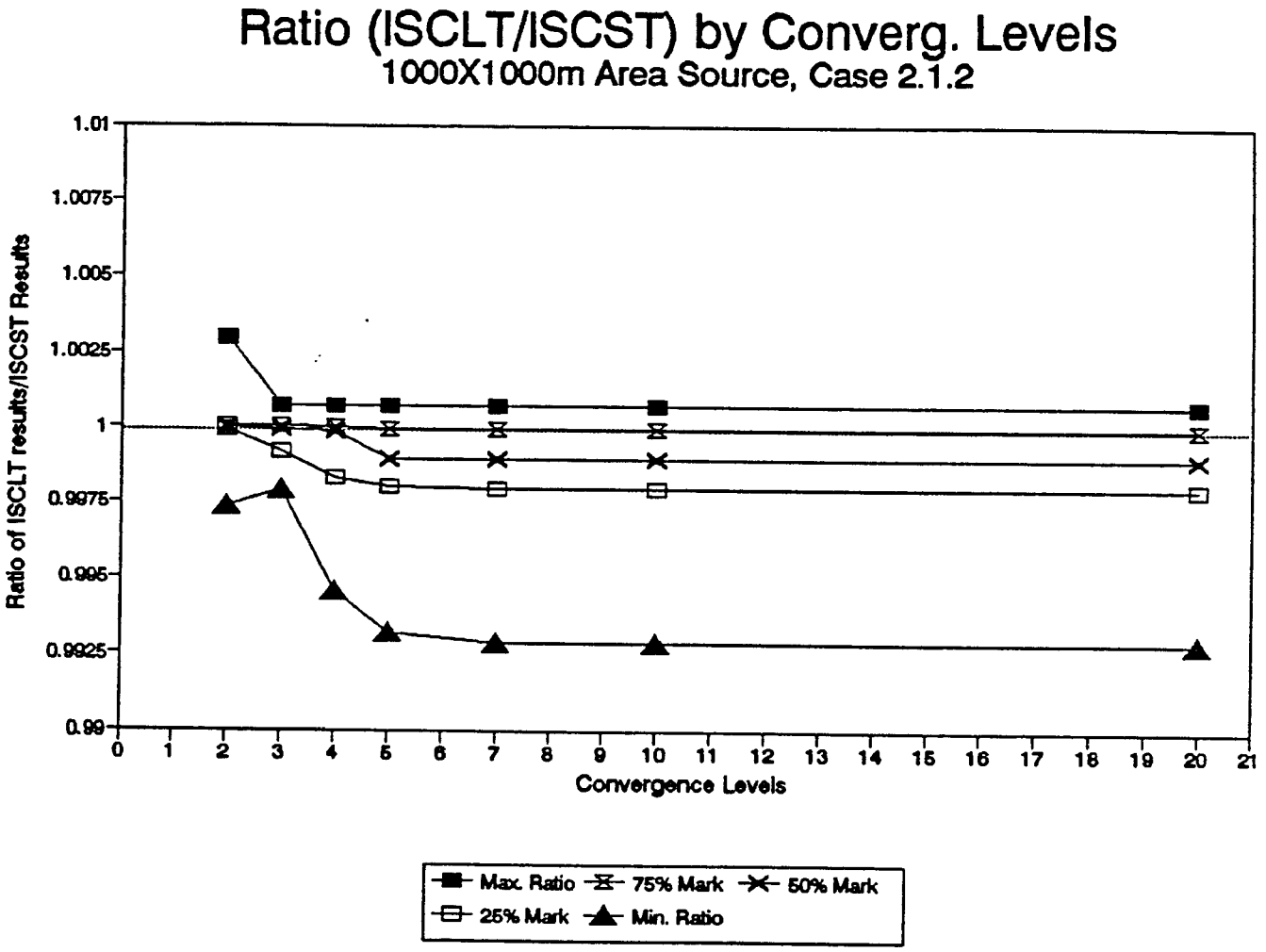

Figure 3.2b. Quartile Plot of Ratios (ISCLT/ISCST) by Convergence Levels For An 1000x1000m Area Source With Idealized Hourly Meteorological Data Set For ISCST Simulation, and the Idealized STAR Data Set For ISCLT Simulation. Stability Category D For All Data. No limit on convergence levels

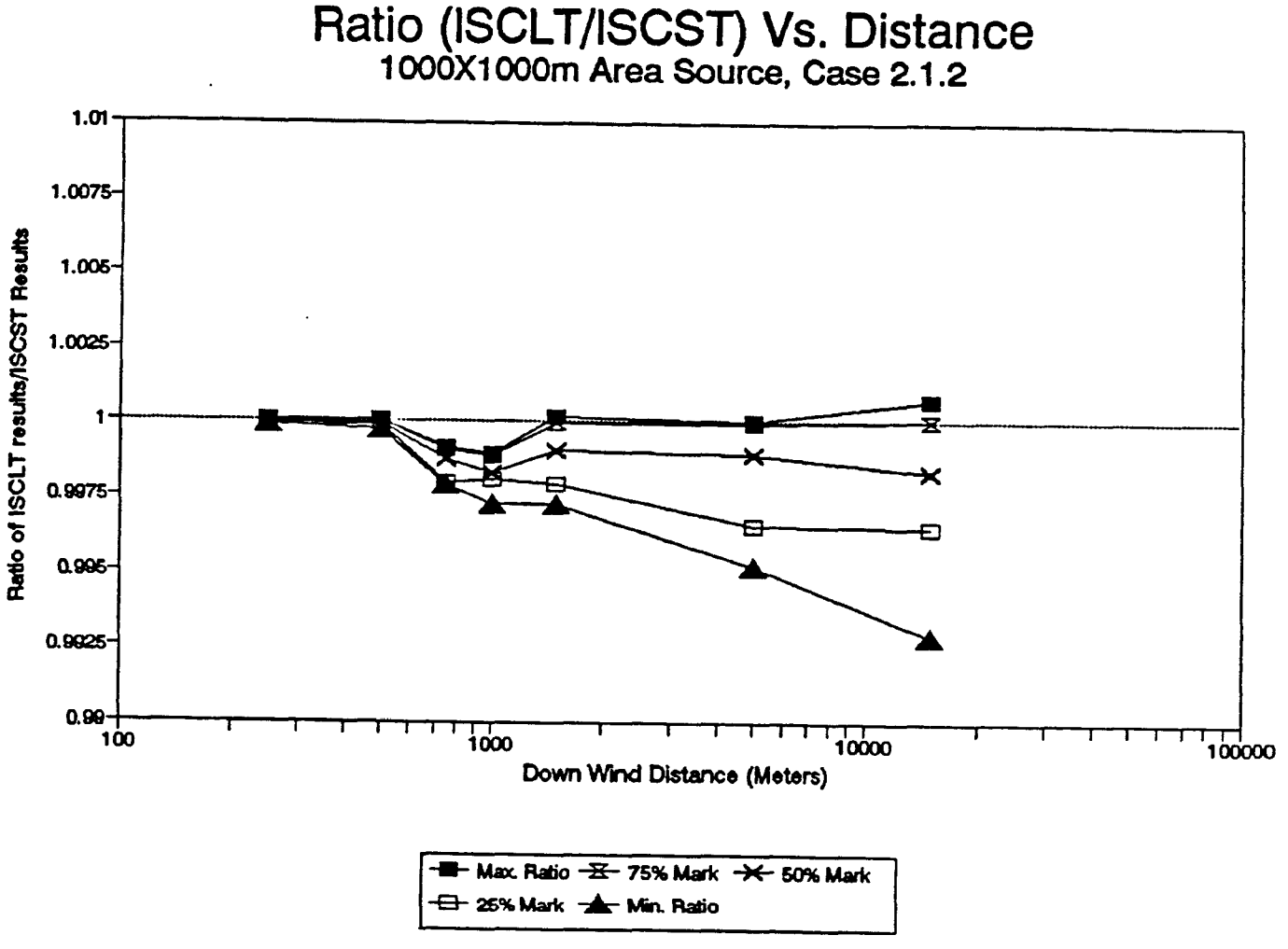

Figure 3.2c. Quartile Plot of Ratios (ISCLT/ISCST) by Downwind Distance For An 1000x1000m Area Source With Idealized Hourly Meteorological Data Set For ISCST Simulation, and the Idealized STAR Data Set For ISCLT Simulation. Stability Category D For All Data.

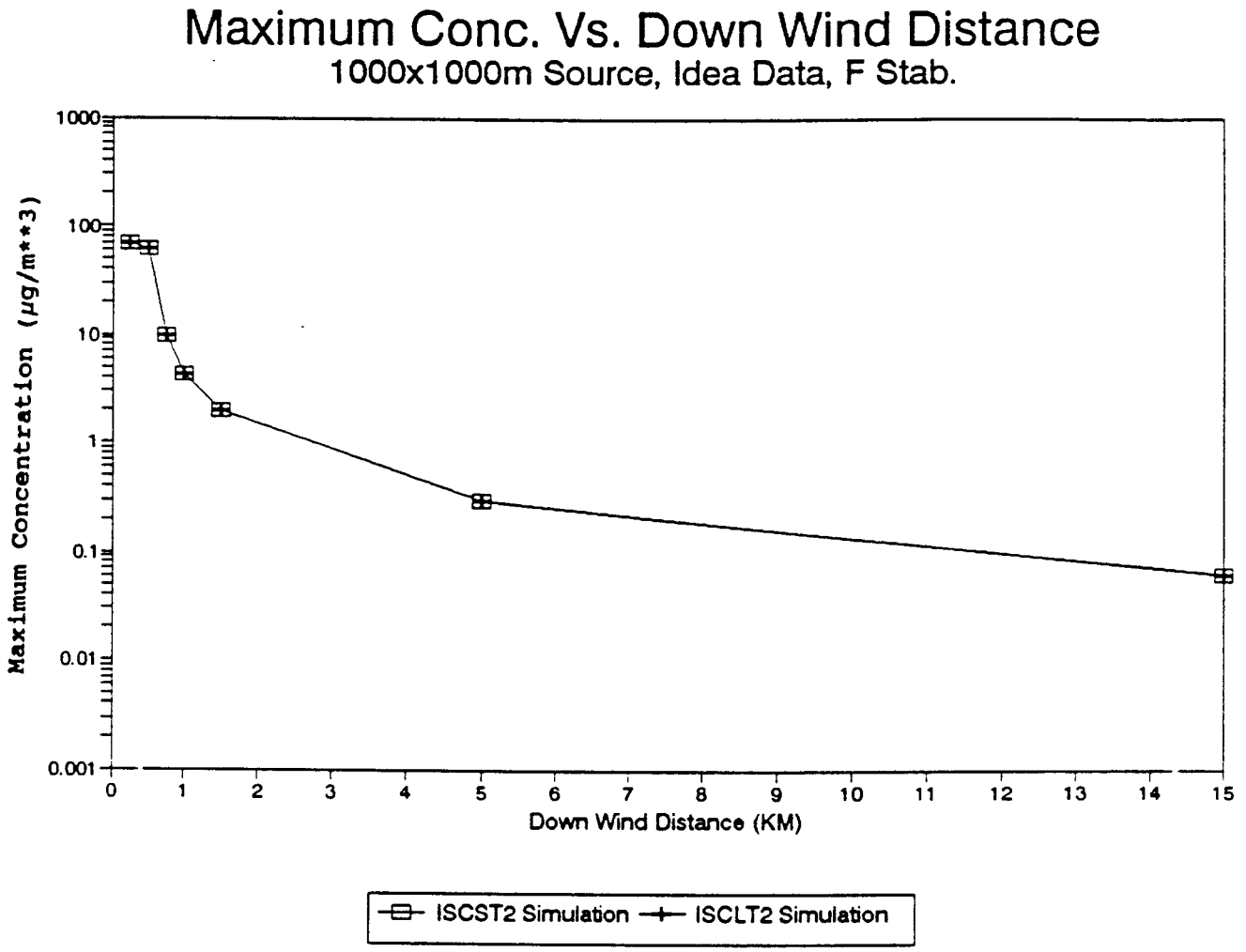

Figure 3.3a. Maximum Concentration Of ISCST Simulation And ISCLT Simulation Plotted With Downwind Distance. 1000x1000m Area Source, F Stability Category

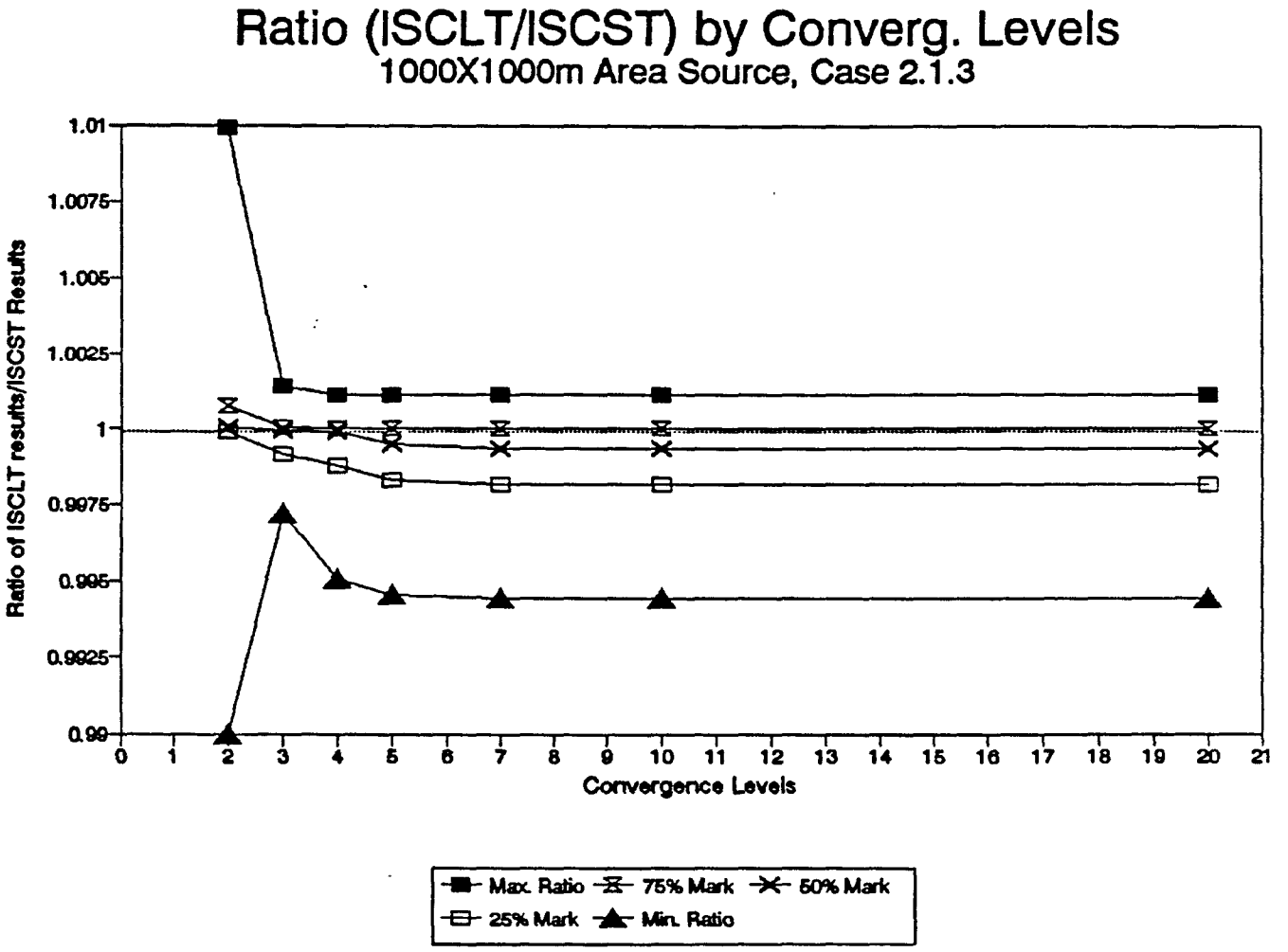

Figure 3.3b. Quantile Plot of Ratios (ISCLT/ISCST) by Convergence Levels For An 1000x1000m Area Source With Idealized Hourly Meteorological Data Set For ISCST Simulation, and the Idealized STAR Data Set For ISCLT Simulation. Stability Category F For All Data.

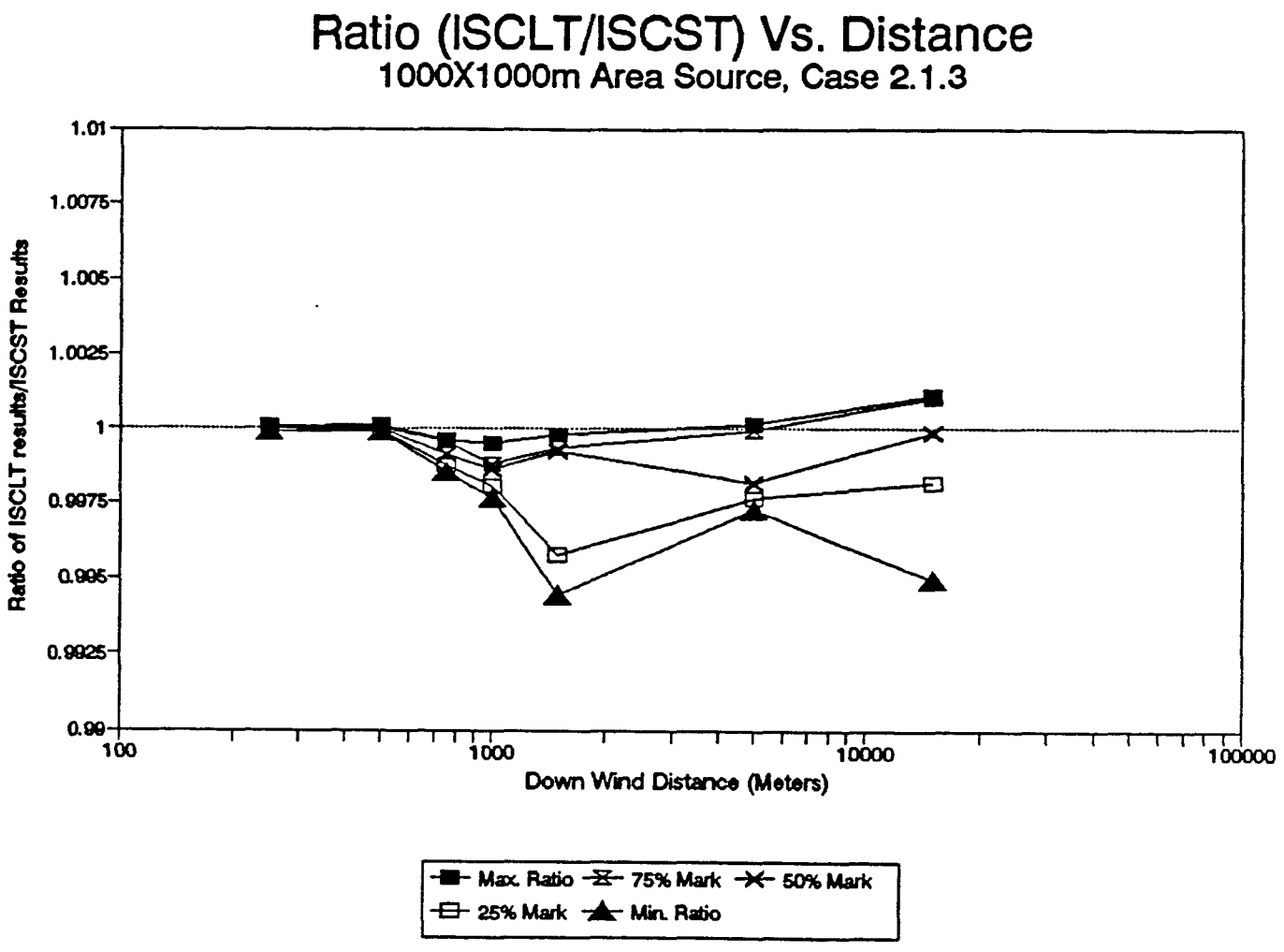

Figure 3.3c. Quartile Plot of Ratios (ISCLT/ISCST) by Downwind Distance For An 1000x1000m Area Source With Idealized Hourly Meteorological Data Set For ISCST Simulation, and the Idealized STAR Data Set For ISCLT Simulation. Stability Category F For All Data. No limit on convergence levels.

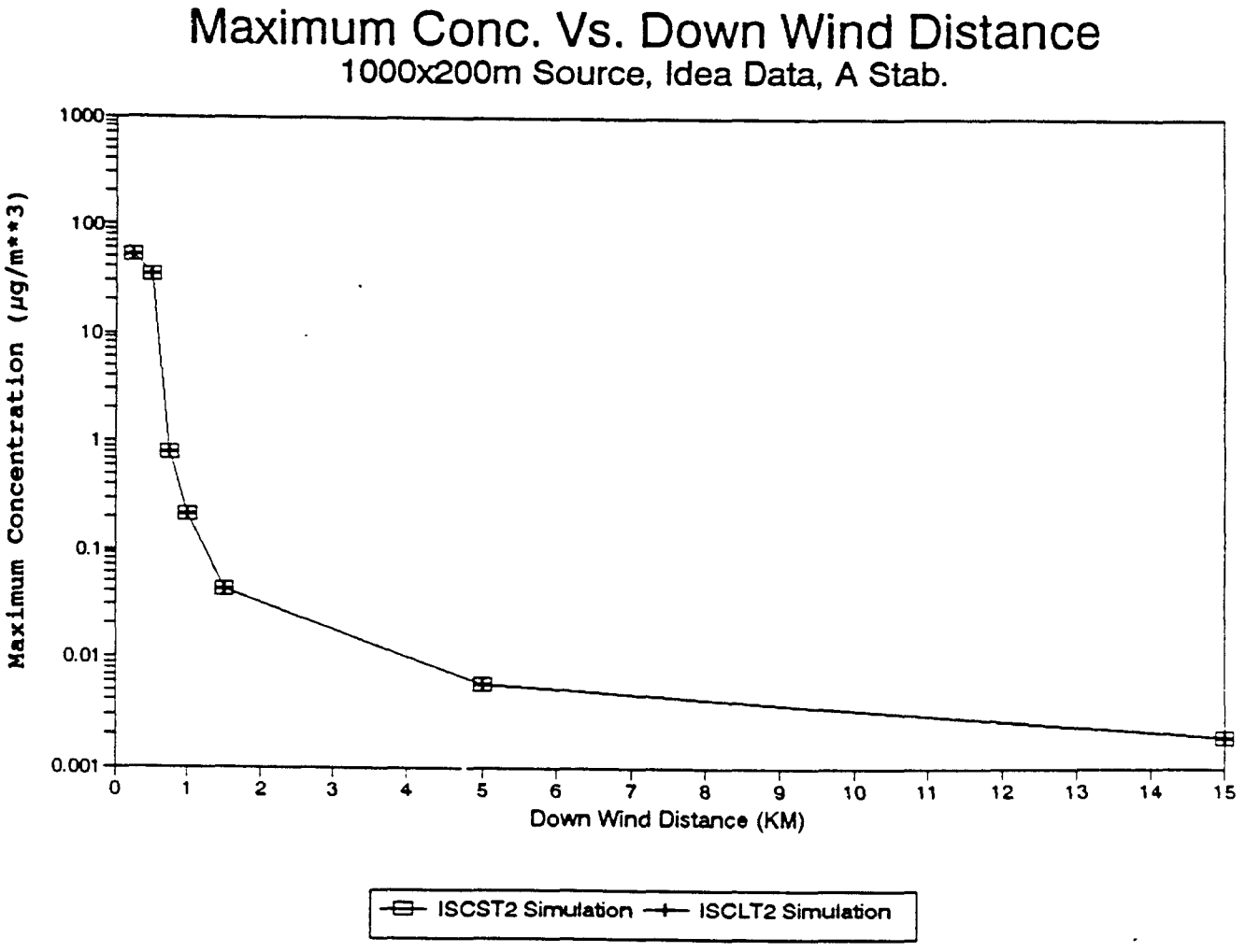

Figure 3.4a. Maximum Concentration Of ISCST Simulation And ISCLT Simulation Plotted With Downwind Distance. 1000x200m Area Source, A Stability Category

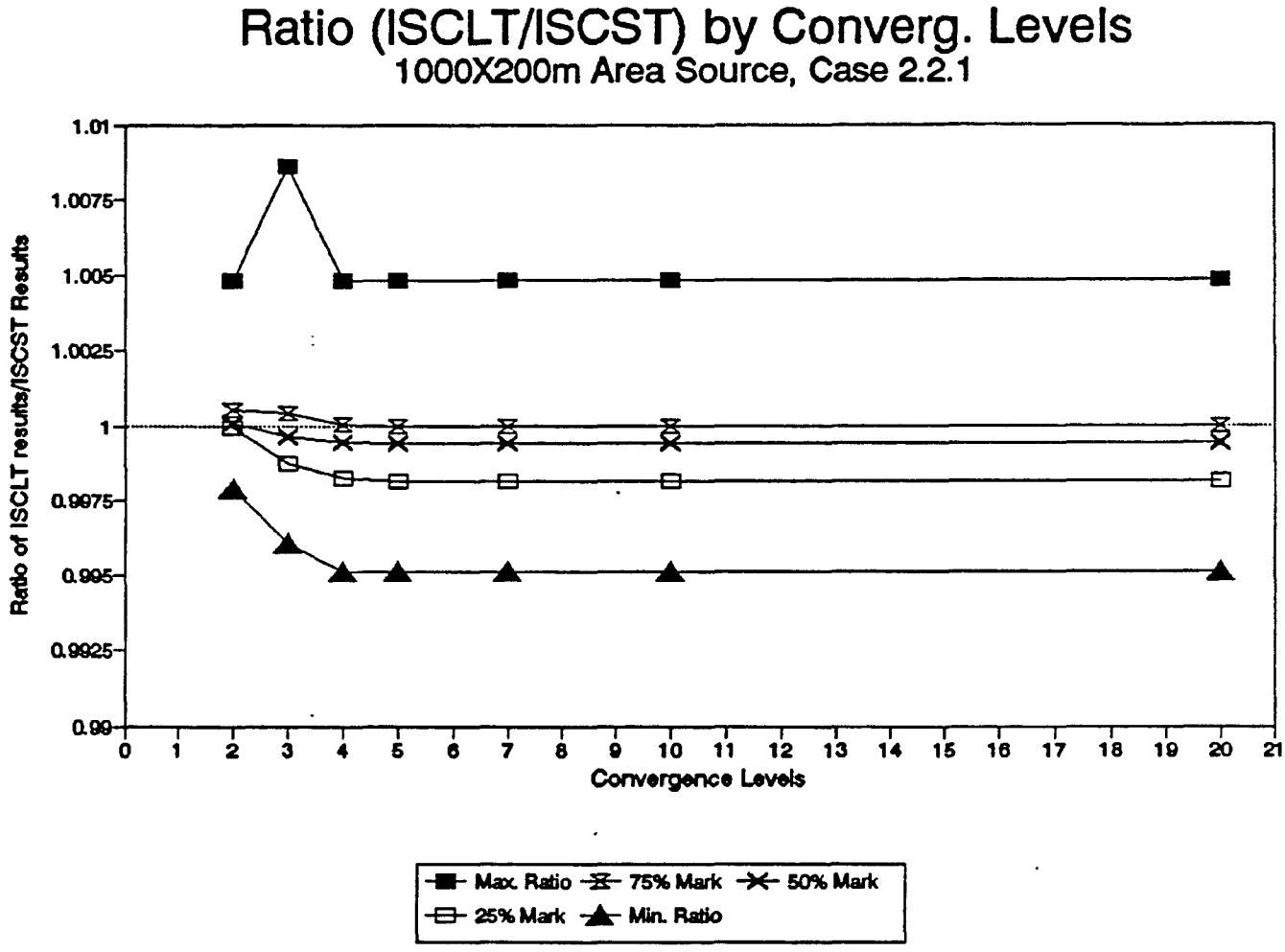

Figure 3.4b. Quartile Plot of Ratios (ISCLT/ISCST) by Convergence Levels For An 1000x200m Area Source With Idealized Hourly Meteorological Data Set For ISCST Simulation, and the Idealized STAR Data Set For ISCLT Simulation. Stability Category A For All Data.

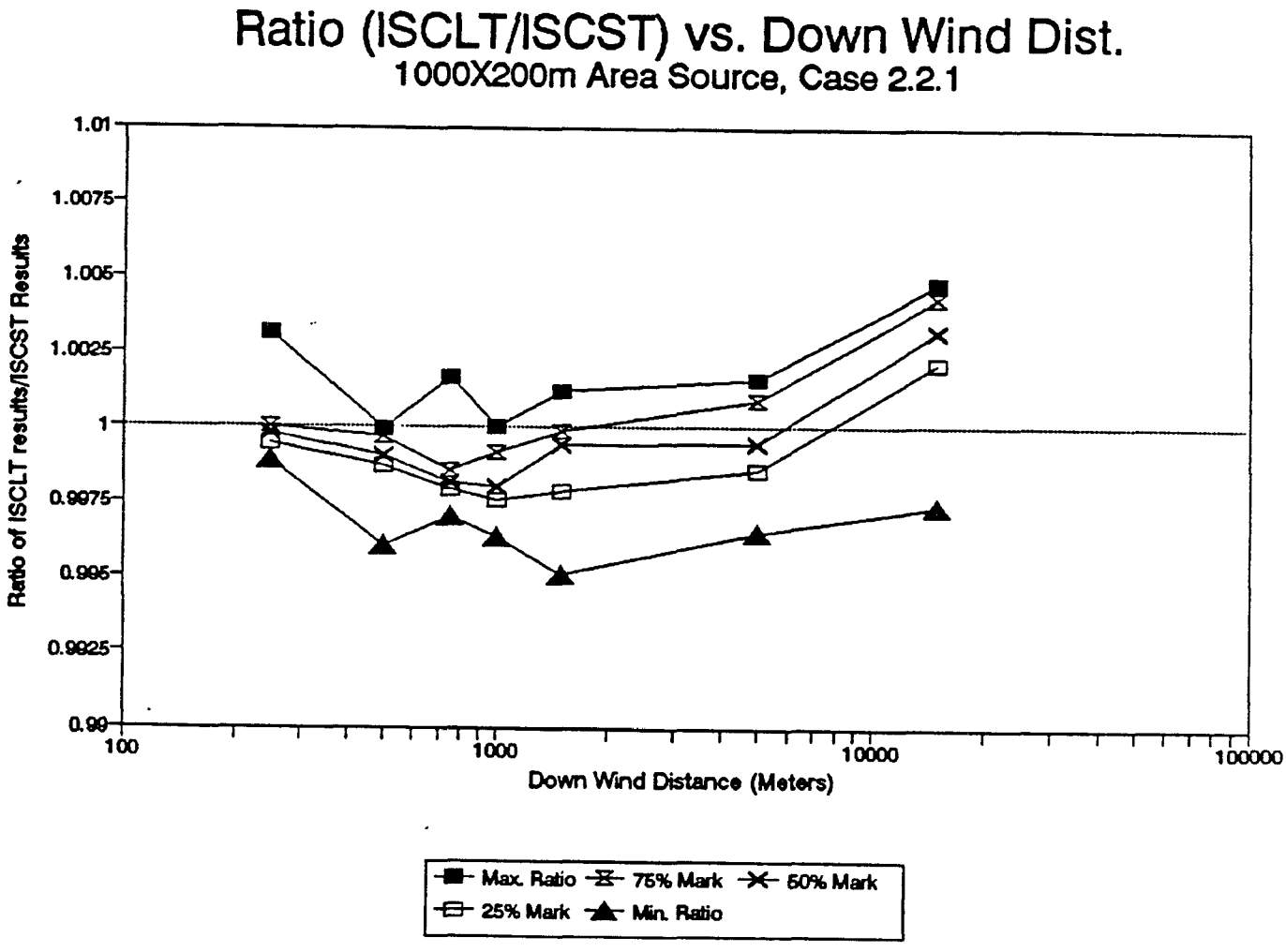

Figure 3.4c. Quartile Plot of Ratios (ISCLT/ISCST) by Downwind Distance For An 1000x200m Area Source With Idealized Hourly Meteorological Data Set For ISCST Simulation, and the Idealized STAR Data Set For ISCLT Simulation. Stability Category A For All Data. No limit on convergence levels.

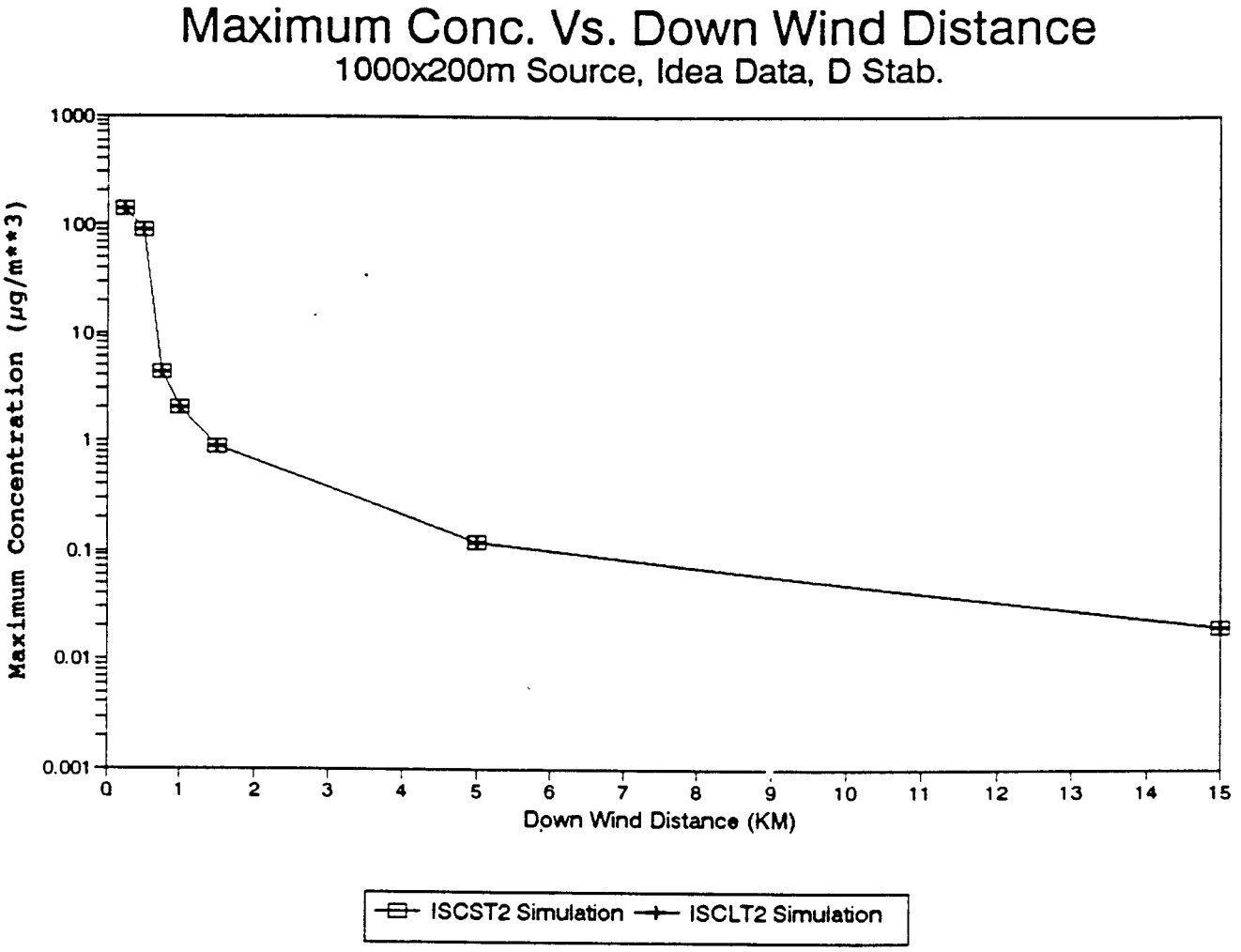

Figure 3.5a. Maximum Concentration Of ISCST Simulation And ISCLT Simulation Plotted With Downwind Distance. 1000x200m Area Source, D Stability Category

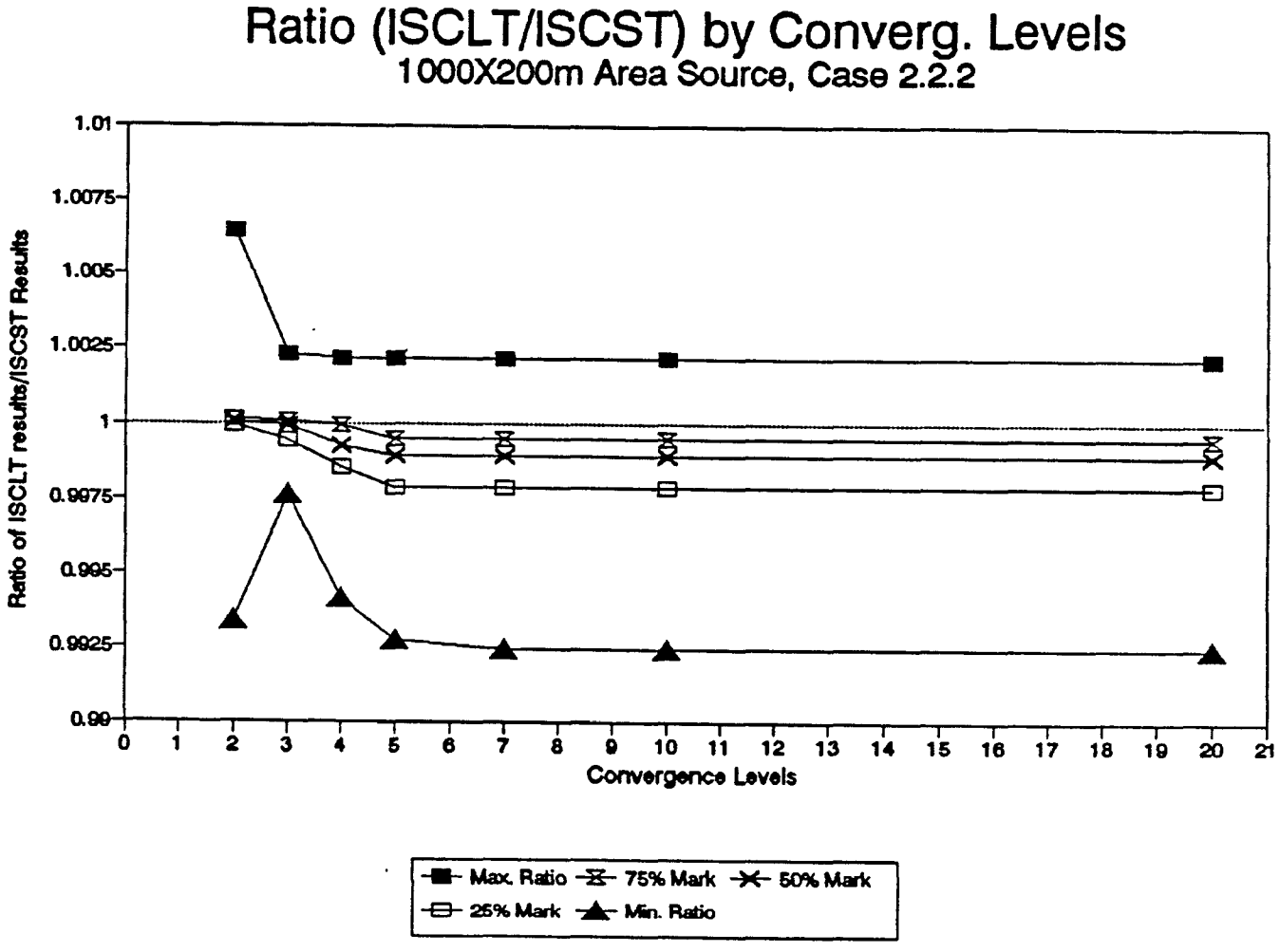

Figure 3.5b. Quartile Plot of Ratios (ISCLT/ISCST) by Convergence Levels For An 1000x200m Area Source With Idealized Hourly Meteorological Data Set For ISCST Simulation, and the Idealized STAR Data Set For ISCLT Simulation. Stability Category D For All Data.

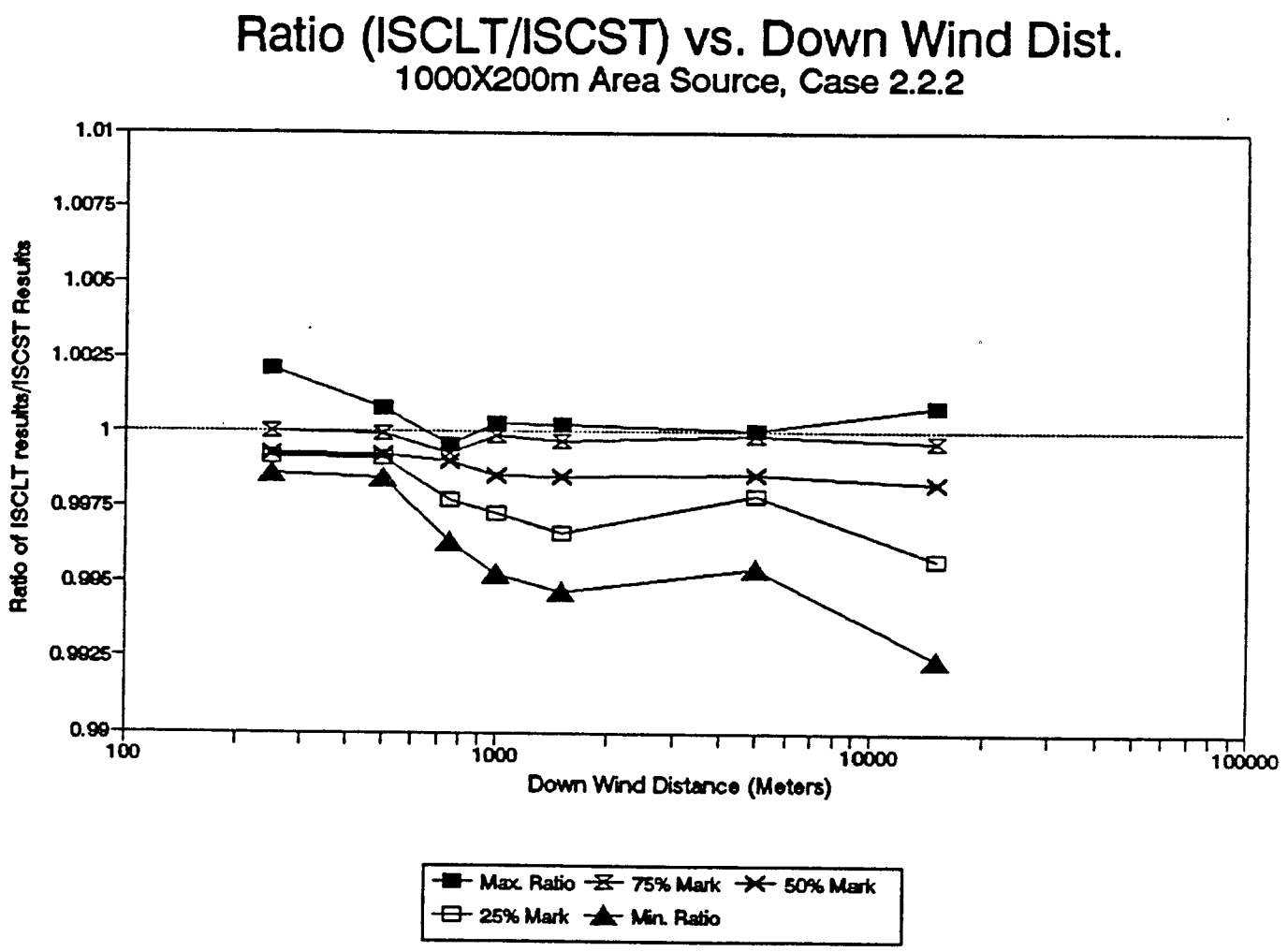

Figure 3.5c. Quartile Plot of Ratios (ISCLT/ISCST) by Downwind Distance For An 1000x200m Area Source With Idealized Hourly Meteorological Data Set For ISCST Simulation, and the Idealized STAR Data Set For ISCLT Simulation. Stability Category D For All Data. No limit on convergence levels.

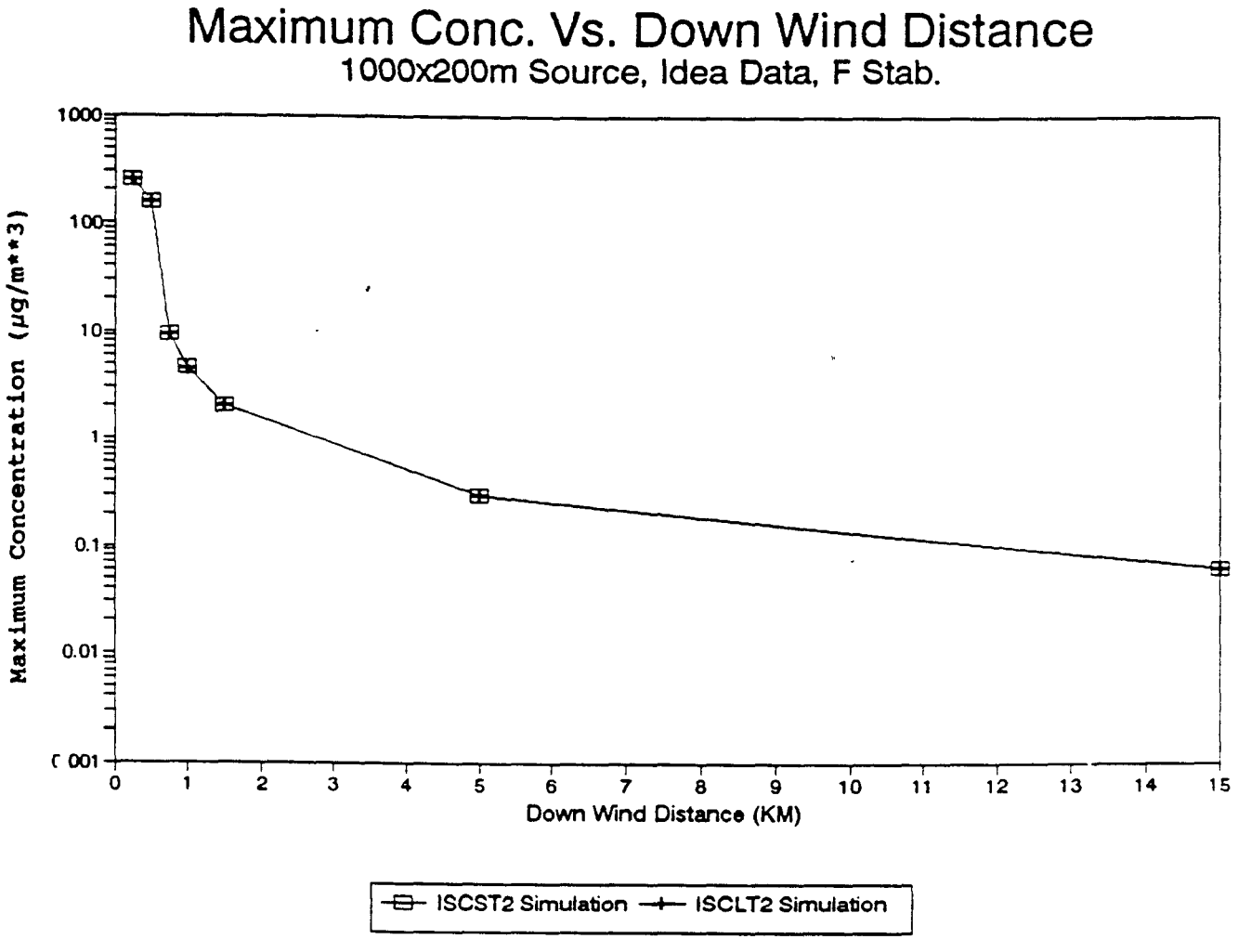

Figure 3.6a. Maximum Concentration Of ISCST Simulation And ISCLT Simulation Plotted With Downwind Distance. 1000x200m Area Source, F Stability Category

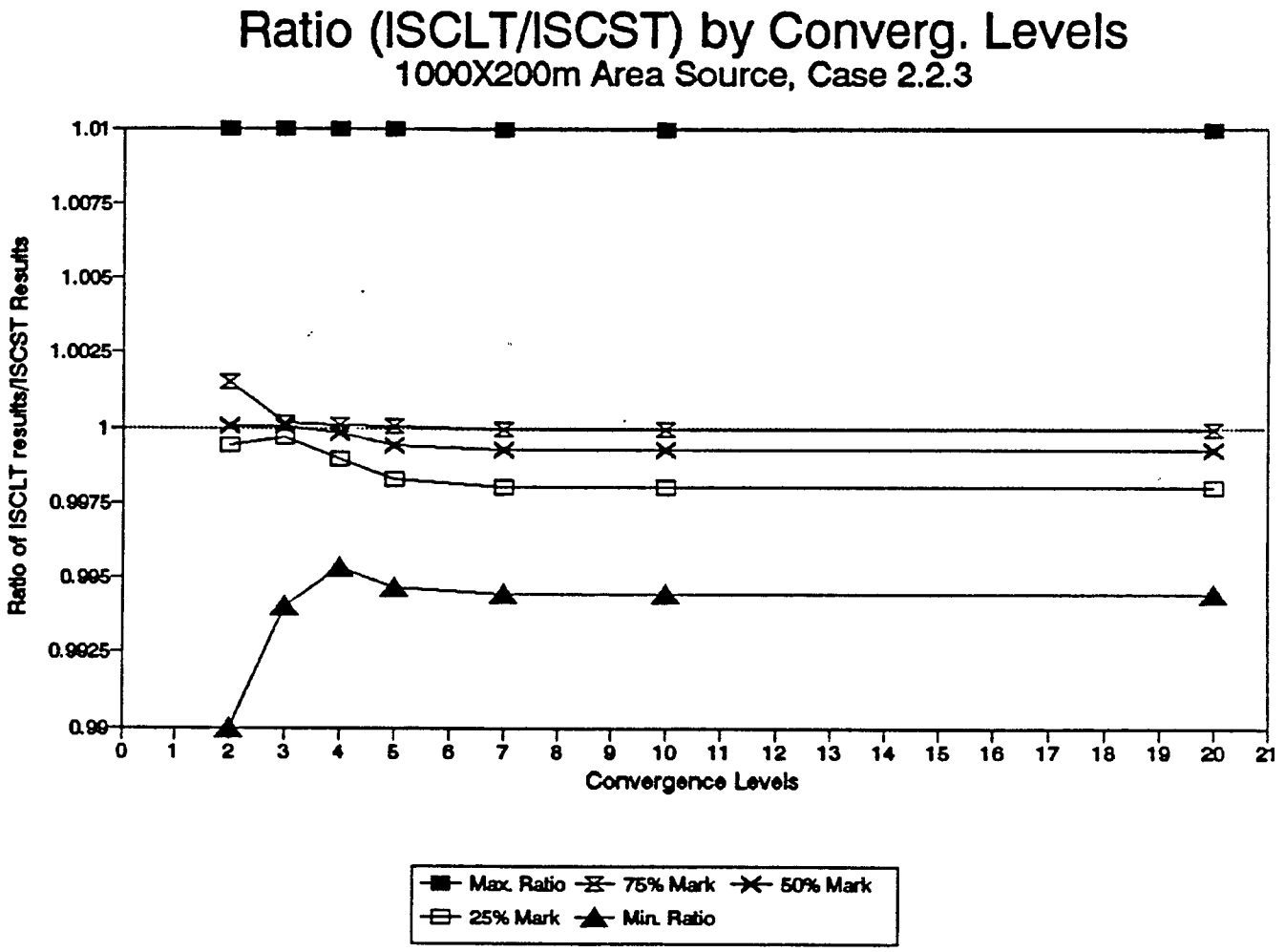

Figure 3.6b. Quartile Plot of Ratios (ISCLT/ISCST) by Convergence Levels For An 1000x200m Area Source With Idealized Hourly Meteorological Data Set For ISCST Simulation, and the Idealized STAR Data Set For ISCLT Simulation. Stability Category F For All Data.

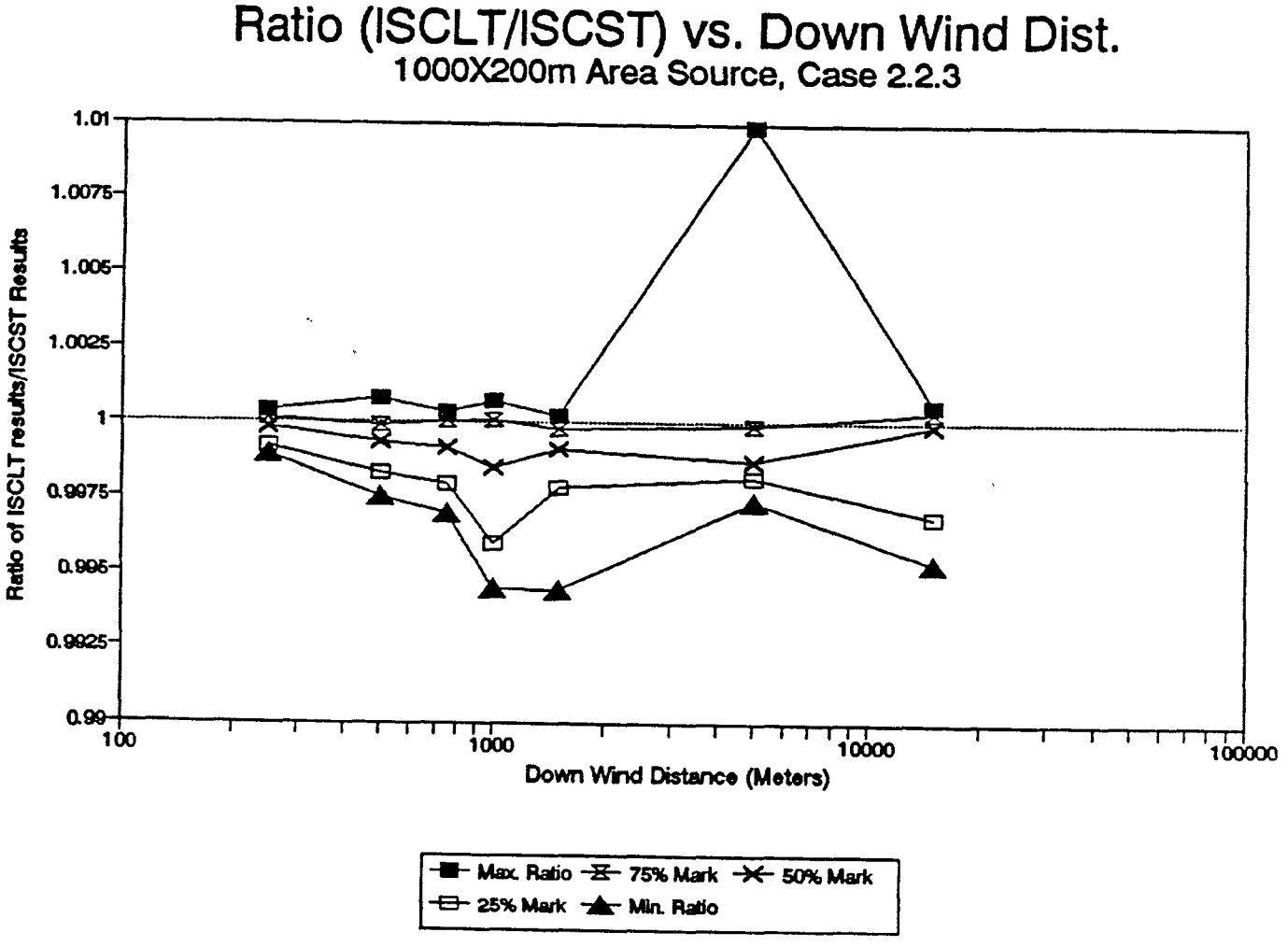

Figure 3.6c. Quartile Plot of Ratios (ISCLT/ISCST) by Downwind Distance For An 1000x200m Area Source With Idealized Hourly Meteorological Data Set For ISCST Simulation, and the Idealized STAR Data Set For ISCLT Simulation. Stability Category F For All Data. No limit on convergence levels.

3.2.2. Large Area Source With Idealized Hourly Meteorology Data Using Random Wind Directions

In the previous section, it was assumed that the frequency of occurrence was equal for all sectors. Using very idealized meteorological data to implement that assumption, the ISCLT2 model successfully reproduces the sector average concentration values calculated by the ISCST2 model. However, such a test does not challenge the algorithm for more realistic meteorological conditions, and especially for the smoothing function applied to the frequency distribution by ISCLT2 for cases of non-uniform distributions. Therefore, a similar test was performed comparing ISCLT2 and ISCST2 results using more realistic meteorology data distributions.

The ISCLT2 model was run for the same two area sources and receptor networks described in the previous section, with an actual STAR meteorological data summary from Raleigh-Durham, NC, (RDU) for the 1987 annual period. In order to simulate the sector averages with the ISCST2 model, an hourly meteorological data file was generated that produces the same frequency distribution as the 1987 RDU annual STAR summary. The wind speeds and mixing heights in the hourly meteorological data file were set to match the corresponding values used by the ISCLT2 model. To approximate the sector average impacts, the hourly wind directions were randomly distributed within the applicable 22.5 degree sector for use with the ISCST2 model. It is worth noting that, although the generated hourly data set eliminates the discrepancies for the wind speeds and mixing heights, there is no guarantee that the wind directions are uniformly distributed within the wind sector. Therefore, some discrepancies between the ISCLT2 and ISCST2 results are expected.

Figure 3.7a-c shows the results for the 1000x1000m square source, and Figure 3.8a-c shows the results for the 1000x200m rectangular source. Part a of each figure shows the maximum concentrations as a function of distance for both the ISCLT2 and ISCST2 models. As with the very idealized case presented earlier, the concentrations from the two models are almost indistinguishable. Parts b and c of the figures show the quartiles of the ratio of ISCLT2/ISCST2 results for all receptors, first as a function of convergence level used for the ISCLT2 model, and second as a function of distance with no limit on the convergence levels. The ratios show very close agreement between ISCLT2 and ISCST2, less than a one percent difference, for receptors located within and near the area source. The maximum differences increase to about 5 percent for receptors located further downwind of the area source, but most ratios still fall within $\pm$ 2 percent. The larger differences at downwind receptors are attributed to the fact that the ISCST2 model results are based on randomly placed wind directions, rather than on a uniform distribution. For sectors with relatively small frequencies of occurrence in the STAR data file, the number of hours generated

for the ISCST2 input file will be relatively few, and these hours may not approximate a sector average impact very well.

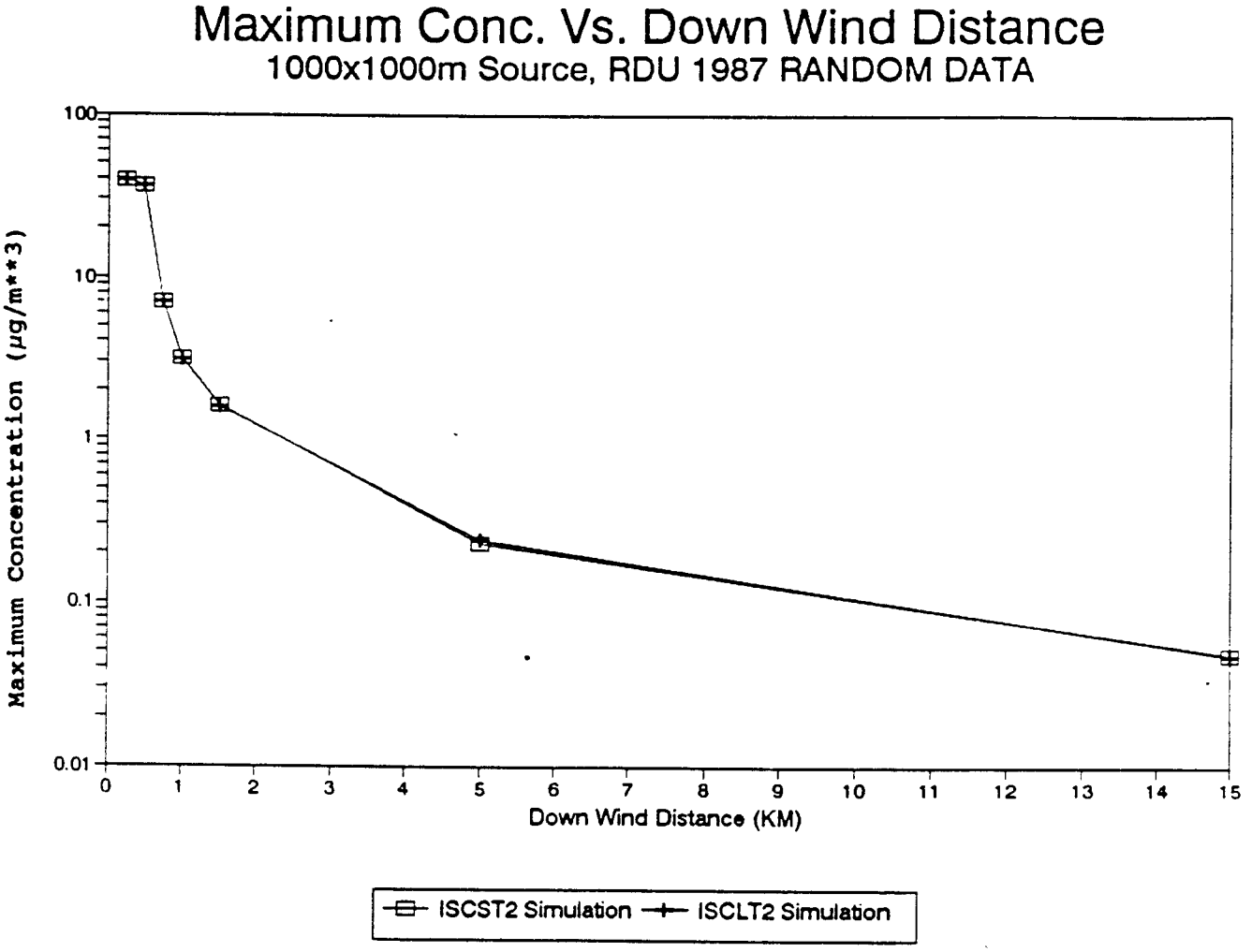

Figure 3.7a. Maximum Concentration Of ISCST Simulation And ISCLT Simulation Plotted With Downwind Distance. 1000x1000m Area Source, RDU 1987 Random Hourly And STAR Data

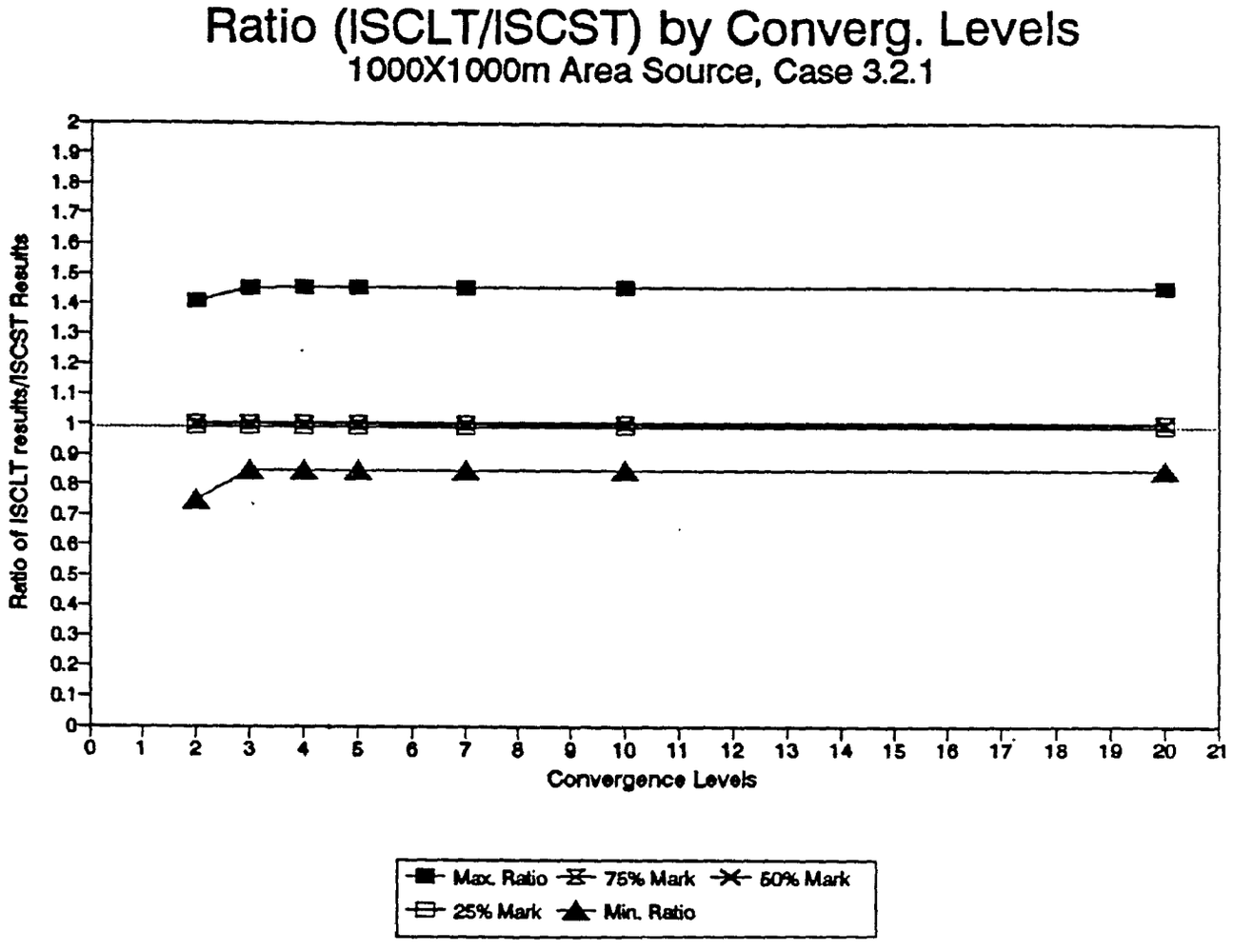

Figure 3.7b. Quartile Plot of Ratios (ISCLT/ISCST) by Convergence Levels For An 1000x1000m Area Source With RDU 1987 Random Hourly Meteorological Data Set For ISCST Simulation, and the RDU 1987 STAR Data Set For ISCLT Simulation.

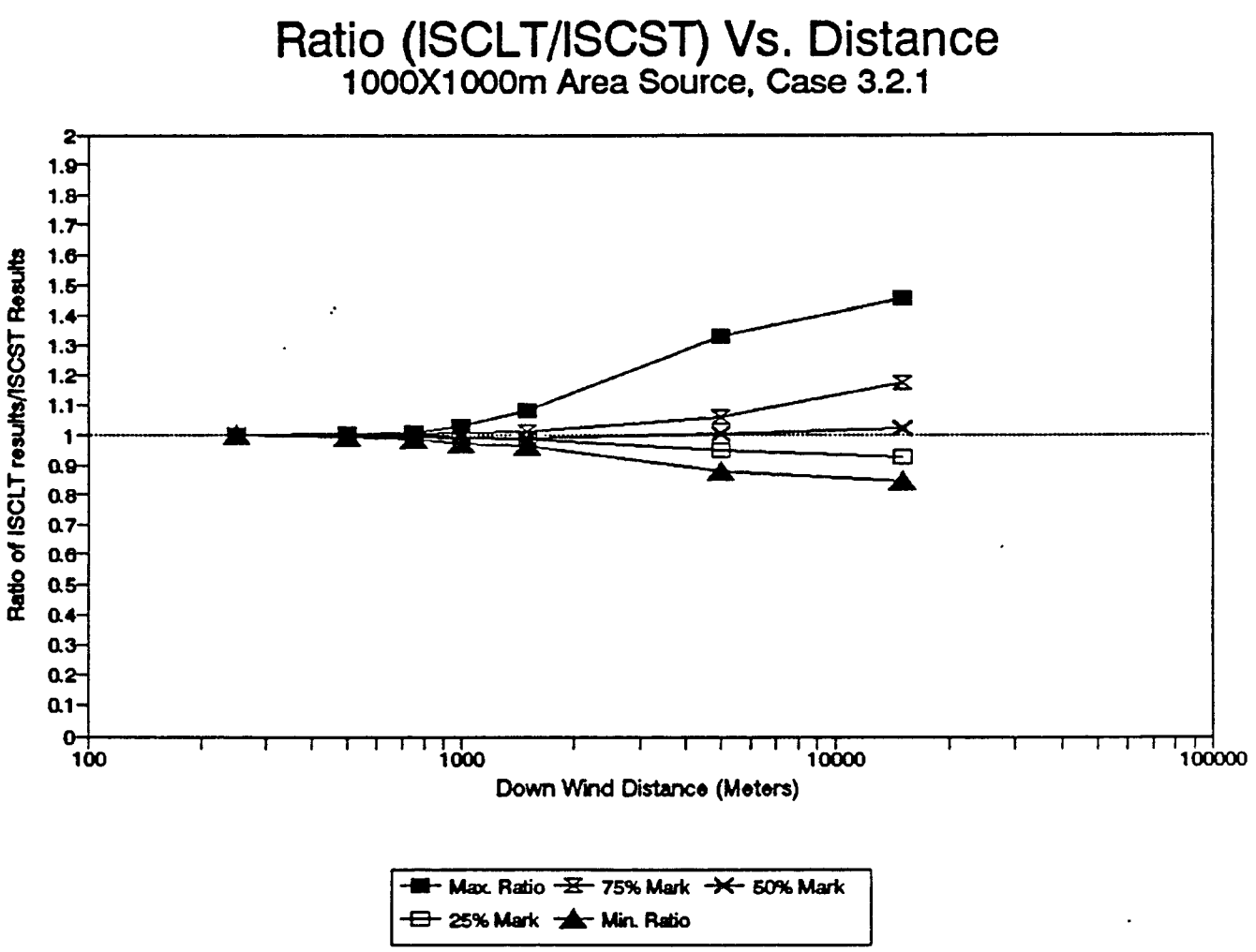

Figure 3.7c. Quartile Plot of Ratios (ISCLT/ISCST) by Downwind Distance For An 1000x1000m Area Source With RDU 1987 Random Hourly Meteorological Data Set For ISCST Simulation, and the RDU 1987 STAR Data Set For ISCLT Simulation. No Limit On Convergence Levels.

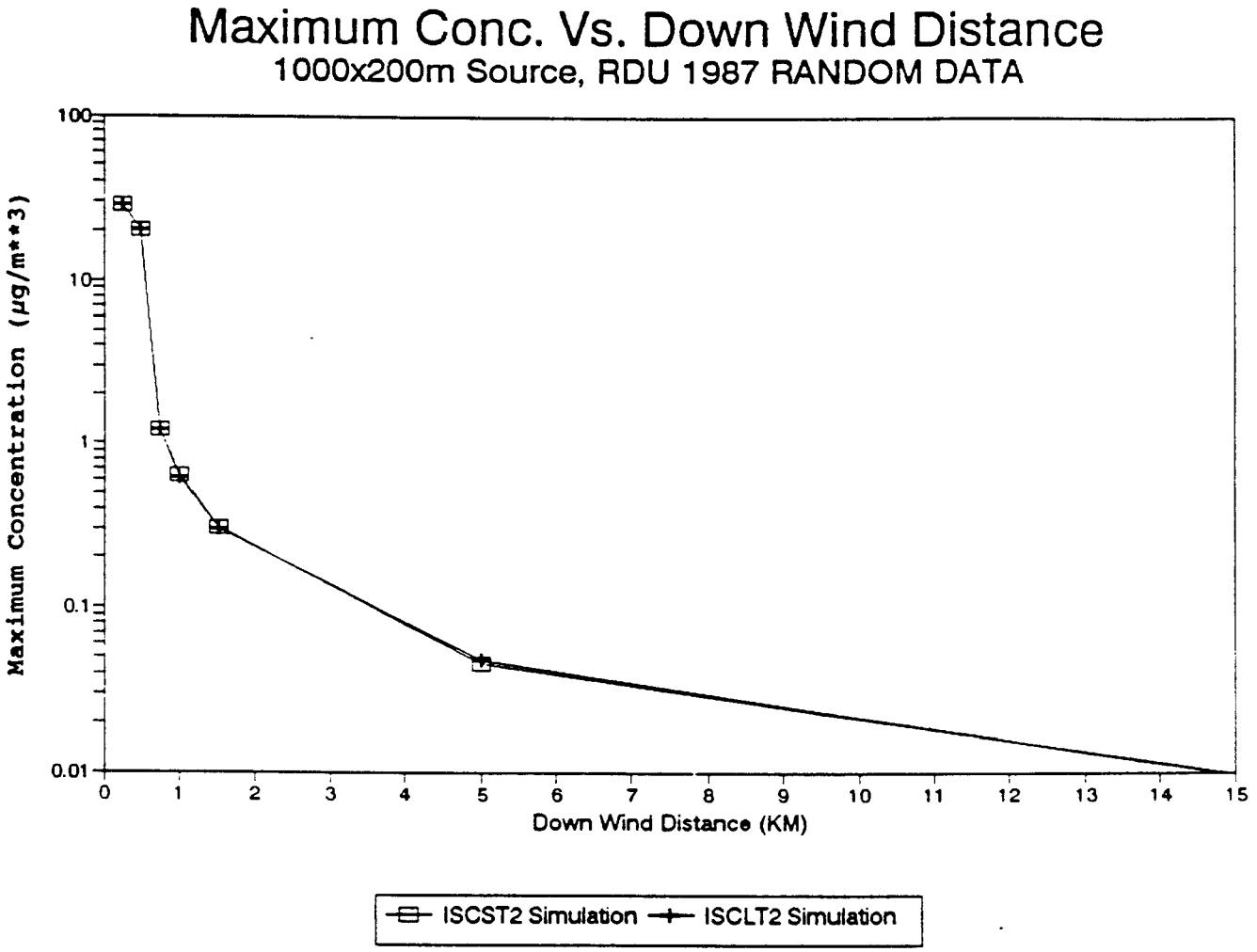

Figure 3.8a. Maximum Concentration Of ISCST Simulation And ISCLT Simulation Plotted With Downwind Distance. 1000x200m Area Source, RDU 1987 Random Hourly And STAR Data

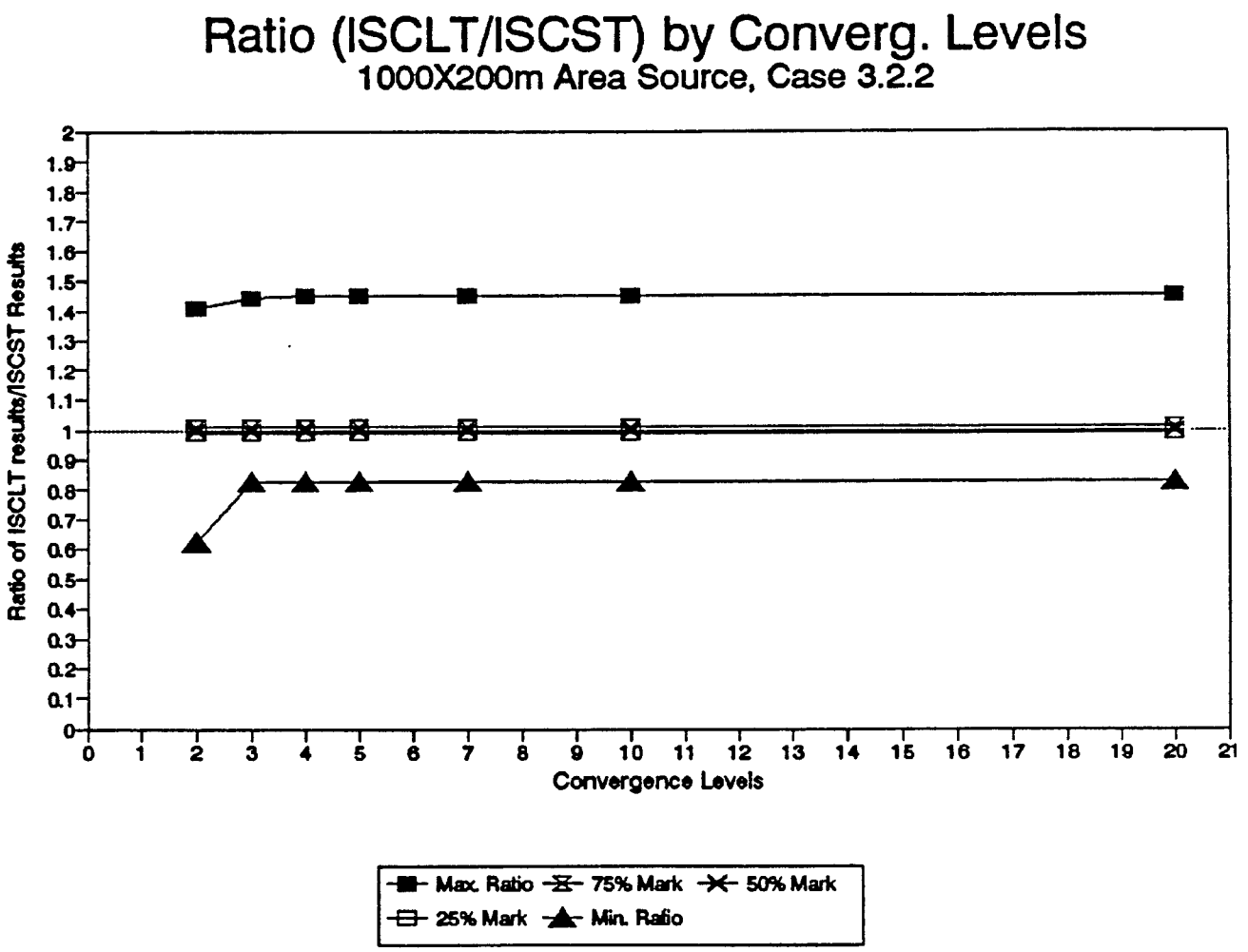

Figure 3.8b. Quartile Plot of Ratios (ISCLT/ISCST) by Convergence Levels For An 1000x200m Area Source With RDU 1987 Random Hourly Meteorological Data Set For ISCST Simulation, and the RDU 1987 STAR Data Set For ISCLT Simulation.

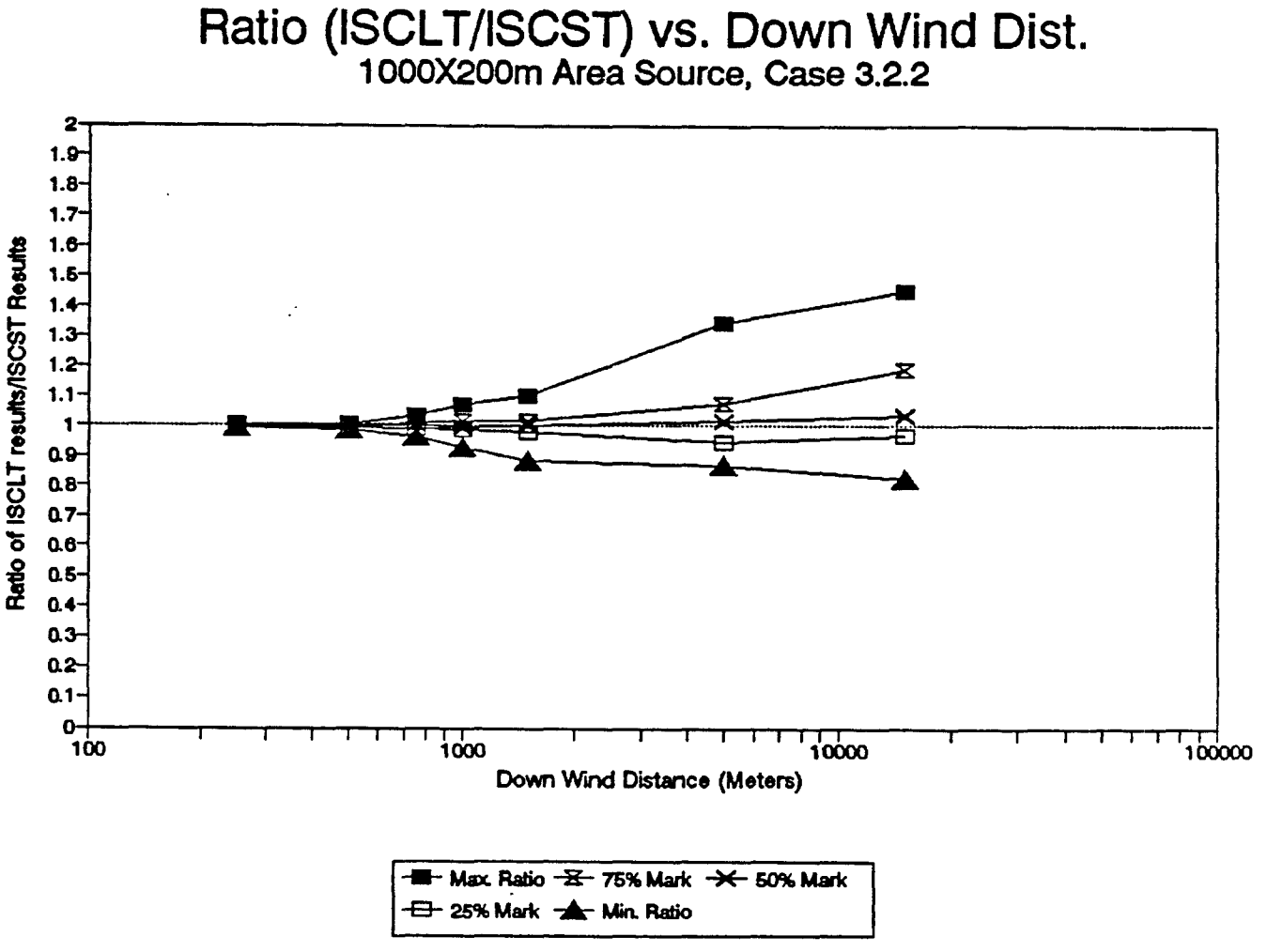

Figure 3.8c. Quartile Plot of Ratios (ISCLT/ISCST) by Downwind Distance For An 1000x200m Area Source With RDU 1987 Random Hour Meteorological Data Set For ISCST Simulation, and the RDU 1987 STAR Data Set For ISCLT Simulation. No Limit On Convergence Levels.

3.2.3. Examining The Source Geometry And Rotation Effects

In the first part of the this study, a 100x100m area source and a 400x100m area source are examined using idealized STAR meteorological data. The purpose of this test is to verify the accuracy and reasonableness of the algorithm for simple variations of source-receptor geometry. A polar network of receptors is used. The origin of this polar network is located at the center of the area source. This polar network uses distance rings of 5, 10, 25, 50, 70, 150, 300, and 500 meters, with 32 receptors in each ring, these receptors are 11.25 degrees apart from each other.

Two separate STAR meteorological data files are used in these exercises. In the first file, all of the winds are assumed to occur within the 22.5 degree sector centered on 0 degree. In the second file, winds are assumed to occur only in the 22.5 degree sector centered on 45 degree.

In the second part of the this study, the same receptor network and meteorological data files are used. The only difference is that the 100x100m area source is divided into four 50x50m area sources, and the 400x100m area source is divided into four 100x100m area sources. The results of these runs are compared with the single source results. The purpose of this experiment is to assure that the algorithm handles source geometry correctly.

Because the algorithm is also designed to handle rectangular sources oriented other than north-south (i.e. rotated), several tests have been performed to examine this capability. The source defined above is rotated for 45.0 degrees clockwise. The wind directions in the STAR data set are changed accordingly to show the effects of the rotation.

The various combinations used to test the source geometry and rotation effects are summarized in Table 3.1.

Table 3.1. The Tests For Source Geometry And Rotation Effects

Case No.	Area Source	Source Rotated From North	Wind Speed Category	Stability Category	Wind Direction
3.3.1.1	100x100m	0	2	A	0 N
3.3.1.2	100x100m	0	2	A	45 NE
3.3.1.3	100x100m	45	2	A	45 NE
3.3.2.1	400x100m	0	2	A	0 N
3.3.2.2	400x100m	0	2	A	45 NE
3.3.2.3	400x100m	45	2	A	45 NE

Figures 3.9 - 3.11 depict contour diagrams for the concentration values for each case with the 100x100m square shaped area source. The first feature is that the results for north wind are symmetric across the centerline. The second feature is that the results for the algorithm appear very reasonable for cases involving rotation of the source and/or wind direction. Figures 3.12 - 3.14 depict contour diagrams for the concentration values for each case with the 400x100m rectangular shaped area source. The results for this source also appear to be reasonable.

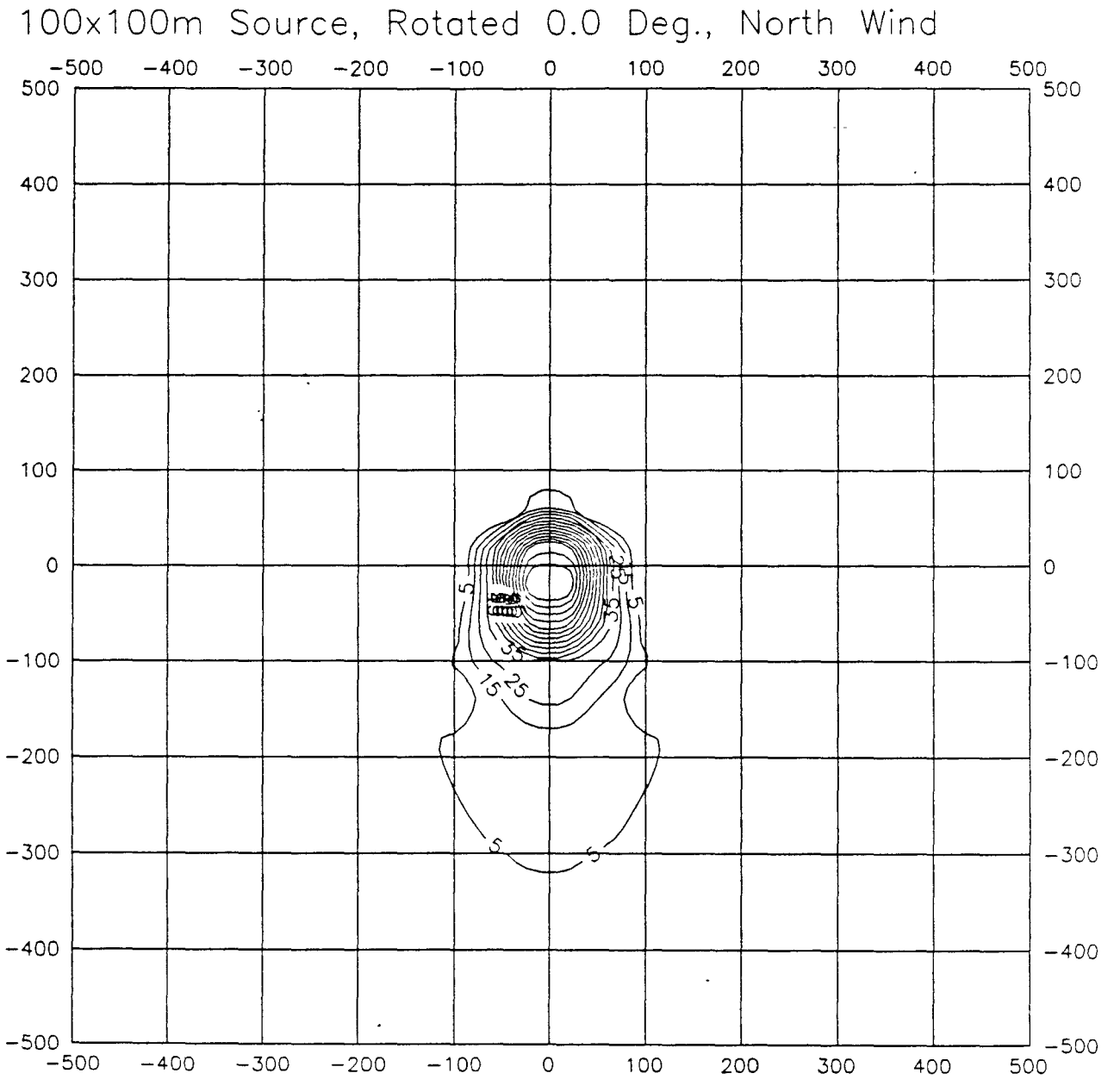

Figure 3.9. Contour Diagram of Annual Average Rural Concentration ($\mu g/m^3$) for An 100x100m Area Source With Winds Come Only From 0 Degree North.

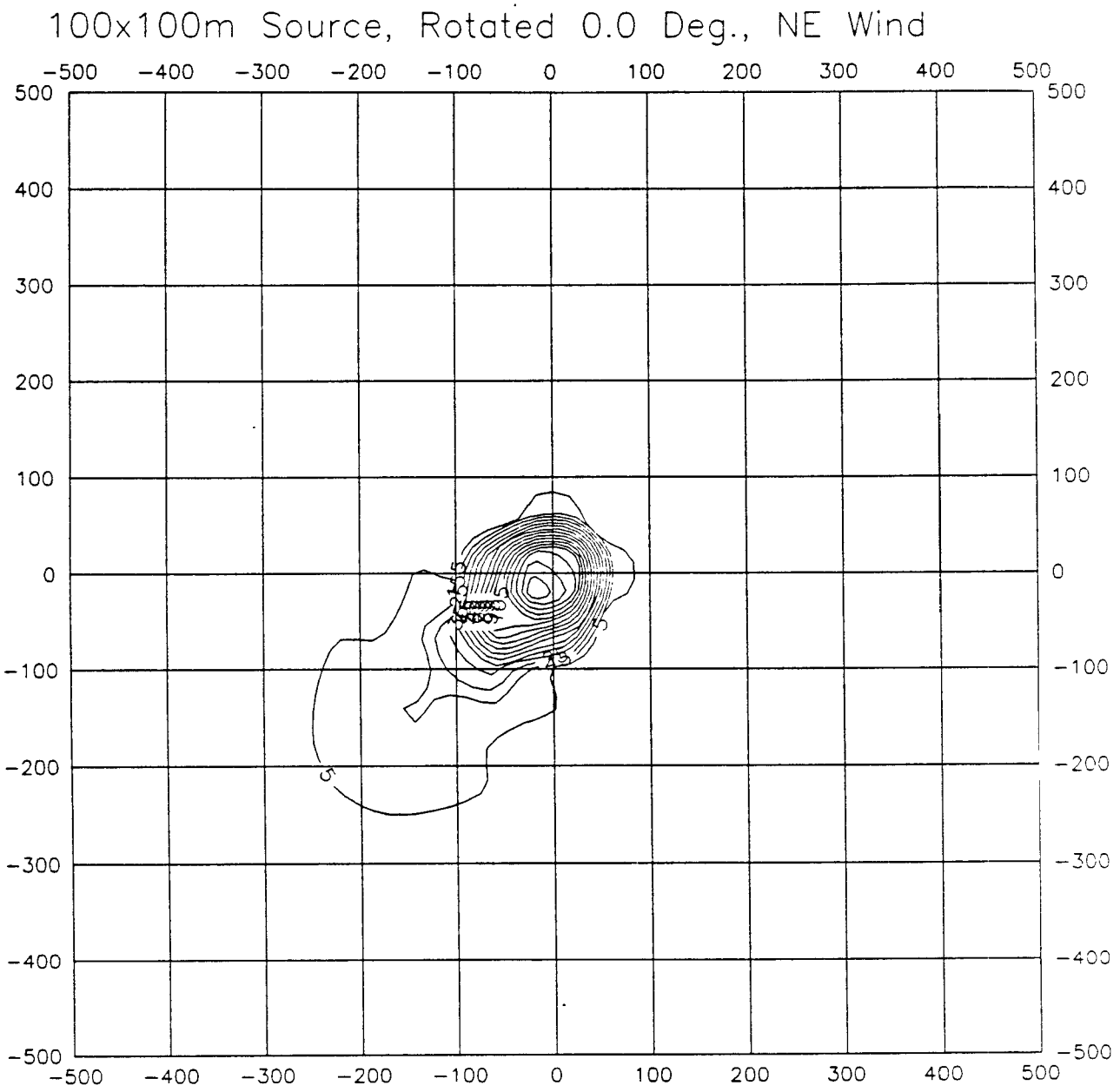

Figure 3.10. Contour Diagram of Annual Average Rural Concentration ($\mu g/m^3$) for An 100x100m Area Source With Winds Come Only From 45.0 Degree Northeast.

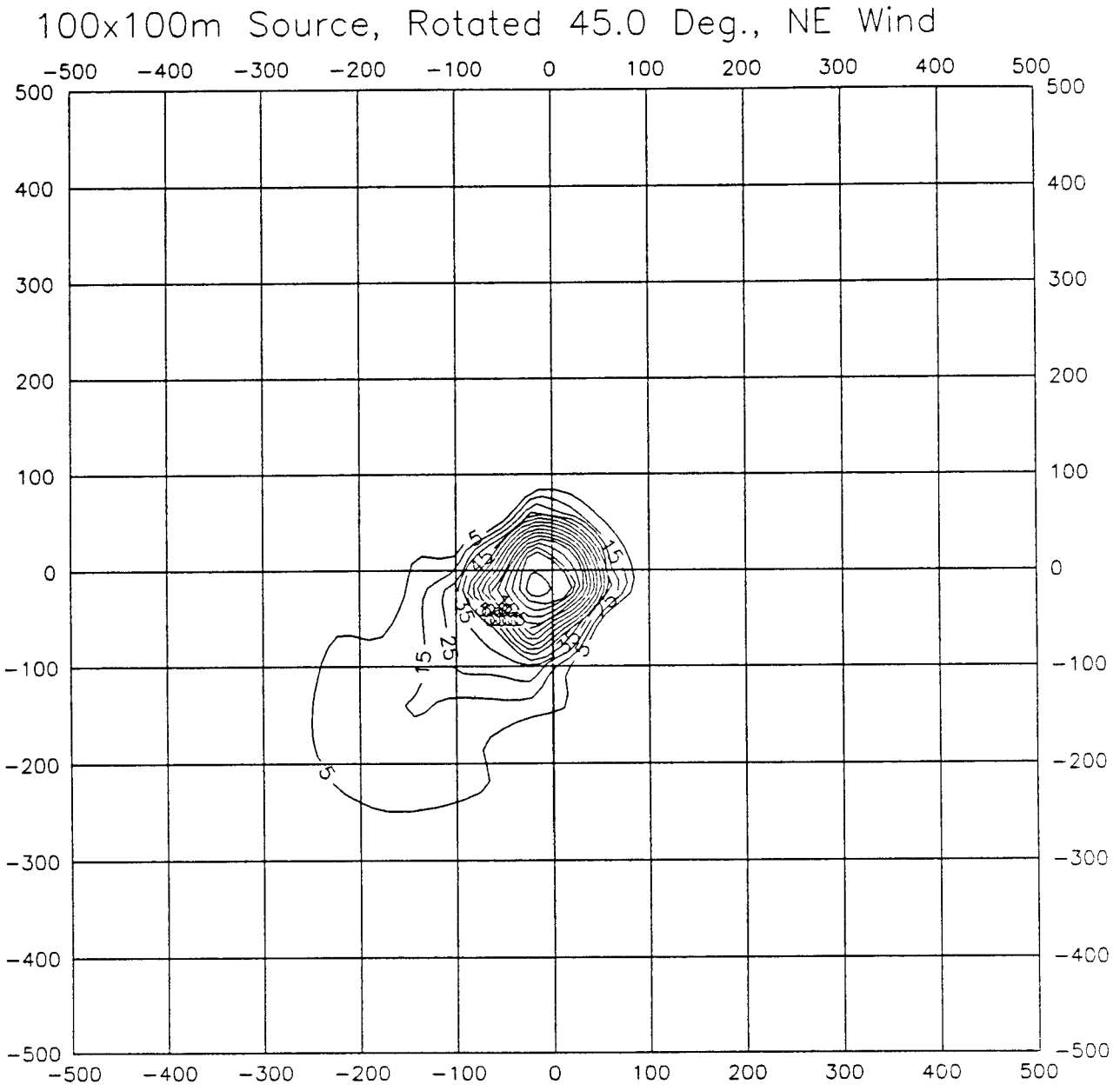

Figure 3.11. Contour Diagram of Annual Average Rural Concentration ($\mu g/m^3$) for An 100x100m Area Source With 45.0 Degree Rotation and Winds Come Only From 45.0 Degree Northeast.

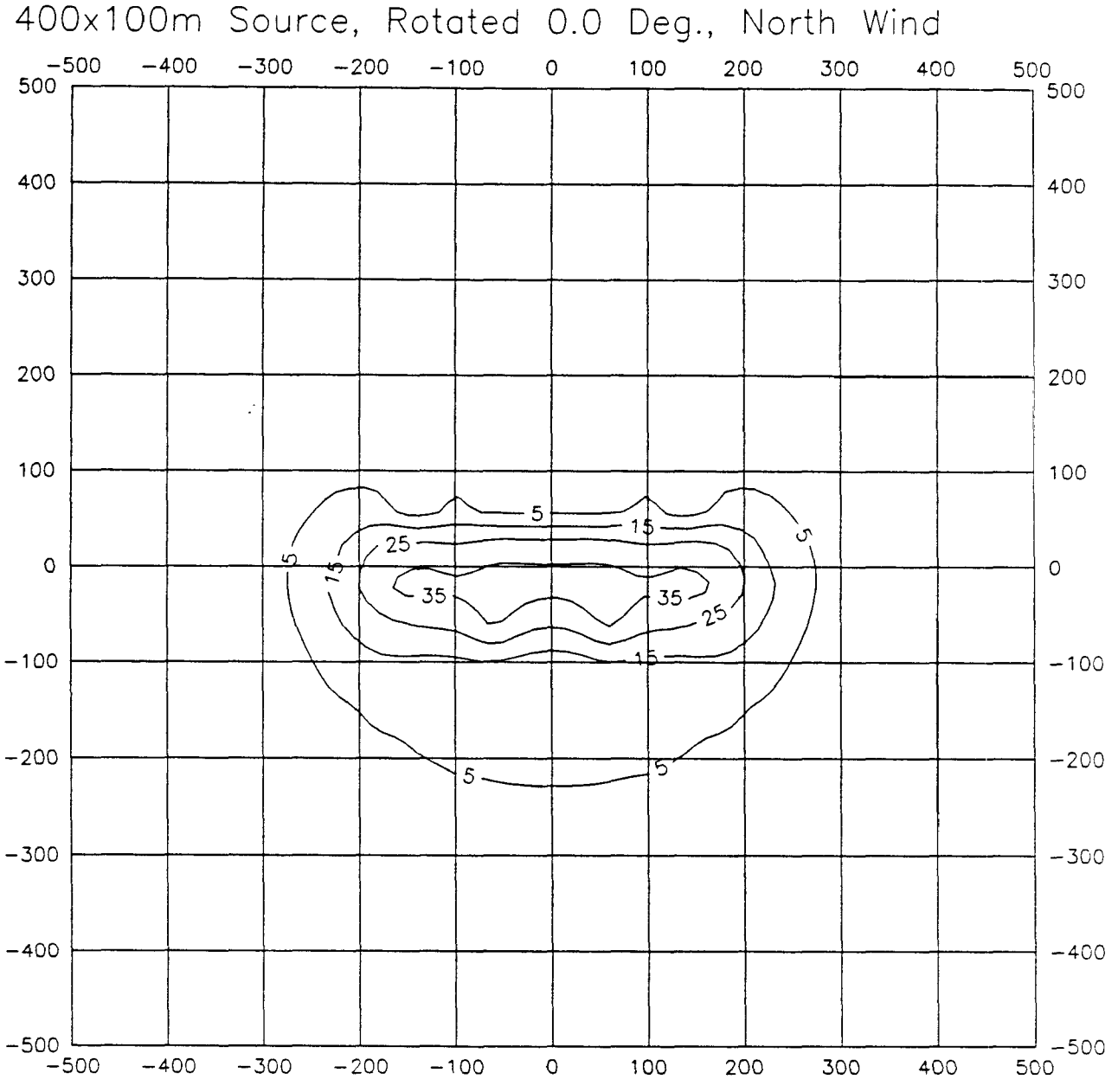

Figure 3.12. Contour Diagram of Annual Average Rural Concentration ($\mu g/m^3$) for An 400x100m Area Source With Winds Come Only From 0 Degree North.

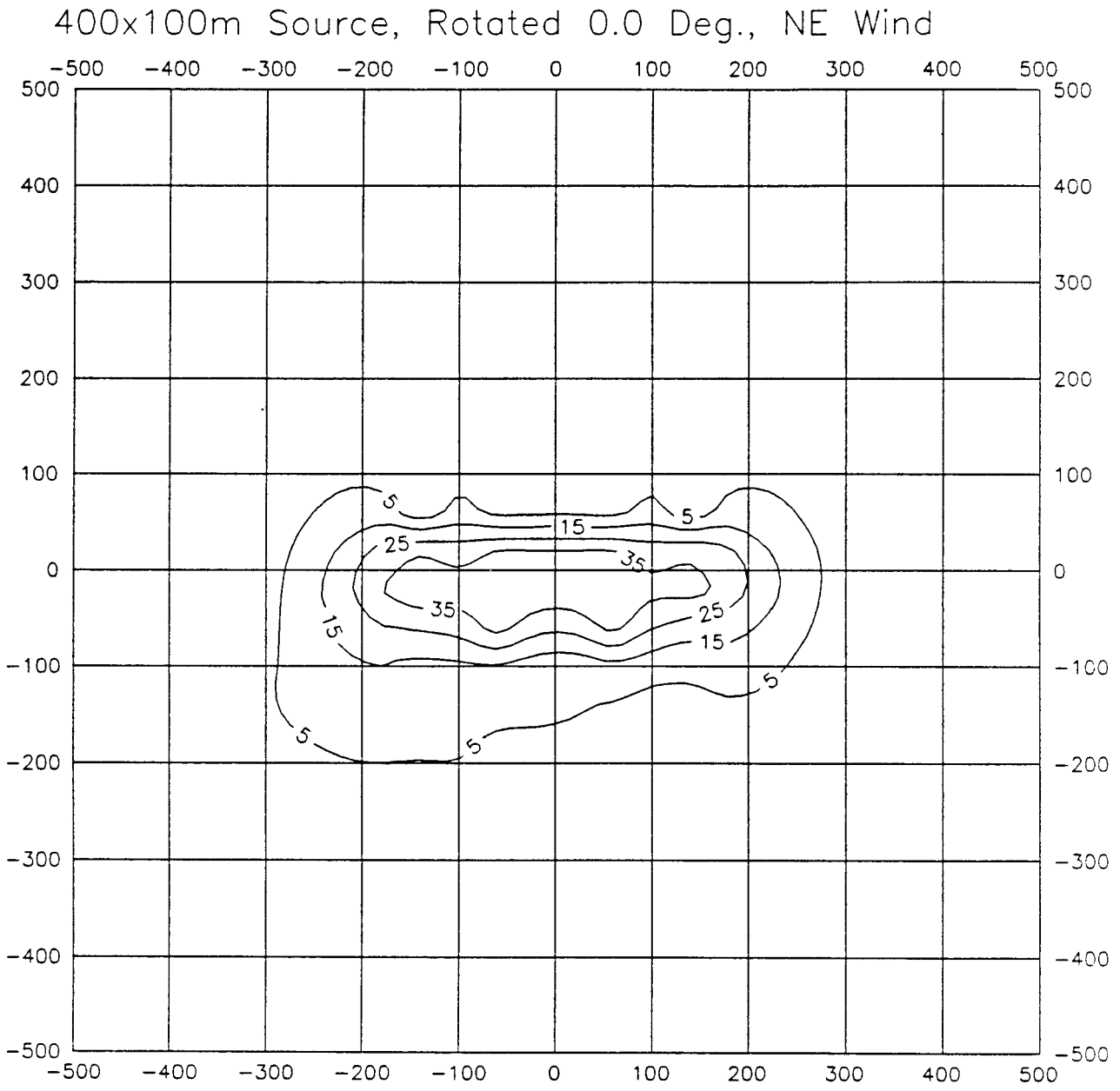

Figure 3.13. Contour Diagram of Annual Average Rural Concentration ($\mu g/m^3$) for An 400x100m Area Source With Winds Come Only From 45.0 Degree Northeast.

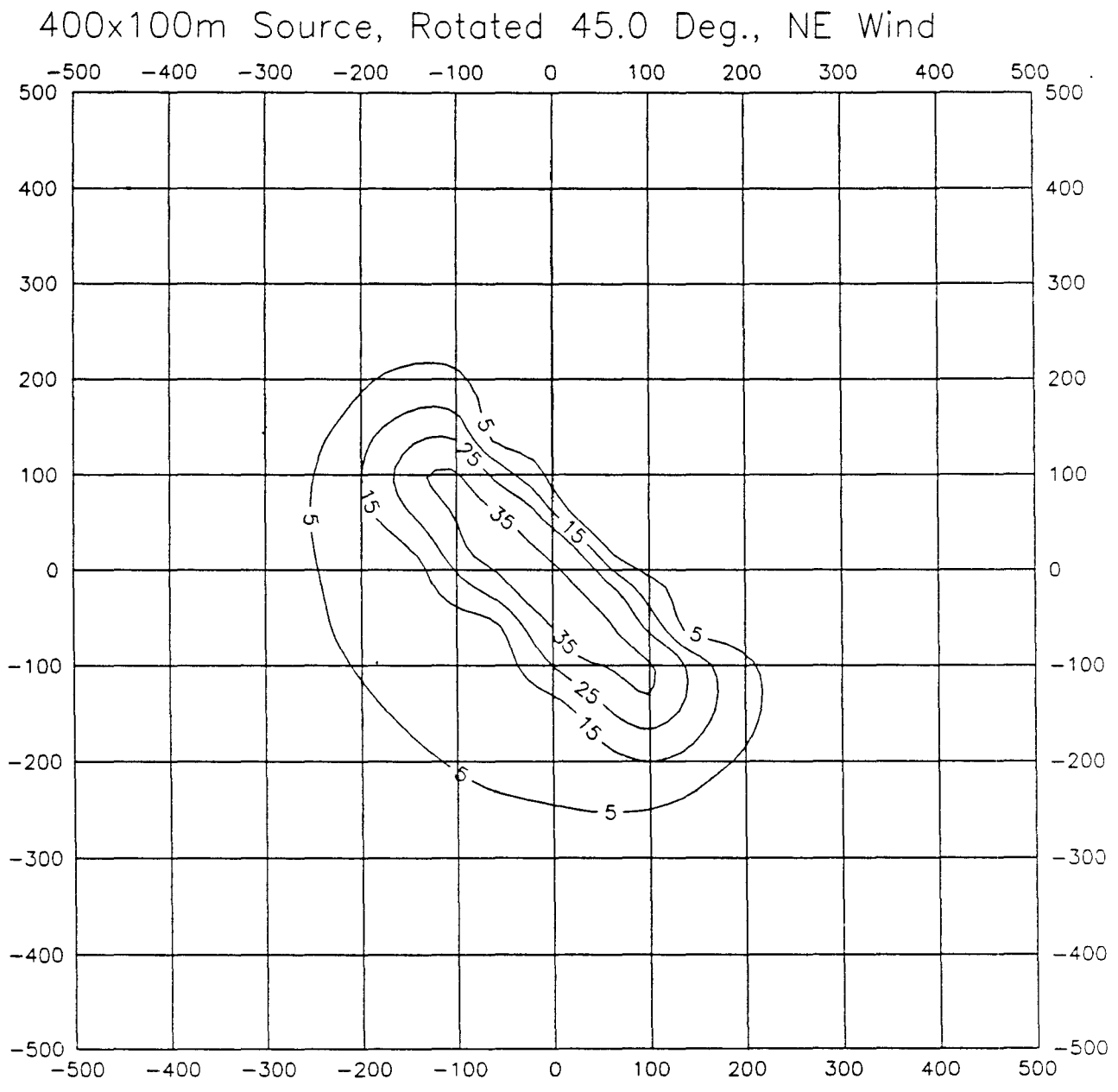

Figure 3.14. Contour Diagram of Annual Average Rural Concentration ($\mu g/m^3$) for An 400x100m Area Source With 45.0 Degree Rotation and Winds Come Only From 45.0 Degree Northeast.

The results for the 10 maximum concentration values of a 100x100m square shaped area source are listed in Table 3.2(a) -(c). Part A of the table lists the results for winds coming from North for the whole year. Part B of the table lists the results for winds coming from 45.0 degree Northeast. Part C of the table lists the results for the area source rotated clockwise for 45 degrees and the winds coming from 45.0 degree Northeast. The left hand columns of each table contain the results generated by a 100x100m single source setup, while the right hand columns of these tables list results from four 50x50m sources subdivided from the 100x100m area source.

The results for the 10 maximum concentration values of a 400x100m square shaped area source are listed in Table 3.3(a) -(c). Part A of the table lists the results for winds coming from North for the whole year. Part B of the table lists the results for winds coming from 45.0 degree Northeast. Part C of the table lists the results for the area source rotated clockwise for 45 degrees and the winds coming from 45.0 degree Northeast. The left hand columns of each table contain the results generated by a 400x100m single source setup, while the right hand columns of these tables list results from four 100x100m sources subdivided from the 400x100m area source.

The differences between the single source simulation and the simulation involving subdividing the source are very small, normally less than 0.1 percent. For instance, Table 3.2a shows highest concentrations of 173.9104 versus 173.9131, or a difference of about 0.002 percent. These minor differences probably result from truncation errors within the single precision calculation in the numerical integration.

Table 3.2a. 10 Maximum Annual Averages For Case 3.3.1.1

Rank	Results Of One 100x100 Area Source	Results Of Four 50x50 Area Sources
1	173.910400 (.00, -50.00)	173.913100 (.00, -50.00)
2	172.949300 (-9.75, -49.04)	172.938900 (-9.75, -49.04)
3	172.851200 (9.75, -49.04)	172.708100 (9.75, -49.04)
4	170.573000 (19.13, -46.19)	170.506600 (19.13, -46.19)
5	170.508100 (-19.13, -46.19)	170.492100 (-19.13, -46.19)
6	166.425400 (27.78, -41.57)	166.376100 (-27.78, -41.57)
7	166.407500 (-27.78, -41.57)	166.294900 (27.78, -41.57)
8	162.357200 (.00, -25.00)	162.002600 (.00, -25.00)
9	162.019400 (4.88, -24.52)	161.688800 (-4.88, -24.52)
10	161.908300 (-4.88, -24.52)	161.591700 (4.88, -24.52)

Table 3.2b. 10 Maximum Annual Averages For Case 3.3.1.2

Rank	Results Of One 100x100 Area Source	Results Of Four 50x50 Area Sources
1	179.183000 (-50.00, -50.00)	179.172000 (-50.00, -50.00)
2	173.940900 (-35.36, -35.36)	173.849100 (-35.36, -35.36)
3	173.082100 (-27.78, -41.57)	173.137500 (-41.57, -27.78)
4	173.013100 (-41.57, -27.78)	173.011700 (-27.78, -41.57)
5	170.628900 (-46.19, -19.13)	170.366600 (-19.13, -46.19)
6	170.439900 (-19.13, -46.19)	170.257700 (-46.19, -19.13)
7	165.939900 (-49.04, -9.75)	165.835600 (-9.75, -49.04)
8	165.885700 (-9.75, -49.04)	165.664000 (-49.04, -9.75)
9	164.349500 (-17.68, -17.68)	163.815600 (-17.68, -17.68)
10	163.958400 (-13.89, -20.79)	163.423600 (-13.89, -20.79)

Table 3.2c. 10 Maximum Annual Averages For Case 3.3.1.3

Rank	Results Of One 100x100 Area Source	Results Of Four 50x50 Area Sources
1	173.910100 (-35.36, -35.36)	173.912700 (-35.36, -35.36)
2	172.949200 (-41.57, -27.78)	172.938800 (-41.57, -27.78)
3	172.851000 (-27.78, -41.57)	172.708000 (-27.78, -41.57)
4	170.572900 (-19.13, -46.19)	170.506500 (-19.13, -46.19)
5	170.508000 (-46.19, -19.13)	170.492000 (-46.19, -19.13)
6	166.425300 (-9.75, -49.04)	166.376000 (-49.04, -9.75)
7	166.407400 (-49.04, -9.75)	166.294800 (-9.75, -49.04)
8	162.357100 (-17.68, -17.68)	162.002500 (-17.68, -17.68)
9	162.019300 (-13.89, -20.79)	161.688700 (-20.79, -13.89)
10	161.908200 (-20.79, -13.89)	161.591600 (-13.89, -20.79)

Table 3.3a. 10 Maximum Annual Averages For Case 3.3.2.1

Rank	Results Of One 400x100 Area Source	Results Of Four 100x100 Area Sources
1	43.721260 (50.00, -50.00)	43.733450 (.00, -50.00)
2	43.721240 (.00, -50.00)	43.703520 (50.00, -50.00)
3	43.720490 (-50.00, -50.00)	43.703520 (-50.00, -50.00)
4	43.614000 (-9.75, -49.04)	43.634800 (-9.75, -49.04)
5	43.613990 (9.75, -49.04)	43.510310 (9.75, -49.04)
6	43.290850 (19.13, -46.19)	43.255700 (-19.13, -46.19)
7	43.290830 (-19.13, -46.19)	43.210060 (19.13, -46.19)
8	42.799210 (27.78, -41.57)	42.696900 (-27.78, -41.57)
9	42.799150 (-27.78, -41.57)	42.687830 (27.78, -41.57)
10	42.517910 (58.79, -39.28)	42.447700 (58.79, -39.28)

Table 3.3b. 10 Maximum Annual Averages For Case 3.3.2.2

Rank	Results Of One 400x100 Area Source	Results Of Four 100x100 Area Sources
1	47.265880 (-50.00, -50.00)	47.312110 (-9.75, -49.04)
2	47.210750 (-9.75, -49.04)	47.264860 (-50.00, -50.00)
3	47.099850 (9.75, -49.04)	47.101670 (9.75, -49.04)
4	47.077460 (.00, -50.00)	47.060090 (.00, -50.00)
5	46.998490 (-19.13, -46.19)	47.007680 (-19.13, -46.19)
6	46.793360 (19.13, -46.19)	46.802980 (19.13, -46.19)
7	46.571220 (50.00, -50.00)	46.573250 (50.00, -50.00)
8	46.541280 (-27.78, -41.57)	46.542540 (-27.78, -41.57)
9	46.348590 (-58.79, -39.28)	46.344420 (-58.79, -39.28)
10	46.272030 (27.78, -41.57)	46.271140 (27.78, -41.57)

Table 3.3c. 10 Maximum Annual Averages For Case 3.3.2.3

Rank	Results Of One 400x100 Area Source	Results Of Four 100x100 Area Sources
1	43.721220 (.00, -70.71)	43.733390 (-35.36, -35.36)
2	43.721210 (-35.36, -35.36)	43.703460 (.00, -70.71)
3	43.720460 (-70.71, .00)	43.703460 (-70.71, .00)
4	43.613970 (-41.57, -27.78)	43.634770 (-41.57, -27.78)
5	43.613960 (-27.78, -41.57)	43.510270 (-27.78, -41.57)
6	43.290820 (-19.13, -46.19)	43.255680 (-46.19, -19.13)
7	43.290800 (-46.19, -19.13)	43.210020 (-19.13, -46.19)
8	42.799180 (-9.75, -49.04)	42.696870 (-49.04, -9.75)
9	42.799130 (-49.04, -9.75)	42.687810 (-9.75, -49.04)
10	42.517880 (13.79, -69.35)	42.447680 (13.79, -69.35)

3.2.4. Large Area Source With Actual Meteorological Conditions

Previous tests using idealized meteorological data have verified that the numerical integration has been correctly implemented within the ISCLT2 model, and results from the algorithm for various source-receptor geometries appear reasonable. This section presents results for tests of the algorithm using actual meteorological conditions. The first tests show comparisons between the ISCLT2 model and the ISCST2 model, both using the numerical integration algorithm and appropriate meteorological data. The ISCLT2 results are based on the RDU 1987 STAR meteorological data and the ISCST2 results are based on the hourly meteorological data generated by the RAMMET meteorological preprocessor for the same RDU 1987 data. Both models were used to calculate annual average concentrations. Figure 3.15 shows the results of the ISCLT2/ISCST2 comparisons for the 1000x1000m area source. Figure 3.15a shows the maximum concentration values for both models as a function of downwind distance. While the results show reasonable close agreement, there is a trend for ISCLT2 to have smaller maximum concentration values than ISCST2 as the downwind distance increases. Figure 3.15b shows the quartiles of the ISCLT2/ISCST2 ratios as a function of ISCLT2 convergence level, and Figure 3.15c shows the ratios of ISCLT2/ISCST2 by downwind distance. These plots include ratios for all receptor locations. Figure 3.15b shows that the ratios do not change significantly beyond convergence level 3, indicating that the ISCLT2 model results are converging fairly quickly. Most of the ratios are around 1.1, indicating that the ISCLT2 model predicts concentrations that are about 10 percent higher than the ISCST2 model for this case. Figure 3.15c shows that the ratio of about 1.1 is very consistent for receptors located within and near the area, and that the range of ratios increases with increasing downwind distance. These results using actual meteorological conditions are very encouraging, showing that the ISCLT2 and ISCST2 models produce fairly consistent results using the numerical integration algorithm for the receptors of most concern located within and near the area. Figures 3.16a to 3.16c show similar results for the 1000x200m rectangular area source.

As mentioned previously, the differences between the ISCLT2 and ISCST2 models result from the fact that the two models use different meteorology data sets. The STAR frequency summaries used by the ISCLT2 model lose the detail of specific combinations of wind speed, direction, stability class and mixing height that occur within the hourly meteorological data input to the ISCST2 model, and these specific combinations which may cause high hourly concentrations have a significant impact on the annual averages generated by the ISCST2 model. Comparing these results with those obtained using the idealized meteorology data confirms this hypothesis.

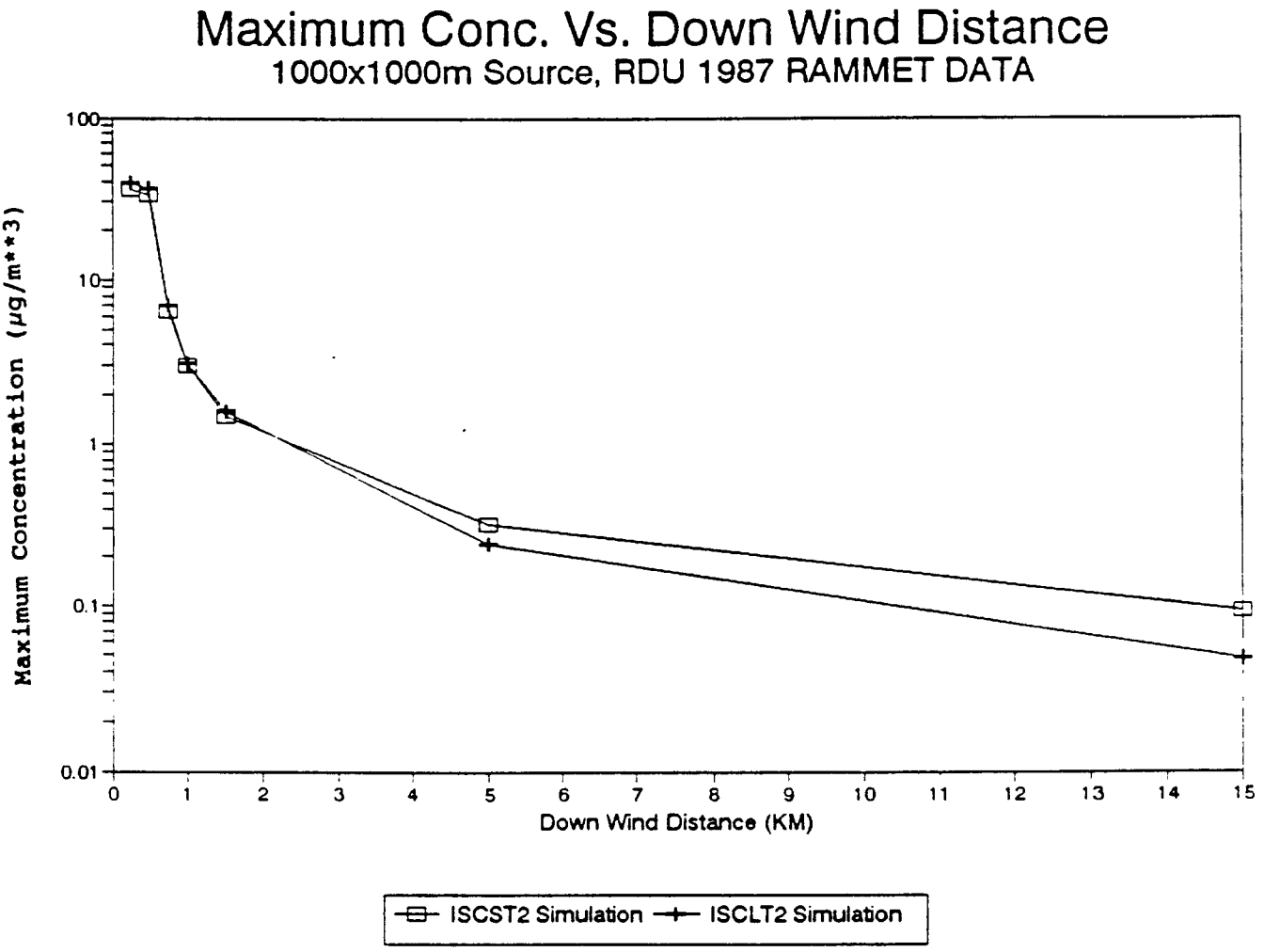

Figure 3.15a. Maximum Concentration Of ISCST Simulation And ISCLT Simulation Plotted With Downwind Distance. 1000x1000m Area Source, RDU 1987 Data.

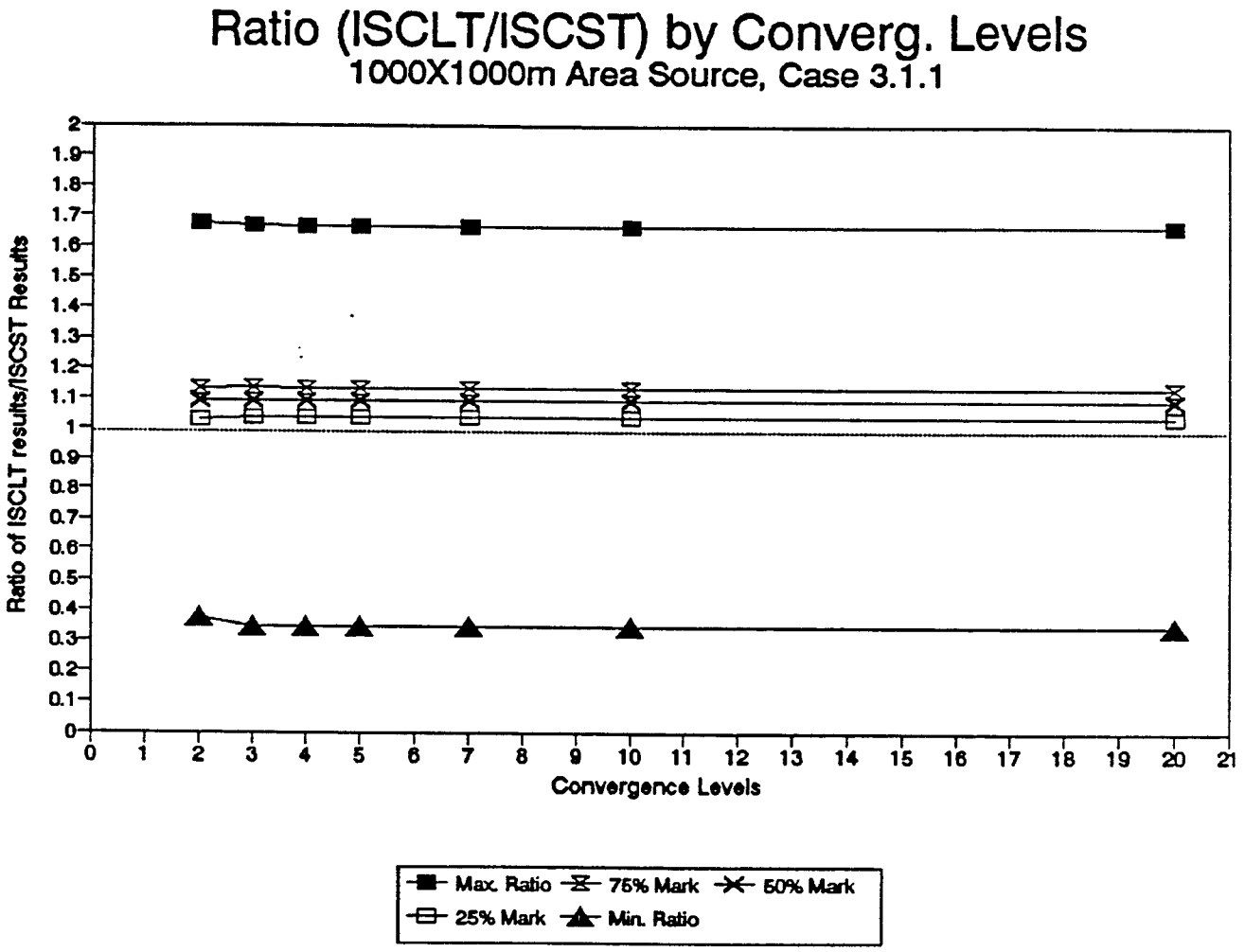

Figure 3.15b. Quartile Plot of Ratios (ISCLT/ISCST) by Convergence Levels For An 1000x1000m Area Source With RDU 1987 RAMMET Hourly Meteorological Data Set For ISCST Simulation, and the RDU 1987 STAR Data Set For ISCLT Simulation.

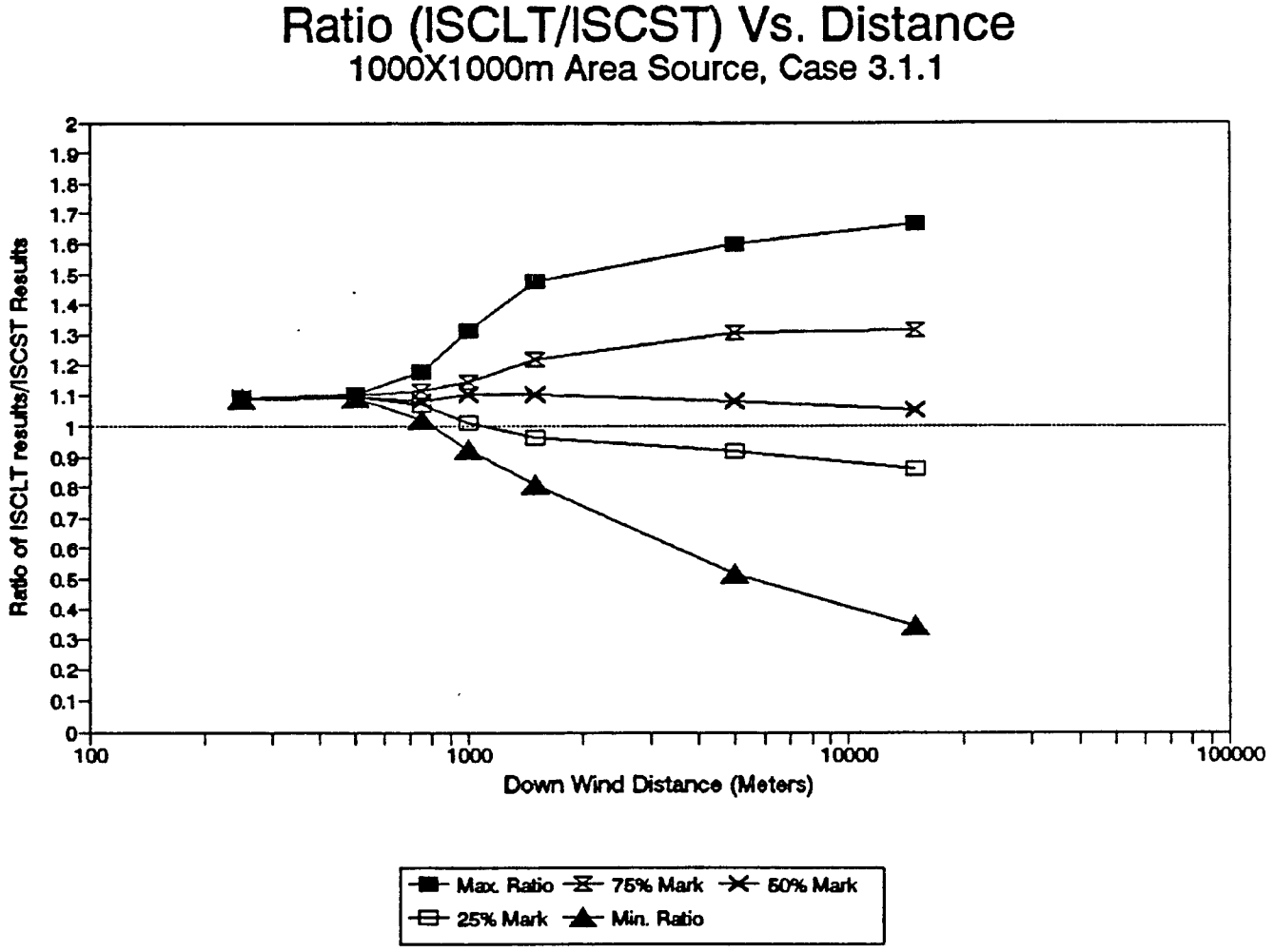

Figure 3.15c. Quartile Plot of Ratios (ISCLT/ISCST) by Downwind Distance For An 1000x1000m Area Source With RDU 1987 RAMMET Hourly Meteorological Data Set For ISCST Simulation, and the RDU 1987 STAR Data Set For ISCLT Simulation. No Limit On Convergence Levels.

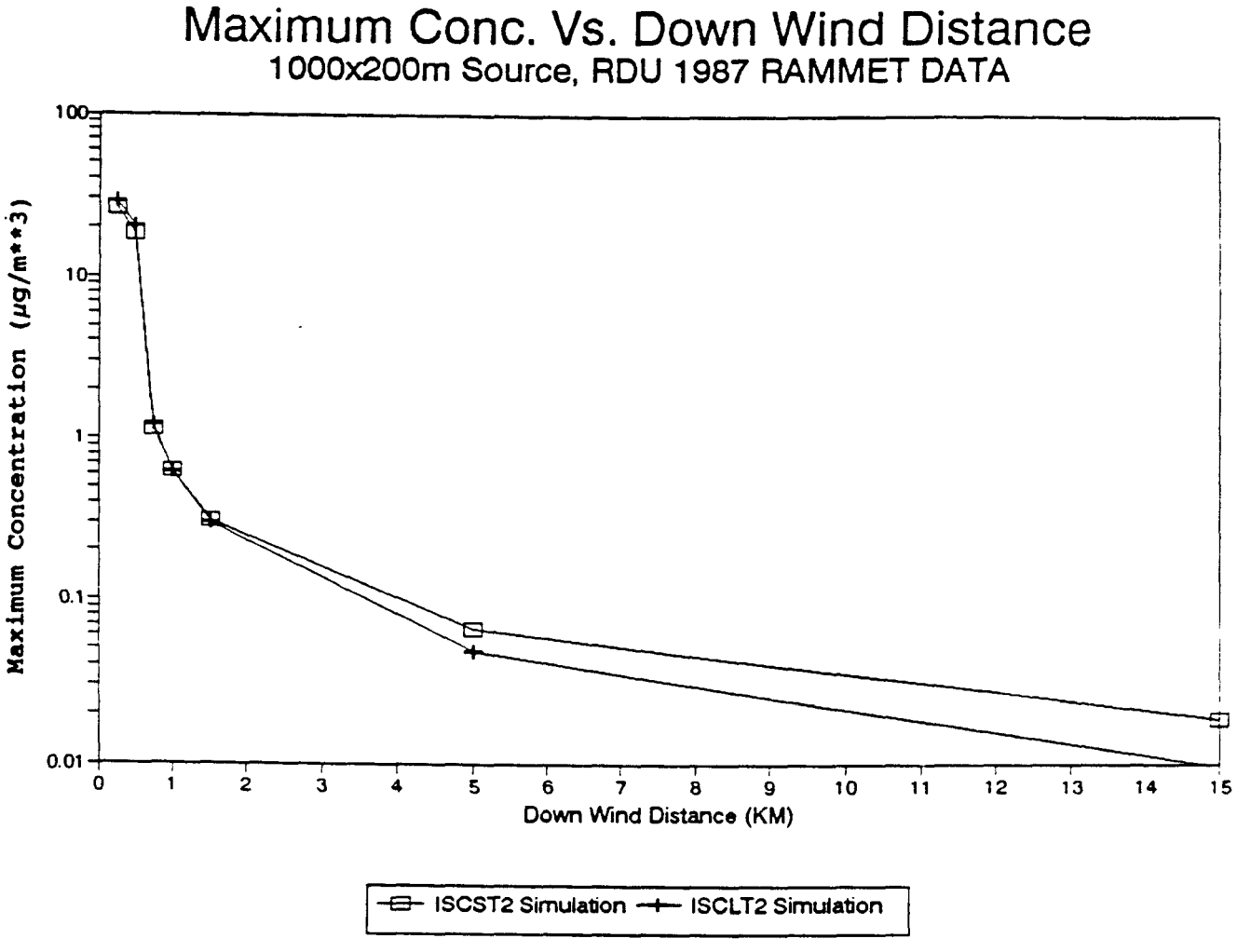

Figure 3.16a. Maximum Concentration Of ISCST Simulation And ISCLT Simulation Plotted With Downwind Distance. 1000x200m Area Source, RDU 1987 Data

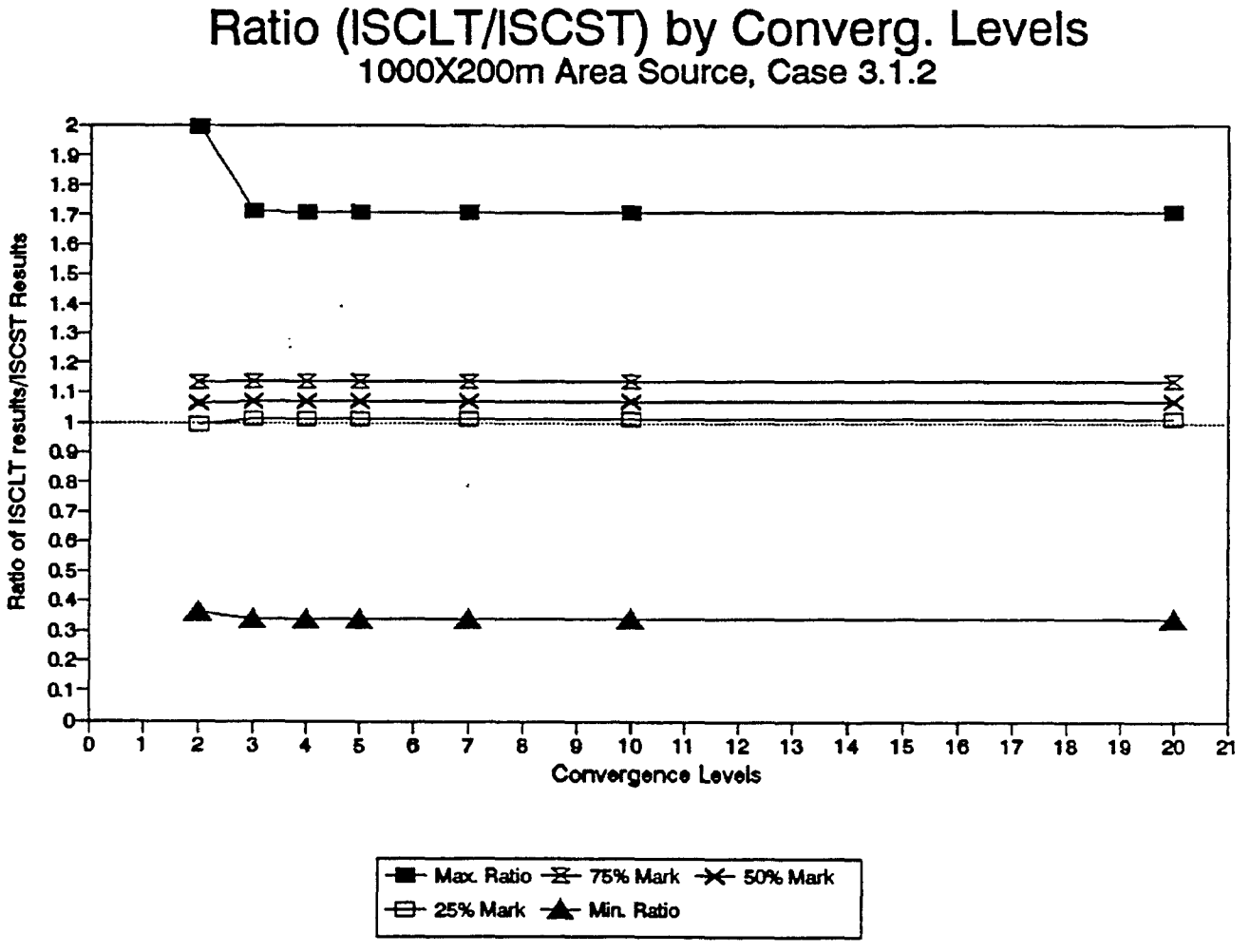

Figure 3.16b. Quartile Plot of Ratios (ISCLT/ISCST) by Convergence Levels For An 1000x200m Area Source With RDU 1987 RAMMET Hourly Meteorological Data Set For ISCST Simulation, and the RDU 1987 STAR Data Set For ISCLT Simulation.

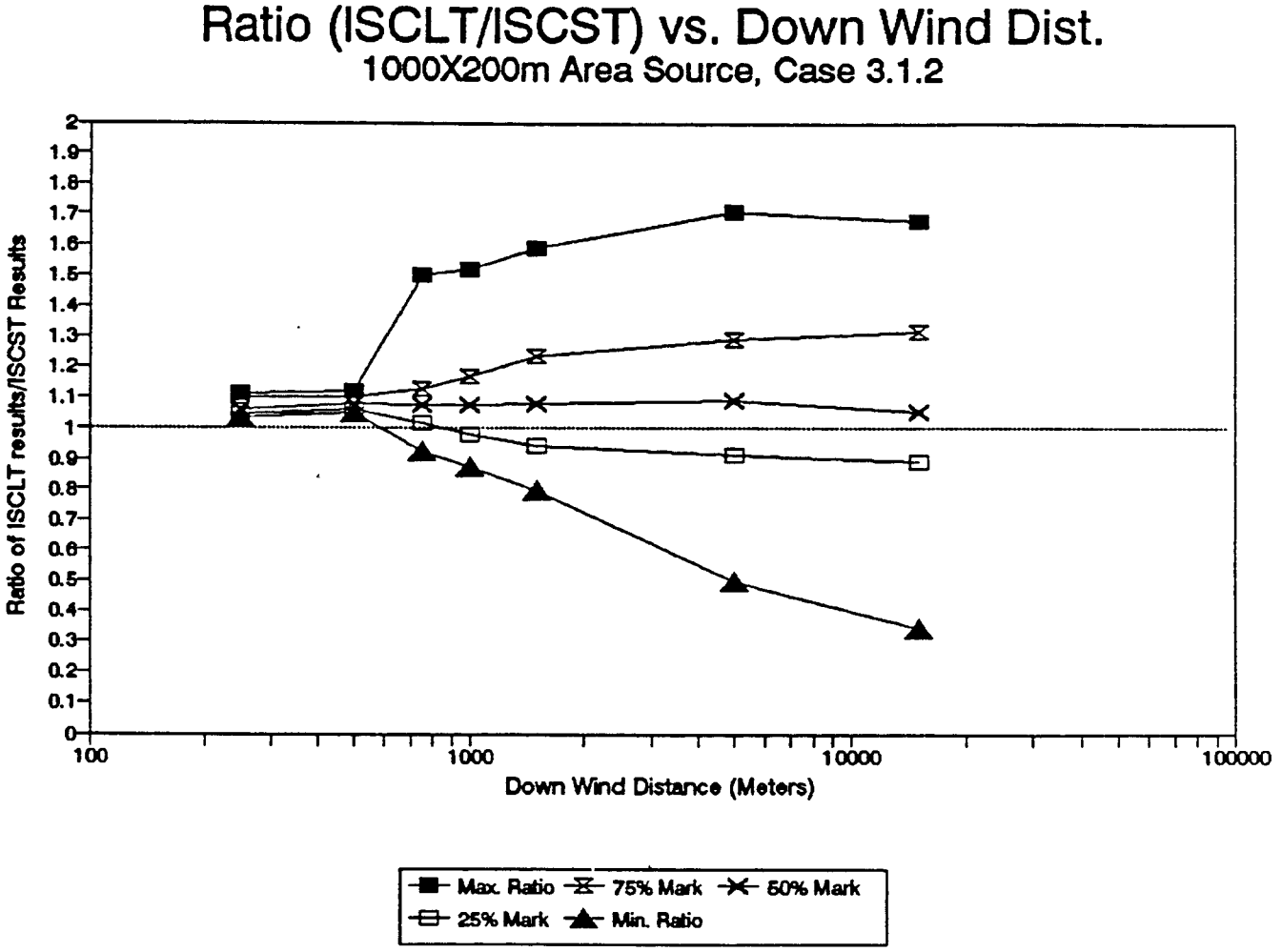

Figure 3.16c. Quartile Plot of Ratios (ISCLT/ISCST) by Downwind Distance For An 1000x200m Area Source With RDU 1987 RAMMET Hour Meteorological Data Set For ISCST Simulation, and the RDU 1987 STAR Data Set For ISCLT Simulation. No Limit On Convergence Levels.

For the large source subdivision study, the 1000x1000m large source has been broken into four 500x500m sources. Also, the 1000x200m source has been broken into five 200x200 sources. The 10 maximum values were examined. Figures 3.17 and 3.18 shows the results of the comparison of the single versus subdivided sources using actual STAR data for RDU 1987. They show the maximum concentration at each of the 7 downwind distances of 250, 500, 750, 1000, 1500, 5000, and 15000 meters. Basically, the maximum concentration values occur inside and nearby the area source. These results show that subdividing the area source does not affect the design value predicted by the model.

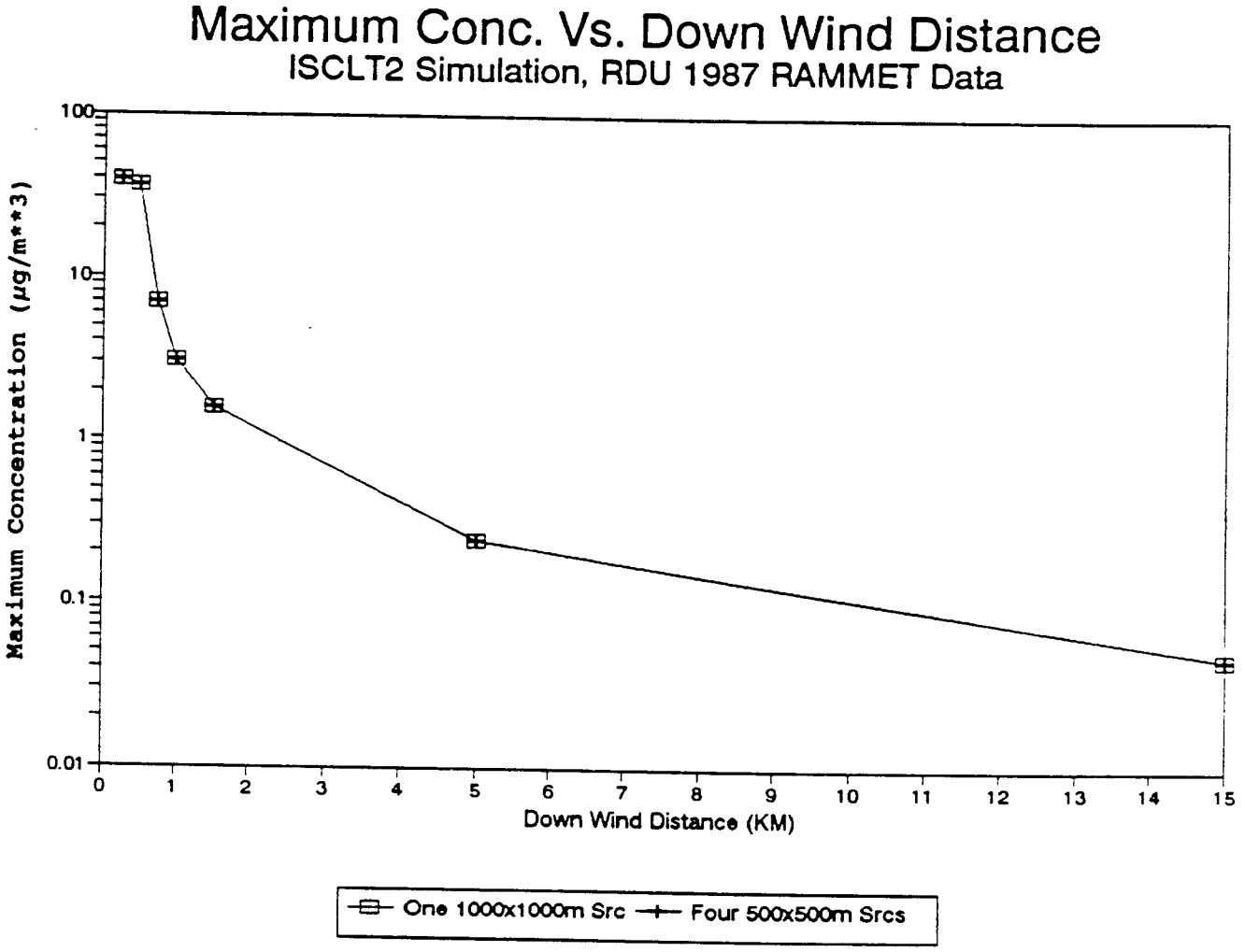

Figure 3.17. Maximum Concentration Of ISCLT Simulation With One 1000x1000m Area Source And ISCLT Simulation With This Source Broken Down Into Four 500x500m Area Sources, RDU 1987 STAR Data

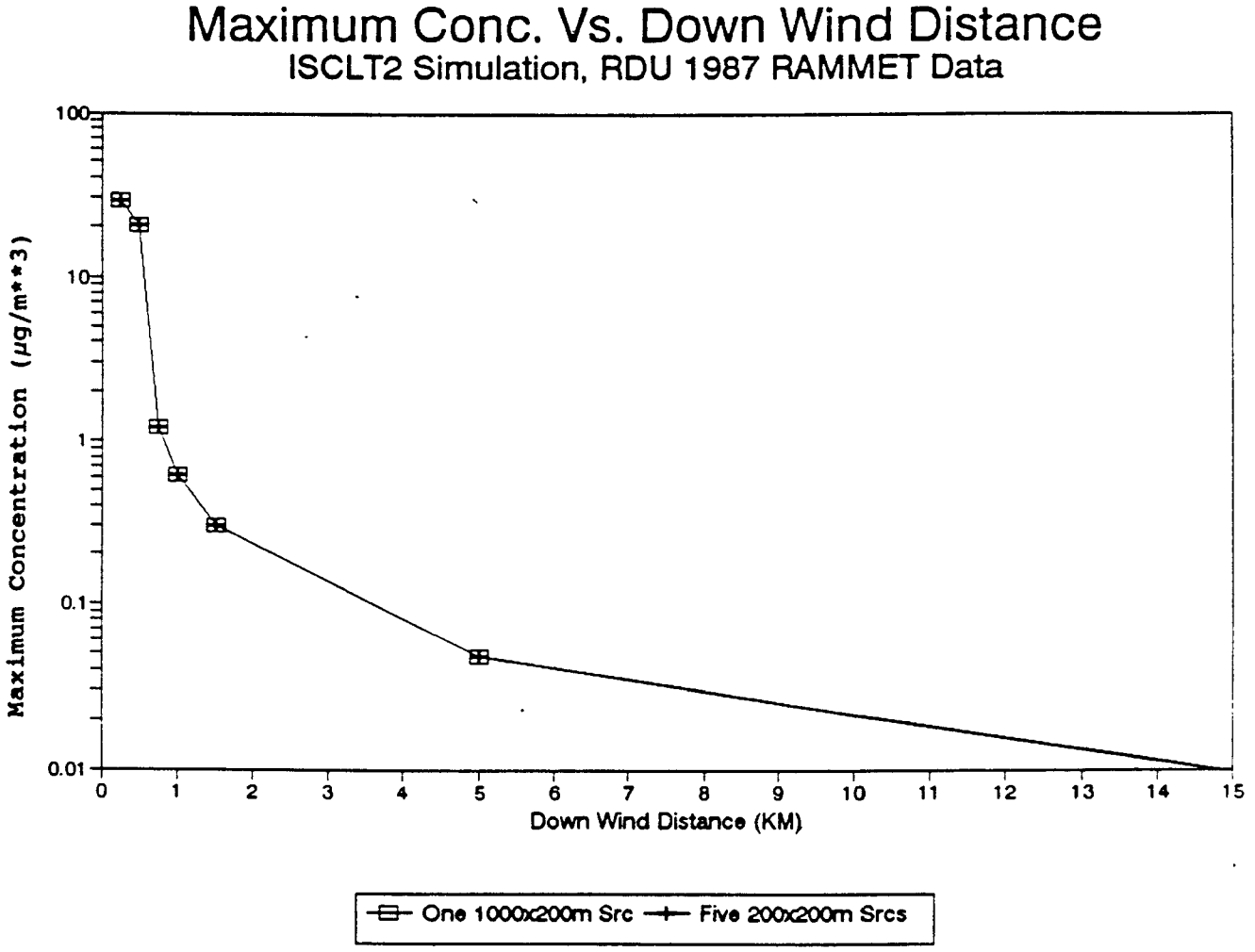

Figure 3.18. Maximum Concentration Of ISCLT Simulation With One 1000x200m Area Source And ISCLT Simulation With This Source Broken Down Into Five 200x200m Area Sources, RDU 1987 STAR Data

3.2.5. Convergence Level Consideration

Figure 3.19 shows the ratio formed by dividing the run time of the ISCLT2 model with the numerical integration algorithm by the run time of the ISCST2 model with the same algorithm. These results were obtained using the actual RDU 1987 meteorological data for both models. The run time increases as the ISCLT2 algorithm convergence level goes up. After level 5, the run times are stabilized at a ratio of about 0.4, meaning that the ISCST2 model took about 2.5 times as long to run as the ISCLT2 model for this case. Table 3.4 shows how the maximum annual concentration value at each downwind distance varies by convergence level. In these cases, the maximum concentration value stabilizes after convergence level 2. Overall, the algorithm appears to have converged completely for this case by level 7.

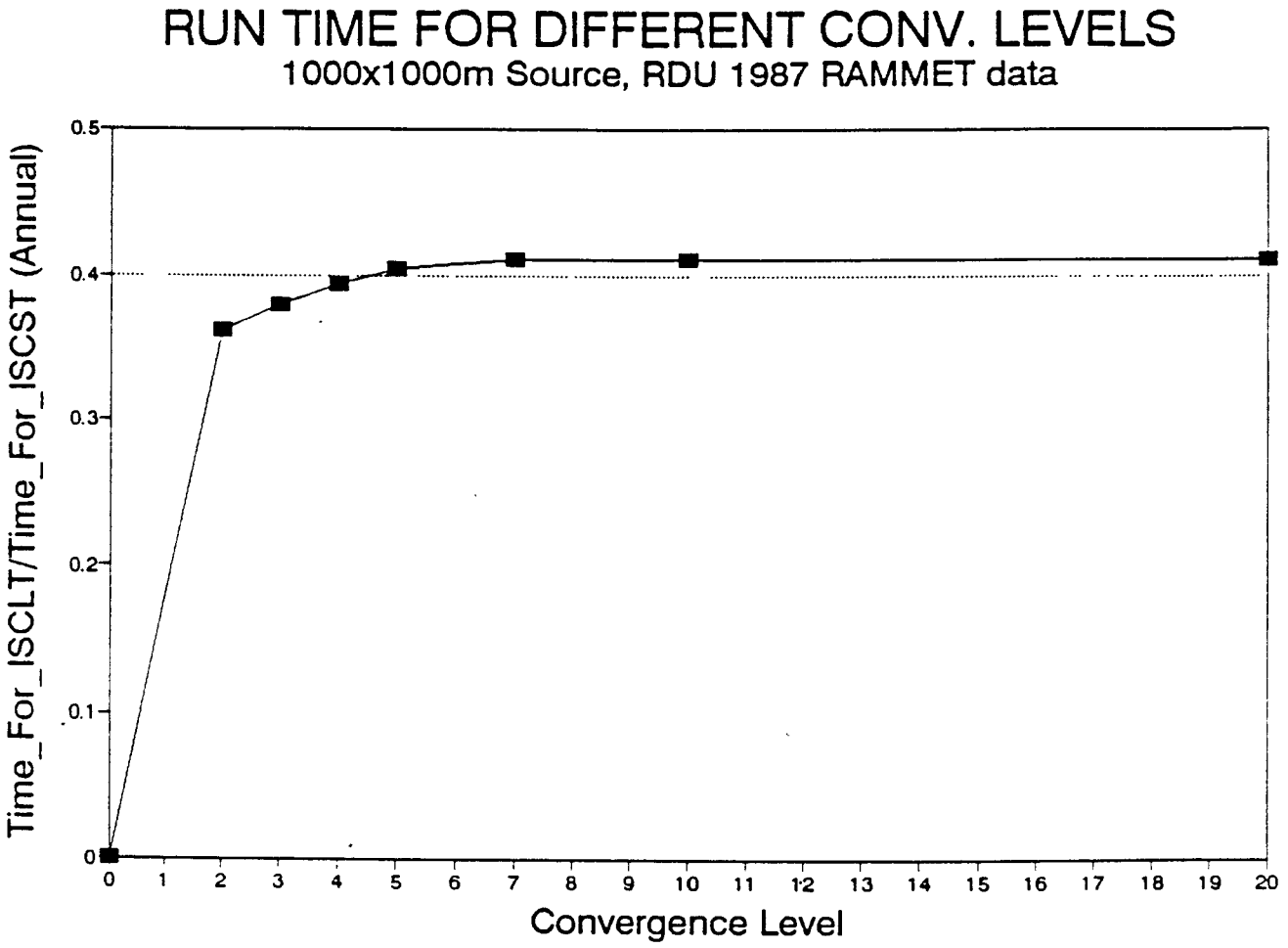

Figure 3.19. Computer Run Time Ratio (ISCLT/ISCST) For Real Life Simulation

Table 3.4a.
Maximum Annual Average Concentration Vs. Downwind Distance
1000x1000m Source, RDU 1987 Star Data

DOWNWIND DISTANCE	CALCULATION STOPS IN LEVEL 2	CALCULATION STOPS IN LEVEL 3	CALCULATION STOPS IN LEVEL 4	CALCULATION STOPS IN LEVEL 5	CALCULATION STOPS IN LEVEL7	CALCULATION STOPS IN LEVEL 10	UNCONDI-TIONAL CON-VERGENCE	ISCST RUN USING RANDOM DATA
250 00000	39.31793	39.31793	39.31793	39.31793	39.31793	39.31793	39.31793	39.27002
500.00000	36.33121	36 33121	36.33121	36.33121	36.33121	36.33121	36.33121	36.29247
750.00000	6.93167	6.91585	6.91292	6.91339	6.91265	6 91255	6.91255	6.90980
1000.00000	3.11843	3.11107	3.10819	3.10749	3.10749	3.10749	3.10749	3.10540
1500.00000	1.59176	1.58582	1.58293	1.58222	1.58214	1.58214	1.58214	1.58267
5000.00000	0.24298	0.24080	0.24076	0.24076	0 24076	0.24076	0.24076	0.23798
15000.00000	0.04811	0 04755	0.04751	0.04749	0 04744	0.04744	0.04744	0.04698

Table 3.4b.
Maximum Annual Average Concentration Vs. Downwind Distance
1000x200m Source, RDU 1987 Star Data

DOWNWIND DISTANCE	CALCULATION STOPS IN LEVEL 2	CALCULATION STOPS IN LEVEL 3	CALCULATION STOPS IN LEVEL 4	CALCULATION STOPS IN LEVEL 5	CALCULATION STOPS IN LEVEL7	CALCULATION STOPS IN LEVEL 10	UNCONDI-TIONAL CON-VERGENCE	ISCST RUN USING RANDOM DATA
250.00000	28.54518	28.55116	28 55116	28.55116	28.55116	28.55116	28.55116	28.51452
500.00000	20.19791	20 19719	20.19719	20.19719	20.19719	20.19719	20 19719	20.18498
750.00000	1.20635	1.20581	1.20513	1.20513	1.20513	1.20513	1.20513	1.20463
1000.00000	0.61886	0.61754	0.61533	0.61498	0.61492	0.61492	0.61492	0.61700
1500.00000	0.29828	0 29871	0 29833	0.29823	0.29820	0 29820	0.29820	0.29850
5000.00000	0 04810	0.04794	0.04793	0.04793	0.04793	0 04793	0 04793	0.04807
15000.00000	0 00990	0.00950	0 00949	0 00949	0.00948	0 00948	0 00948	0 00977

4. THE SENSITIVITY ANALYSIS

4.1. Description Of The Study

The purpose of this study is to evaluate the sensitivity of design concentrations across a range of source characteristics for the new area source algorithm that has been incorporated into the ISC2 Long Term (ISCLT2) model (EPA, 1992). To examine the sensitivity of the design concentrations across a range of source characteristics, five ground-level area sources were modeled, with sizes varying from 10 meters to 1,000 meters in width. An elevated source scenario consisting of a 100-meter wide area with a release height of 10 meters was modeled. An additional case involving a 1,000 meter wide ground level area was modeled with receptors located within and nearby the area. The high annual averages were determined for each of these source scenarios using a full year of meteorological data. All of the sources were modeled as square areas oriented N-S and E-W, since the original ISC algorithm was limited to handling that source geometry. Each scenario was run for one year of STAR data from Pittsburgh, PA (1989); one year of STAR data from Oklahoma City, OK (1989); and one year of STAR meteorological data from Seattle, WA (1989).

Each scenario was run with both the rural and urban mode dispersion options. The only difference between the rural mode and the urban mode that effects the area sources modeled in this study are the lateral and vertical dispersion coefficients, sigma-y and sigma-z. The dispersion coefficients are somewhat larger for the urban mode to account for the increased dispersive capacity of the atmosphere in the urban environment. The regulatory default option was used for all scenarios. This includes a procedure for calculating averages for periods that include calm hours. A pollutant type of "OTHER" was specified, so that no decay was used for either the rural or the urban mode. For the sake of efficiency, all computer runs involving the original algorithm were performed using the ISCLT2 model, rather than the original ISCLT model. In this way, the same input runstream file was used for both algorithms.

A polar receptor network consisting of ground level receptors at five distances and 36 directions (every 10 degrees) was used to determine design concentrations. Since most area sources are ground-level or low-level releases, the maximum impacts can be expected to occur very near the source. However, the virtual point source algorithm does not allow receptors within the area itself, and is known to provide unreasonable concentration estimates very close to the source. The guidance in the ISC2 User's Guide states that if the source-receptor distance is less than the width of the area, then the area should be subdivided and modeled as multiple sources. Therefore, the first distance ring in the polar network was placed at a downwind distance (measured from the center of the area) of 1.5*XINIT meters, where XINIT is the width of the area. This places the nearest receptors at a distance of about one source width from the edge of the area. Additional distance rings were placed at approximately 2.0, 3.0, 5.0 and 10.0 times the initial distance, for a total of 180 receptors. For the ground level sources, the maximum ground level concentrations are expected to occur near the downwind edge of the area, and to decrease beyond that distance. Therefore the maximum concentrations for these source-receptor geometries are expected to occur at the 1.5*XINIT distance. The concentrations at the larger receptor distances were also examined for a few cases in order to compare the algorithms for distances downwind of the maximum concentration.

Additional receptor distances were used for the elevated source to account for the fact that the maximum impact may occur beyond the nearest distance ring. Additional receptor rings were included at distances of 2.0*XINIT, 2.5*XINIT, and 4.0*XINIT for the elevated release height cases to better represent the peak concentration from the refined model.

In order to assess the sensitivity of the design values for receptors located close to and within an area source, an additional scenario was modeled involving a 1,000 meter wide (extra large) ground-level area source with receptors located within the area and near the edge of the area. For the original virtual point source algorithm, this source was subdivided into 4, 16, 64 and 100 separate areas of equal size. This was necessary because the virtual point source algorithm cannot model impacts at receptor locations within the area being modeled.

An emission rate equivalent to 1.0 g/s for the entire area was used for all scenarios. The area source widths, heights of release, emission rates, and receptor distances are shown in Table 4.1 for each scenario. Table 4.2 provides the source inputs for the X-Large (XL), Close-in case for the 4-, 16-, 64-, and 100-source treatment used with the virtual point source algorithm. Figure 4.1 shows the location of the receptors used for the X-Large source with receptors located within and nearby the area.

Table 4.1.
Area Source Scenarios for Sensitivity Analysis

Source Type	Width of Area (m)	Height of Release (m)	Emission Rate ($g/(sm^2)$)	Receptor Distances (m) (measured from the center of the area)
X-Small, GL*	10.0	0.0	1.0E-2	15, 30, 50, 75, 150
Small, GL*	50.0	0.0	4.0E-4	75, 150, 250, 400, 750
Medium, GL*	100.0	0.0	1.0E-4	150, 300, 500, 750, 1500
Large, GL*	500.0	0.0	4.0E-6	750, 1500, 2500, 4000, 7500
X-Large, GL*	1000.0	0.0	1.0E-6	1500, 3000, 5000, 7500,15000
Medium, EL**	100.0	10.0	1.0E-4	150, 200, 250, 300, 400,500, 750,1500
X-Large, CI***, GL	1000.0	0.0	1.0E-6	250, 500, 750, 1000, 1500

*GL means Ground-Level.
**EL means Elevated.
*** CI means Close-in

Table 4.2.
Area Source Inputs for X-Large, Close-in Scenario
(used for the original virtual point source algorithm only)

Scenario Description	Width of Each Sub-Division (m)	Height of Release (m)	Emission Rate ($g/(sm^2)$)	Receptor Distances (measured from the center of the 1000m area) (m)
XL, Close-in 4-sources, (2x2)	500.0	0.0	1.0E-6	250, 500, 750, 1000, 1500
XL, Close-in 16-sources, (4x4)	250.0	0.0	1.0E-6	250, 500, 750, 1000, 1500
XL, Close-in 64-sources, (8x8)	125.0	0.0	1.0E-6	250, 500, 750, 1000, 1500
XL, Close-in 100-sources, (10x10)	100.0	0.0	1.0E-6	250, 500, 750, 1000, 1500

4.2. Results Of The Study

The results of the sensitivity study are presented first for the five ground level sources with receptors located downwind of the area, followed by the results for the elevated source, and then for the ground level source with receptors located within the area.

4.2.1. Ground Level Sources With Downwind Receptors

Tables 4.3 through 4.7 present comparisons of design values (10 highest annual average values) obtained from the numerical integration algorithm in ISCLT2 with values from the original virtual point source algorithm for the five ground level sources of various widths. The source widths range from the very small (10 meter wide) area source in Table 4.3 to the very large (1000 meter wide) area source in Table 4.7.

Part A of each table presents the results using rural dispersion coefficients, and part B for each table presents the results using urban dispersion coefficients. The design values are generally located at the receptors located closest to the area source.

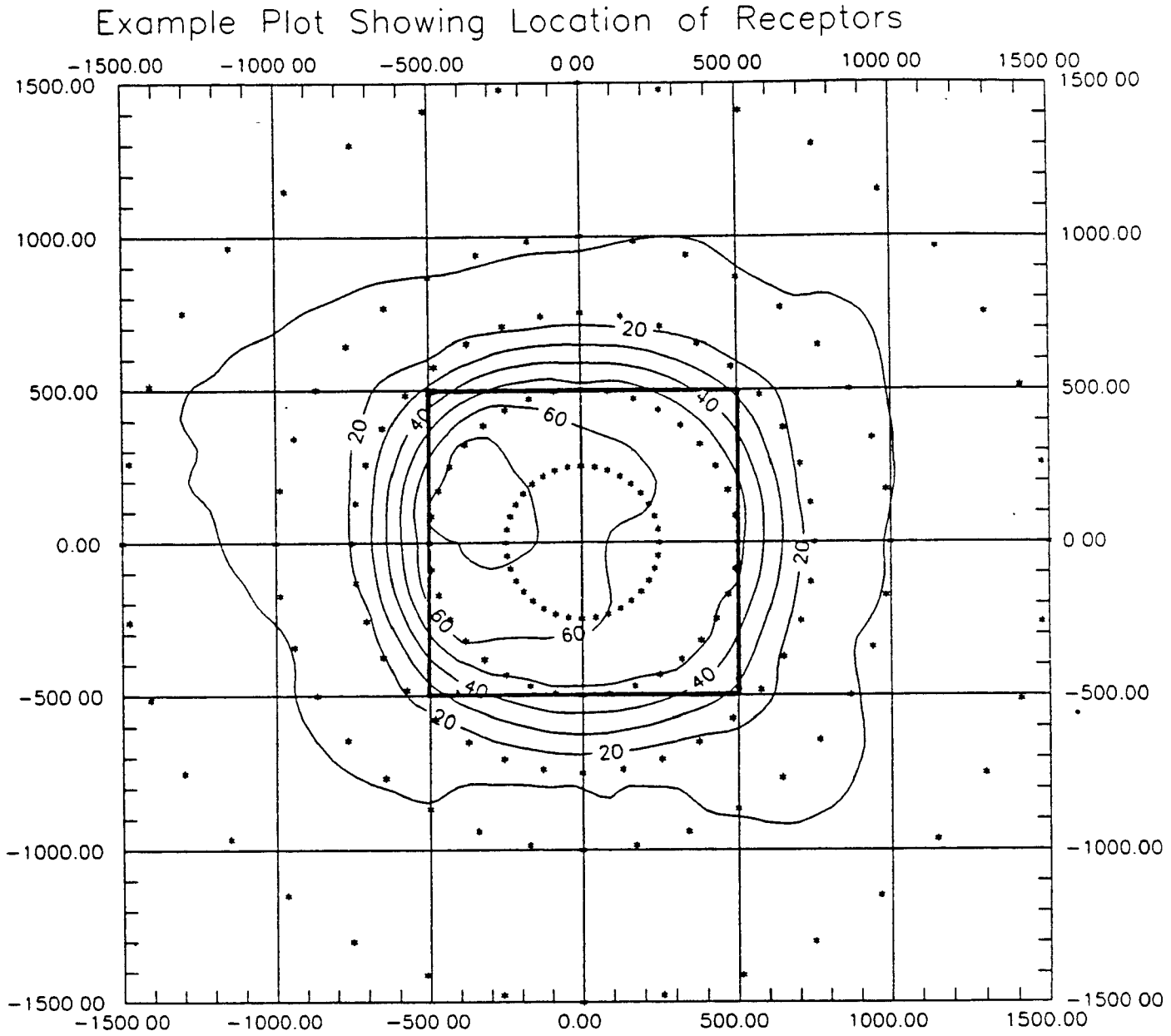

Figure 4.1. Example Contour Plot Showing Location of Receptors Relative to the 1000 Meter Wide Ground Level Source for the X-Large Close-in Case

Table 4.3.
Comparison of Design Concentrations ($\mu g/m^3$) for the Very Small Source (10m Width)

Site, Data & Dispersion Options	Numerical Integration (New)	Virtual Point Source (Old)	Ratio (New/Old)
Pittsburgh 1989, Rural	5469.19800	3137.21600	1.7433285
Okla. City 1989, Rural	7969.95200	4032.40300	1.9764771
Seattle 1989, Rural	9681.49900	4673.74800	2.0714636
Pittsburgh 1989, Urban	2412.35600	1305.56500	1.8477487
Okla. City 1989, Urban	3668.16200	1754.99500	2.0901268
Seattle 1989, Urban	4198.99700	1948.98300	2.0307770

Table 4.4.
Comparison of Design Concentrations ($\mu g/m^3$) for the Small Source (50m Width)

Site, Data & Dispersion Options	Numerical Integration (New)	Virtual Point Source (Old)	Ratio (New/Old)
Pittsburgh 1989, Rural	280.28900	160.42750	1.7413810
Okla. City 1989, Rural	410.25400	206.99070	1.9819924
Seattle 1989, Rural	491.23020	236.76410	2.0747664
Pittsburgh 1989, Urban	98.87118	54.23226	1.8231064
Okla. City 1989, Urban	150.94320	73.34540	2.0579777
Seattle 1989, Urban	171.52150	80.59711	2.1281346

Table 4.5.
Comparison of Design Concentrations ($\mu g/m^3$) for the Medium Source (100m Width)

Site, Data & Dispersion Options	Numerical Integration (New)	Virtual Point Source (Old)	Ratio (New/Old)
Pittsburgh 1989, Rural	78.06039	44.75477	1.7441803
Okla. City 1989, Rural	114.53200	57.90853	1.9778088
Seattle 1989, Rural	136.19110	65.75126	2.0713078
Pittsburgh 1989, Urban	25.43472	14.15101	1.7973784
Okla. City 1989, Urban	39.00346	19.26075	2.0250229
Seattle 1989, Urban	43.95693	20.92982	2.1002058

Table 4.6.
Comparison of Design Concentrations ($\mu g/m^3$) for the Large Source (500m Width)

Site, Data & Dispersion Options	Numerical Integration (New)	Virtual Point Source (Old)	Ratio (New/Old)
Pittsburgh 1989, Rural	4.212339	2.552411	1.6503373
Okla. City 1989, Rural	6.231626	3.329695	1.8715306
Seattle 1989, Rural	7.280537	3.730223	1.9517699
Pittsburgh 1989, Urban	1.217577	0.721960	1.6864882
Okla. City 1989, Urban	1.909762	1.010385	1.8901330
Seattle 1989, Urban	2.060928	1.044501	1.9731221

Table 4.7.
Comparison of Design Concentrations ($\mu g/m^3$) for the Very Large Source (1000m Width)

Site, Data & Dispersion Options	Numerical Integration (New)	Virtual Point Source (Old)	Ratio (New/Old)
Pittsburgh 1989, Rural	1.290841	0.821113	1.5720626
Okla. City 1989, Rural	1.911188	1.071306	1.7839796
Seattle 1989, Rural	2.222102	1.198315	1.8543555
Pittsburgh 1989, Urban	0.355397	0.218373	1.6274768
Okla. City 1989, Urban	0.566046	0.309991	1.8260079
Seattle 1989, Urban	0.593821	0.312113	1.9025834

Overall, the new numerical integration algorithm predicts higher design concentrations than the original virtual point source algorithm. The average ratio of the numerical integration algorithm results over the virtual point source algorithm results (averaged over all three cities and for all averaging periods) ranges from about 2.0 for the 10 meter wide area to about 1.7 for the 1000 meter wide area. This trend toward smaller ratios for larger areas is illustrated in Figure 4.2, which shows the average ratios (averaged across the three meteorological data locations) for the five ground-level sources for downwind receptors only, for both rural and urban dispersion. The ratios are generally larger for the cases with urban dispersion coefficients than for the cases with rural dispersion coefficients.

The most notable feature about these results is that the numerical integration method produces larger concentration estimates than the original virtual point source algorithm. One possible explanation for part of this difference is that the numerical integration algorithm produces larger off-centerline concentration values than the virtual point source algorithm. This is because the numerical integration algorithm provides a more realistic assessment of the lateral distribution of concentration by integrating over the entire source area. The lateral distribution of concentration from the virtual point source algorithm is essentially the distribution of a point source, although some initial lateral spread of the plume is incorporated to account for the area source.

In addition to examining the design values, which all occurred at receptors located on the nearest distance ring for the ground level sources, the results at distances located further downwind were examined briefly to determine whether or not the results converge with distance. Figures 4.3 to 4.8 present the high annual average concentration values versus distance downwind for the 10 meter wide ground level area source for Pittsburgh, Oklahoma City and Seattle data for the cases with both rural and urban dispersion coefficients. Results show that, in all the cases, the maximum concentration values decrease as expected with increasing downwind distance. The figures also show that the results for the two algorithms converge for large downwind distances (beyond about 5 to 7 source widths).

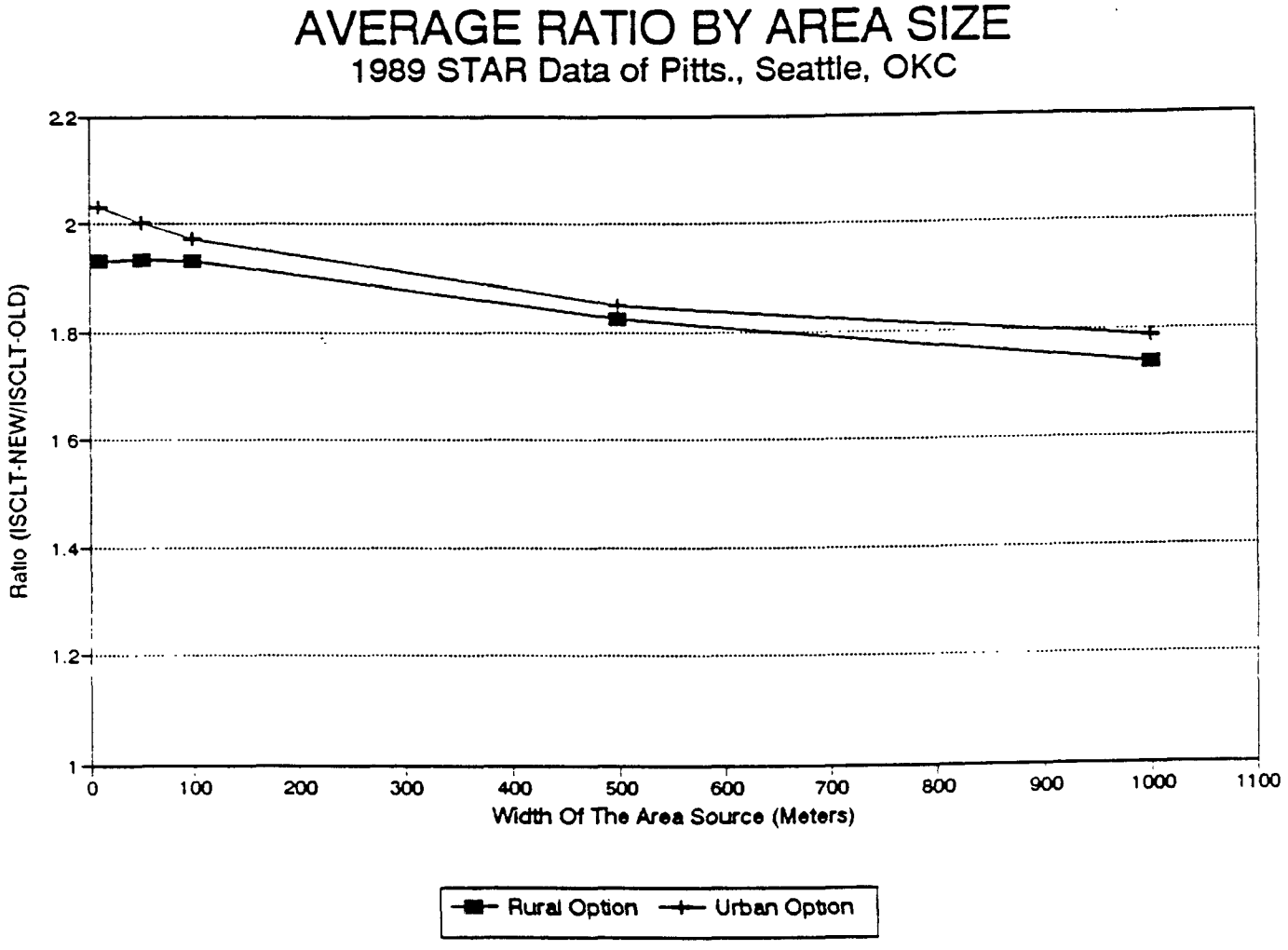

Figure 4.2. Average Ratios (New/Old) by Area Size for Ground Level Sources For Both Rural And Urban Dispersion Coefficients

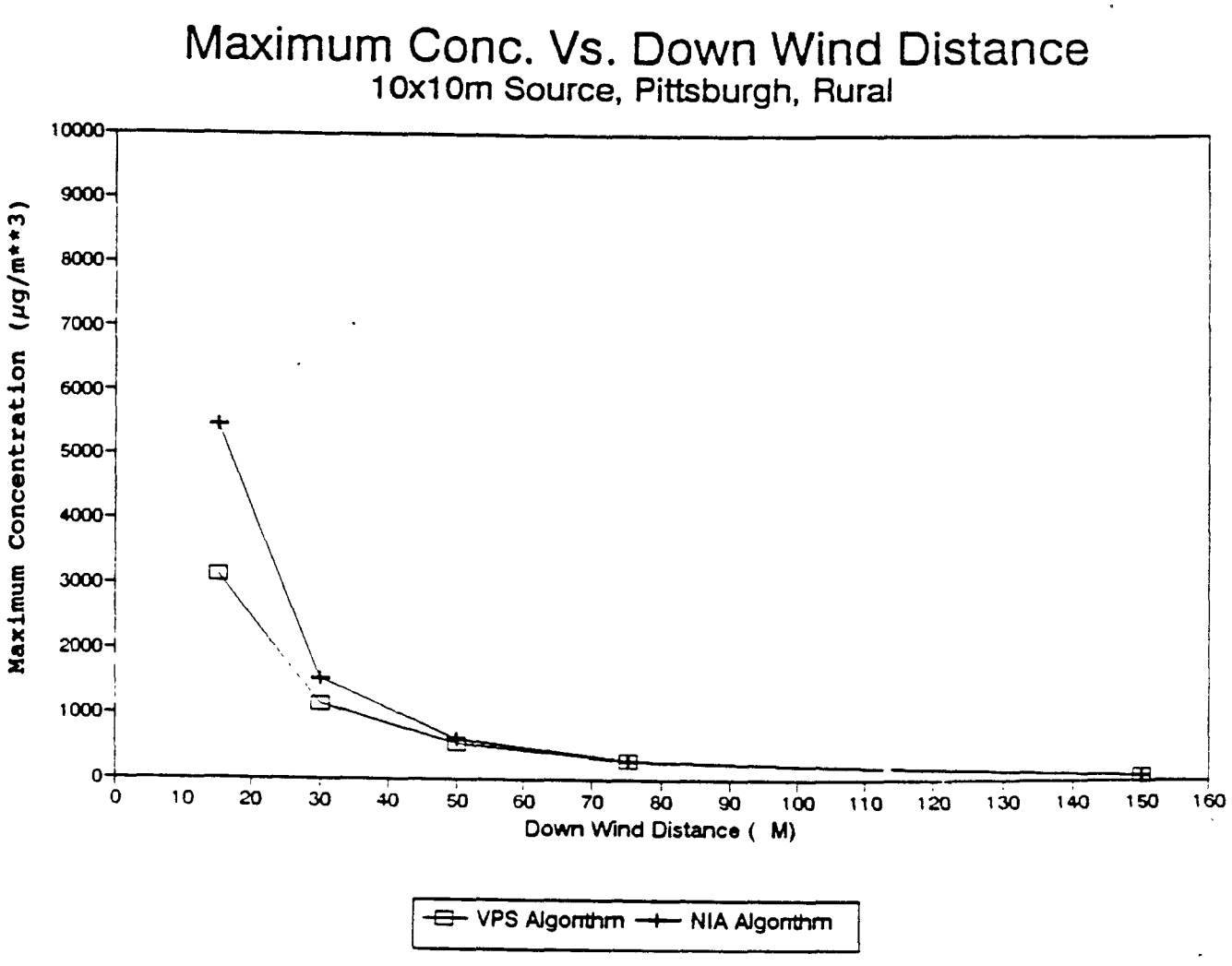

Figure 4.3. High Annual Average Values Versus Distance for the 10 Meter Wide Ground Level Source for Rural Dispersion and Pittsburgh 1989 STAR Data

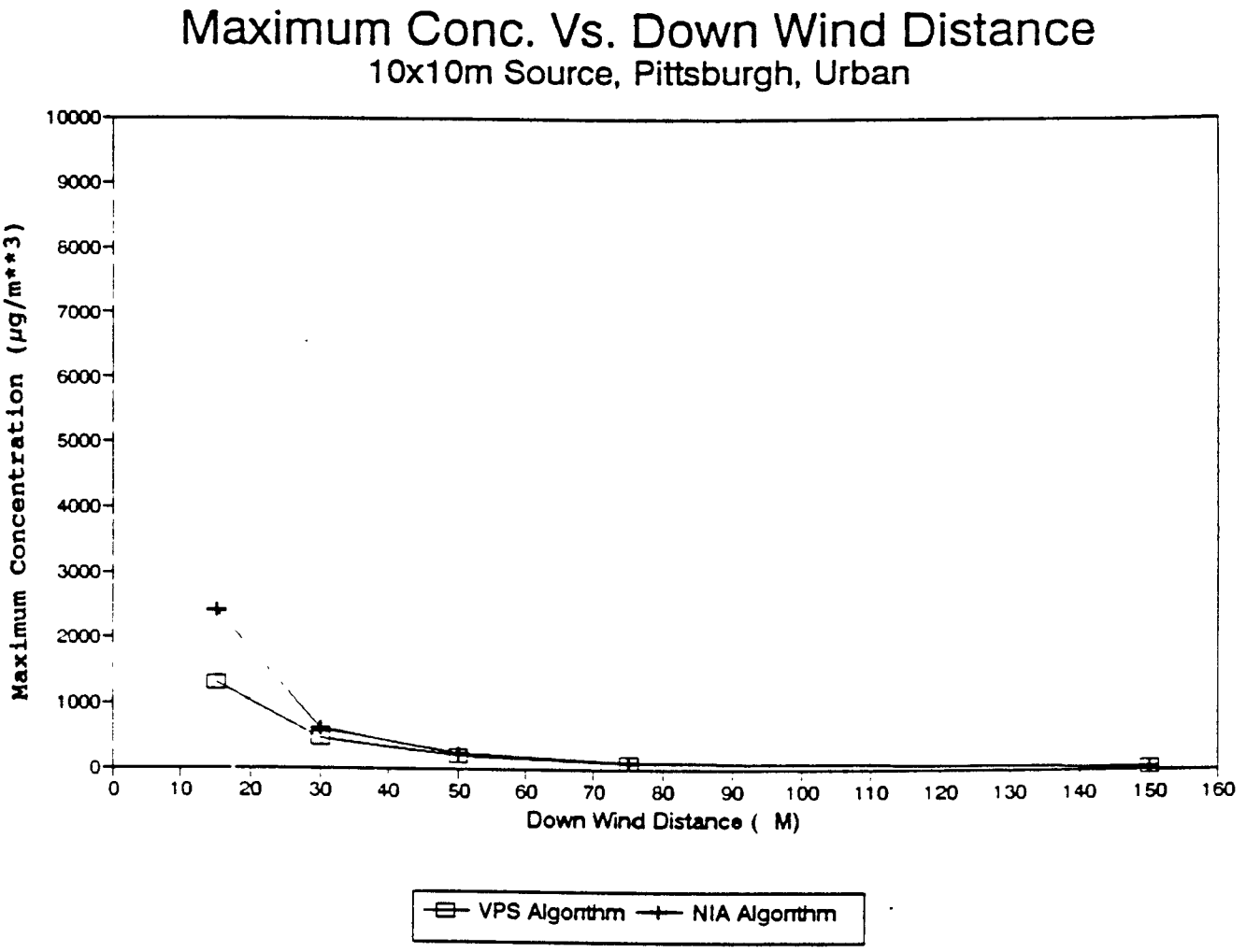

Figure 4.4. High Annual Average Values Versus Distance for the 10 Meter Wide Ground Level Source for Urban Dispersion and Pittsburgh 1989 STAR Data

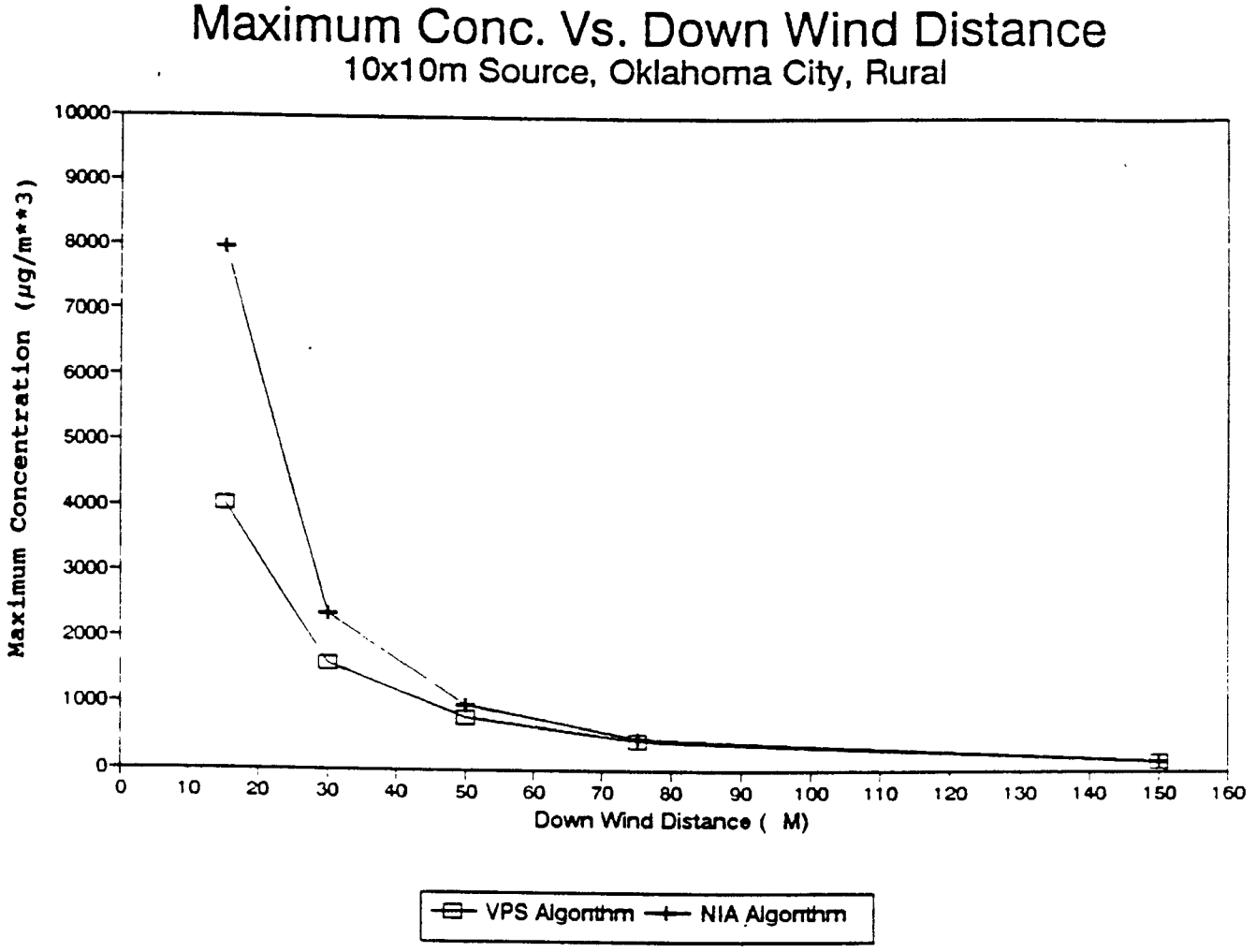

Figure 4.5. High Annual Average Values Versus Distance for the 10 Meter Wide Ground Level Source for Rural Dispersion and Oklahoma City 1989 STAR Data

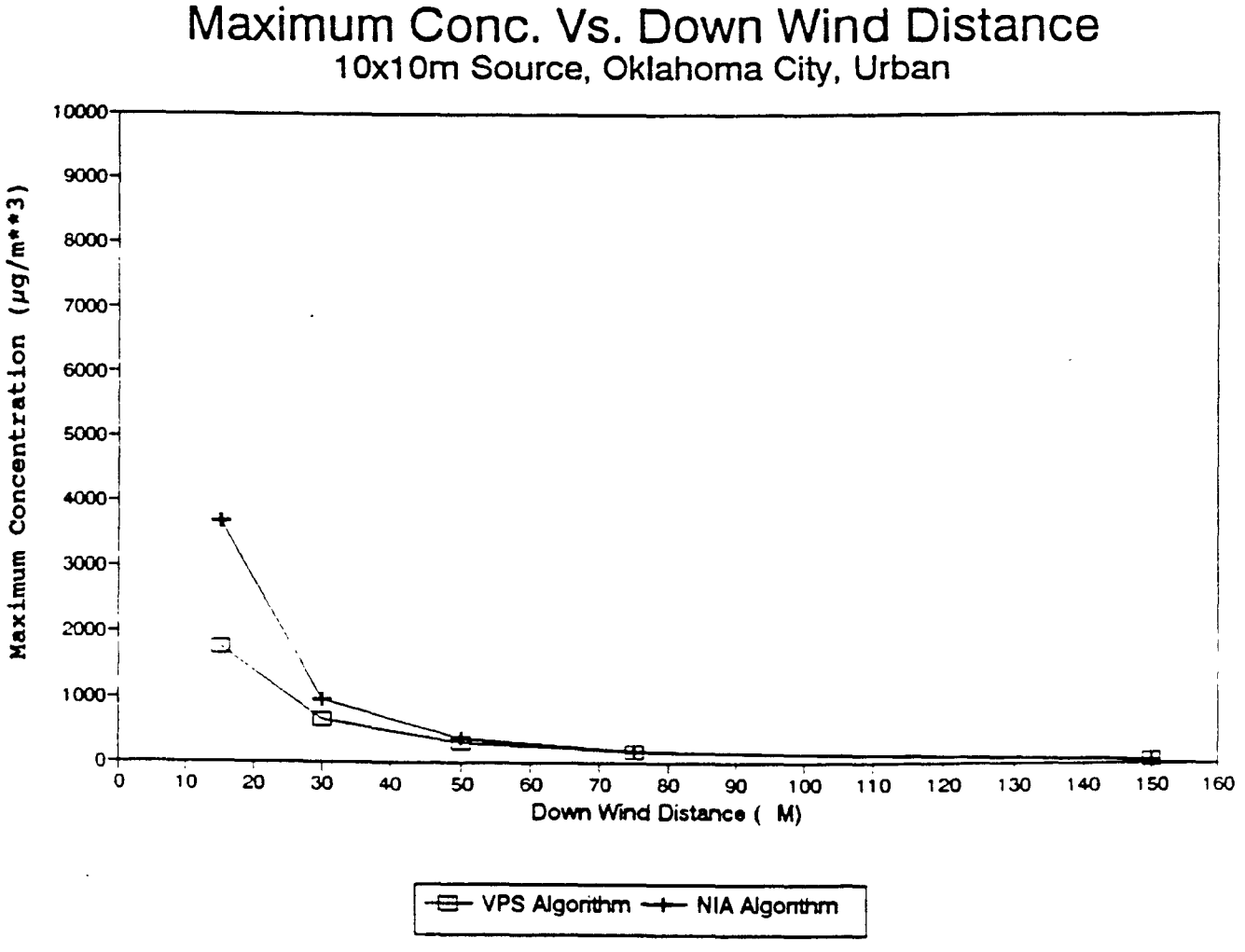

Figure 4.6. High Annual Average Values Versus Distance for the 10 Meter Wide Ground Level Source for Urban Dispersion and Oklahoma City 1989 STAR Data

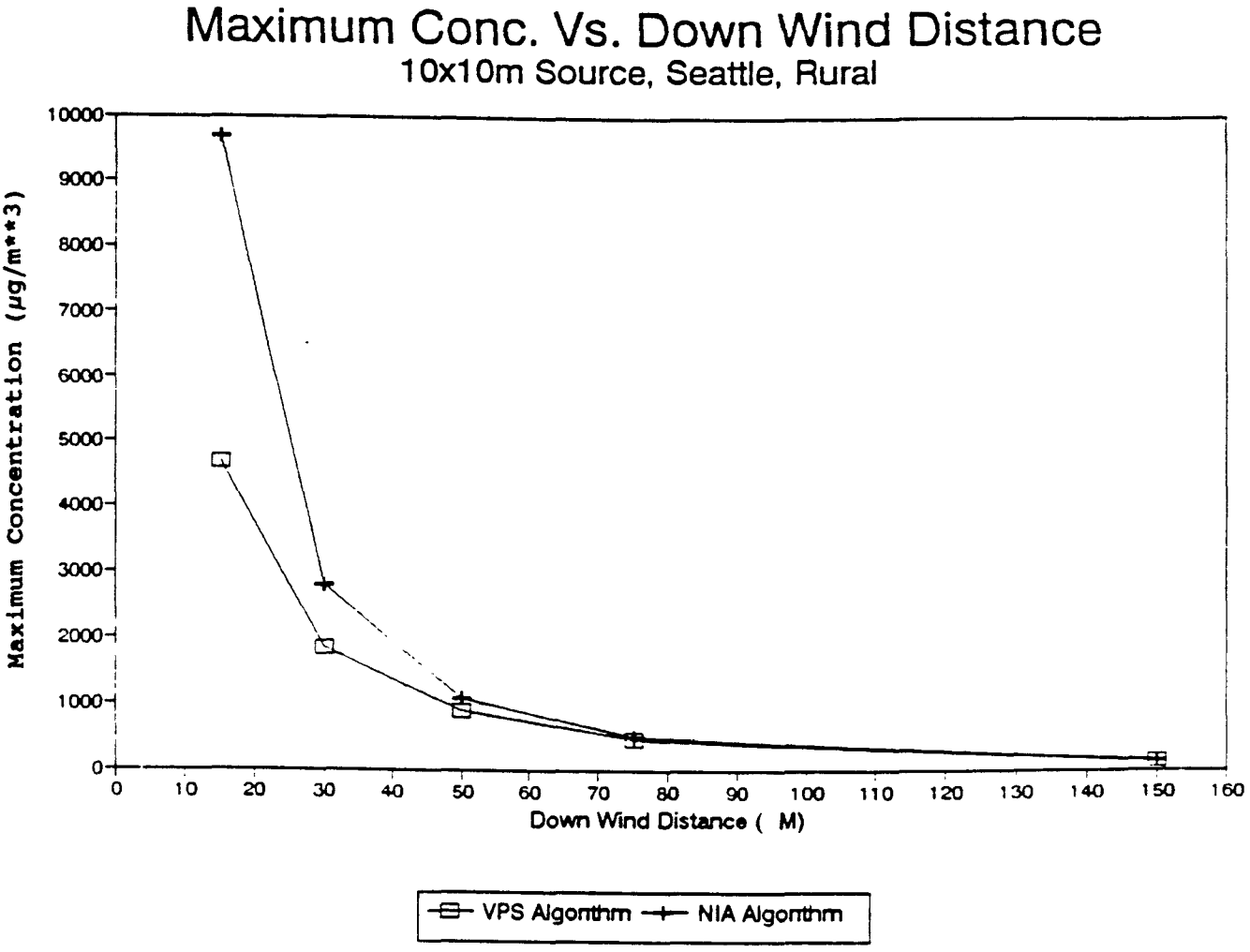

Figure 4.7. High Annual Average Values Versus Distance for the 10 Meter Wide Ground Level Source for Rural Dispersion and Seattle 1989 STAR Data

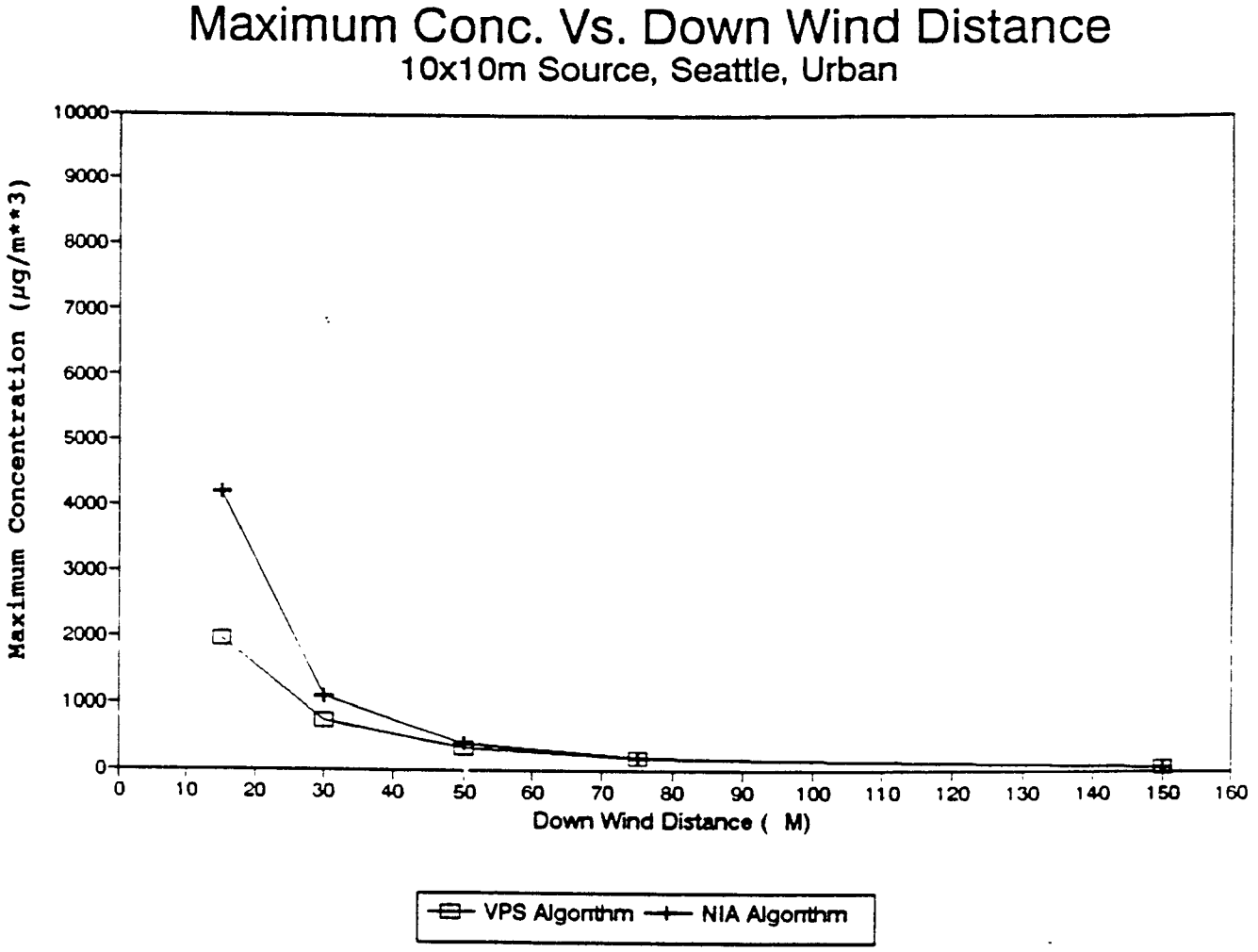

Figure 4.8. High Annual Average Values Versus Distance for the 10 Meter Wide Ground Level Source for Urban Dispersion and Seattle 1989 STAR Data

4.2.2. Elevated Area Source

Table 4.8 presents comparisons of design values obtained from the numerical integration algorithm and the virtual point source algorithm for the 100 meter wide elevated source (10 meter release height). Results are presented for both rural and urban dispersion coefficients. The ratios for the elevated source are smaller than the corresponding ratios for the 100-meter ground level source (see Tables 4.5.). In fact, the ratios for the rural dispersion case are less than 1.0, indicating that the numerical integration algorithm estimates smaller concentrations than the virtual point source algorithm for these cases. Urban ratios are somewhat larger than rural ratios, but are still smaller than the corresponding ratios for the ground-level source.

One possible explanation for these results for the elevated source is that the virtual point source algorithm uses a virtual distance equal to the width of the source for calculating the vertical dispersion parameters. This means that the sigma-z value is growing from the upwind edge of the area source. Since the numerical integration algorithm integrates over the entire area, the vertical dispersion parameter for each element of the integration is representative of the actual distance from that element of the area to the receptor location. For the portion of the area that is closest to the receptor, and therefore having the greatest impact on the receptor, the sigma-z value will be based on the distance from the downwind edge of the area to the receptor location. This difference will result in a smaller overall "effective" vertical dispersion parameter for the numerical integration algorithm than for the virtual point source algorithm. Since this is an elevated source with ground-level receptors, the smaller "effective" vertical dispersion parameter for the numerical integration algorithm will tend to cause smaller ground-level concentrations, as seen for the case of rural dispersion. This tendency competes with the tendency for the numerical integration algorithm to estimate higher concentrations due to differences in the treatment of lateral dispersion.

Table 4.8.
Comparison of Design Concentrations ($\mu g/m^3$) for the Medium Elevated Source (100m Width)

Site, Data & Dispersion Options	Numerical Integration (New)	Virtual Point Source (Old)	Ratio (New/Old)
Pittsburgh 1989, Rural	11.94122	15.29294	0.7808322
Okla. City 1989, Rural	19.64324	21.67913	0.9060898
Seattle 1989, Rural	28.44486	29.69580	0.9578748
Pittsburgh 1989, Urban	16.22476	10.98232	1.4773527
Okla. City 1989, Urban	27.32439	16.86372	1.6203062
Seattle 1989, Urban	33.55091	18.89518	1.7756333

4.2.3. Ground-level Sources With Receptors Within and Nearby the Area Source

Table 4.9 presents comparisons of design values from the numerical integration algorithm and from the virtual point source algorithm for the 1000 meter wide ground level source with receptors located within and nearby the area source. Results are presented for both rural and urban dispersion coefficients. The results for the virtual point source algorithm are presented for each of the subdivided multiple-source scenarios examined using 4, 16, 64 and 100 areas of equal size. The ratios for the cases with receptors within and nearby the area are generally larger than the corresponding ratios for the other ground level cases (see Tables 4.1 through 4.7). As with the other sources examined, the ratios are larger for the case with urban dispersion coefficients than for the case with rural dispersion coefficients. The average ratio for the rural cases is about 3.0, and the average ratio for the urban cases is about 4.0 The results in Tables 4.9 also show that, in general, the design values for the old virtual point source algorithm tend to increase as the number of subdivided areas increases. Since the impact at any receptor located within the area does not include any contribution from the subarea in which the receptor is located, as the number of subareas increases and the size of the subarea decreases, the amount of contribution not accounted for will tend to decrease. In principal, as the number of subareas approaches infinity and the individual subareas approach point sources, the two algorithms should eventually converge.

The receptor locations for the design values are also included in Table 4.9 for the numerical integration algorithm and for the virtual point source case based on 100 subdivided area sources. The locations are given as direction (in degrees) and distance (in meters). Thus, a location of (90,500) means a receptor located along the 90 degree direction radial, measured clockwise from North, at a distance of 500 meters from the center of the area. The receptor locations show good agreement. A more complete picture is provided in Figures 4.9 through 4.21, which display contour plots of high concentrations across the receptor grid for the numerical integration algorithm (NIA) and for the virtual point source (VPS) algorithm based on 100 sources. The rural results are presented first, followed by the urban results, with the numerical integration algorithm results and virtual point source (100-source) results for the same location and averaging period on facing pages to facilitate comparison. The four grid squares located at the center of the diagrams (between X = -500 to 500 and Y = -500 to 500) define the location of the 1000 meter wide area source. The source location and the distribution of receptor points was shown in Figure 4.1 in Section 4.2.

Generally, the contour plots show similar patterns between the two algorithms, although the magnitude of the results is higher for the numerical integration algorithm than the virtual point source. Some of the contour plots exhibit isolated peaks and valleys, and some discontinuities (or "kinks") in the contours. These anomalies are due to the limited number of data points (180) on which the plots are based, and are an artifact of the interpolation and contouring schemes used to generate the plots. Therefore, the fine-scale details should not be given much credence in these plots, although the overall patterns are fairly reliable. Both algorithms show generally reasonable patterns, with the contours showing roughly the square shape of the area across the area source itself. The numerical integration algorithm shows a steeper gradient in the concentration distribution near the edges of the area than the virtual point source algorithm. This trend goes along with the tendency for the numerical integration algorithm to estimate higher concentrations within the area and to converge toward the virtual point source estimate within several source widths downwind of the area. The overall conclusion from these contour diagrams is that the numerical integration algorithm provides a reasonable distribution of concentrations for receptors located within and nearby the area source.

Table 4.9.
Comparison of Annual Average Concentrations ($\mu g/m^3$) for the 1000m Wide Area
With Receptors Located Within and Nearby the Area

Site, Data& Dispersion Option	Numerical Integration (New)	Virtual Point Source (Old) 4 Sources	Virtual Point Source (Old) 16 Sources	Virtual Point Source (Old) 64 Sources	Virtual Point Source (Old) 100 Sources	Ratio New/Old-100
Pittsburgh 1989, Rural	34.19587 (20,250)	2.52315	6.02710	10.01933	11.18408 (10,250)	3.0575488
Okla. City 1989, Rural	26.40565 (330,250)	3.13874	4.96530	8.38680	9.21463 (330,250)	2.8656218
Seattle 1989, Rural	33.36413 (50,250)	3.49210	5.99353	10.09934	11.08371 (60,250)	3.0101951
Pittsburgh 1989, Urban	14.10248 (30,250)	0.73693	1.80160	3.08403	3.47830 (10,250)	4.0544151
Okla. City 1989, Urban	11.19658 (320,250)	0.96177	1.55283	2.69919	2.98885 (330,250)	3.7461202
Seattle 1989, Urban	13.86200 (50,250)	0.98152	1.80063	3.13583	3.48208 (60,250)	3.9809562

Note: Values in parentheses are receptor locations given as direction (degrees from North) and downwind distance (meters).

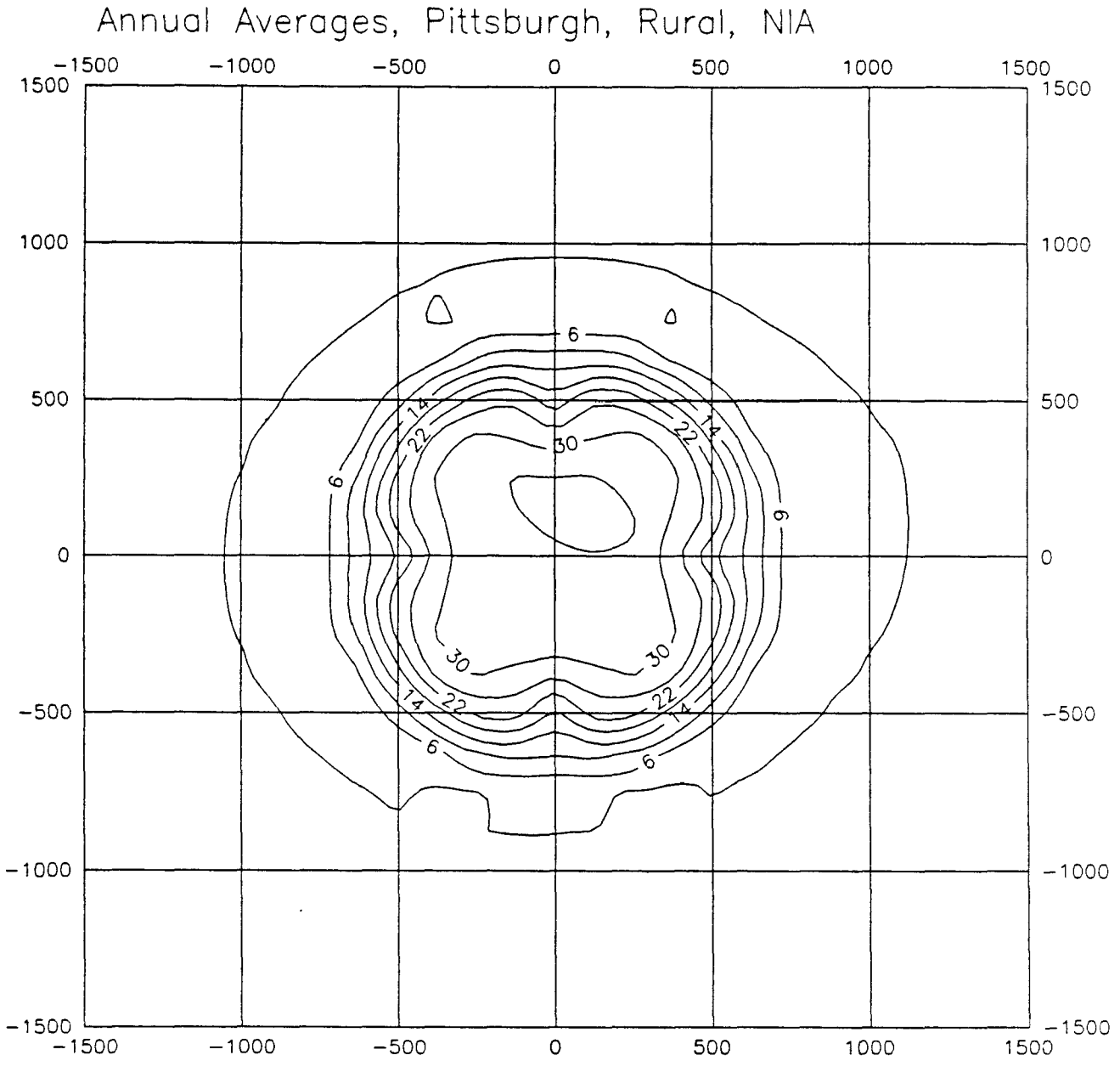

Figure 4.9. Contour Diagram of Annual Average Rural Concentrations ($\mu g/m^3$) from the Numerical Integration Algorithm for the 1000 Meter Wide Ground Level Source with Close-in Receptors Using Pittsburgh 1989 STAR Data.

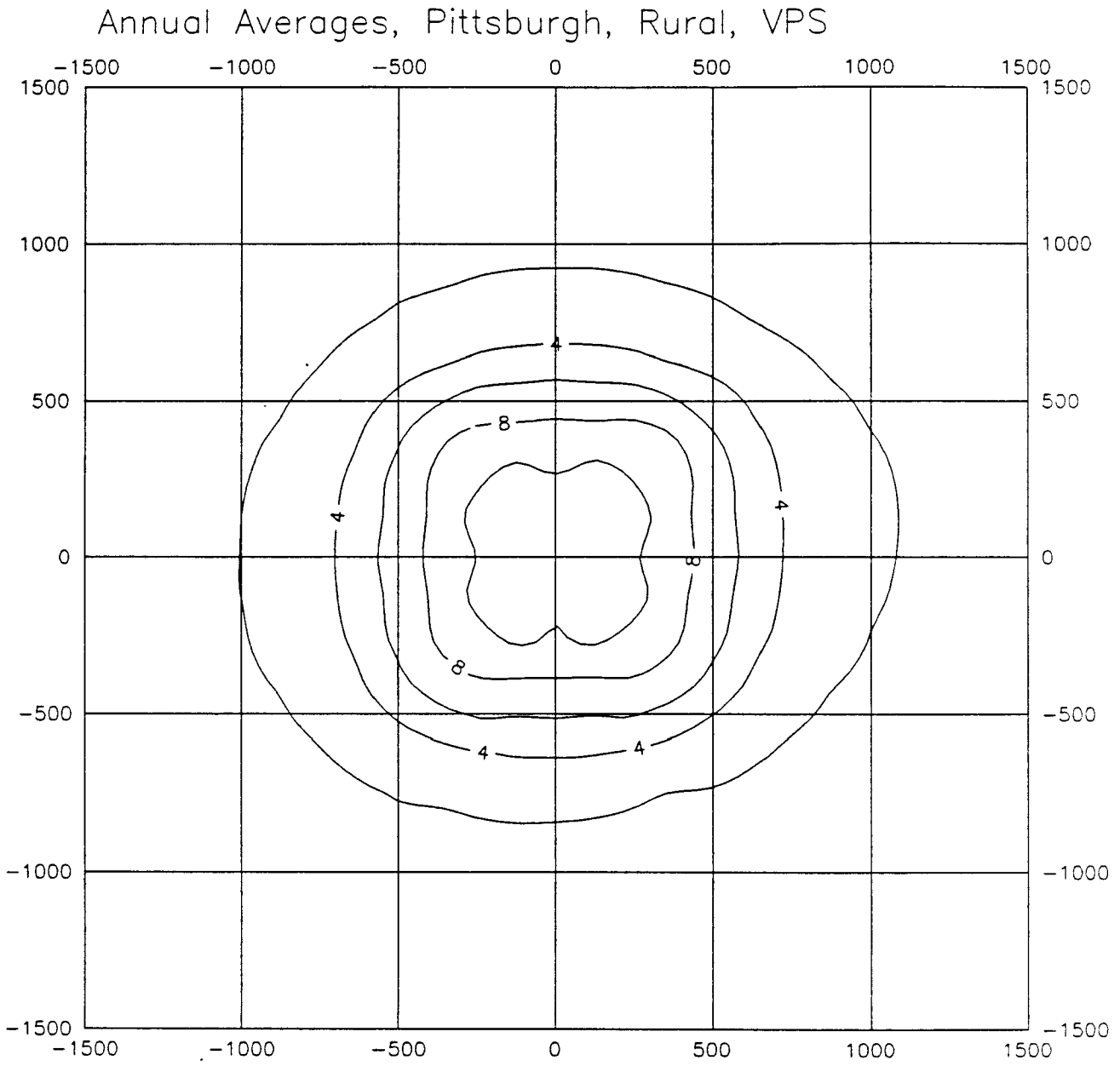

Figure 4.10. Contour Diagram of Annual Average Rural Concentrations ($\mu g/m^3$) from the Virtual Point Source Algorithm for the 1000 Meter Wide Ground Level Source with Close-in Receptors Using Pittsburgh 1989 STAR Data.

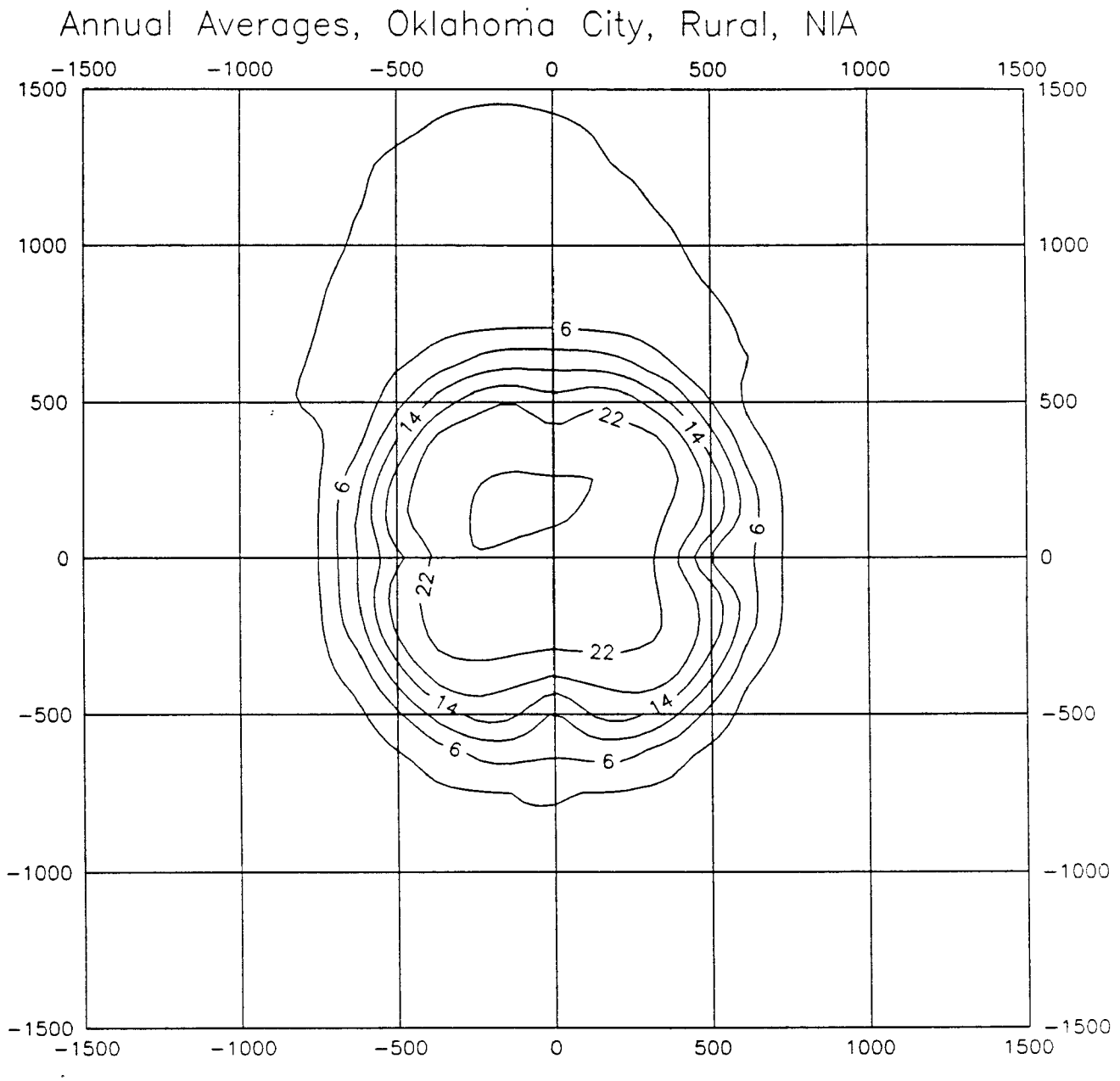

Figure 4.11. Contour Diagram of Annual Average Rural Concentrations ($\mu g/m^3$) from the Numerical Integration Algorithm for the 1000 Meter Wide Ground Level Source with Close-in Receptors Using Oklahoma City 1989 STAR Data.

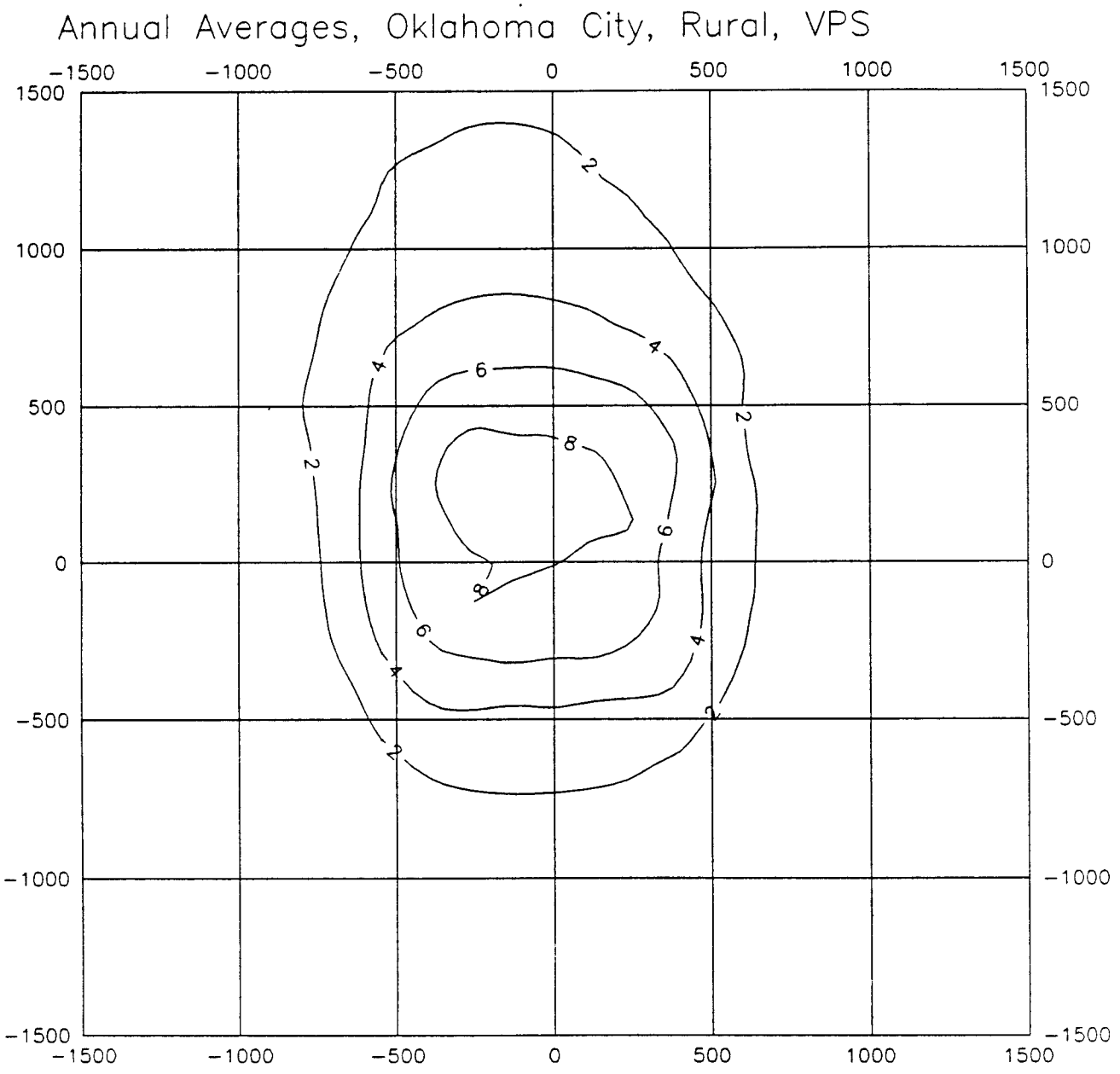

Figure 4.12. Contour Diagram of Annual Average Rural Concentrations ($\mu g/m^3$) from the Virtual Point Source Algorithm for the 1000 Meter Wide Ground Level Source with Close-in Receptors Using Oklahoma City 1989 STAR Data.

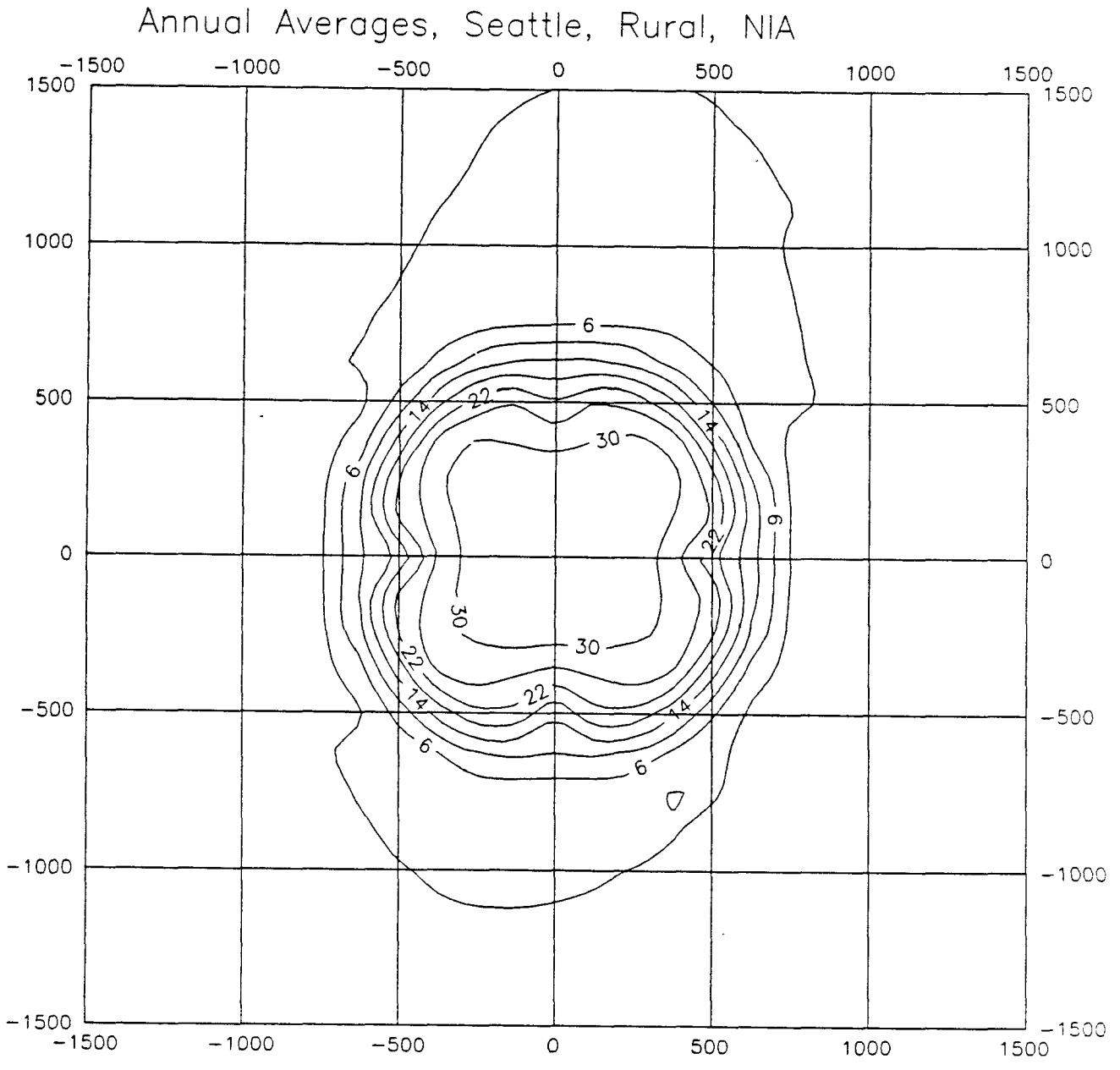

Figure 4.13. Contour Diagram of Annual Average Rural Concentrations ($\mu g/m^3$) from the Numerical Integration Algorithm for the 1000 Meter Wide Ground Level Source with Close-in Receptors Using Seattle 1989 STAR Data.

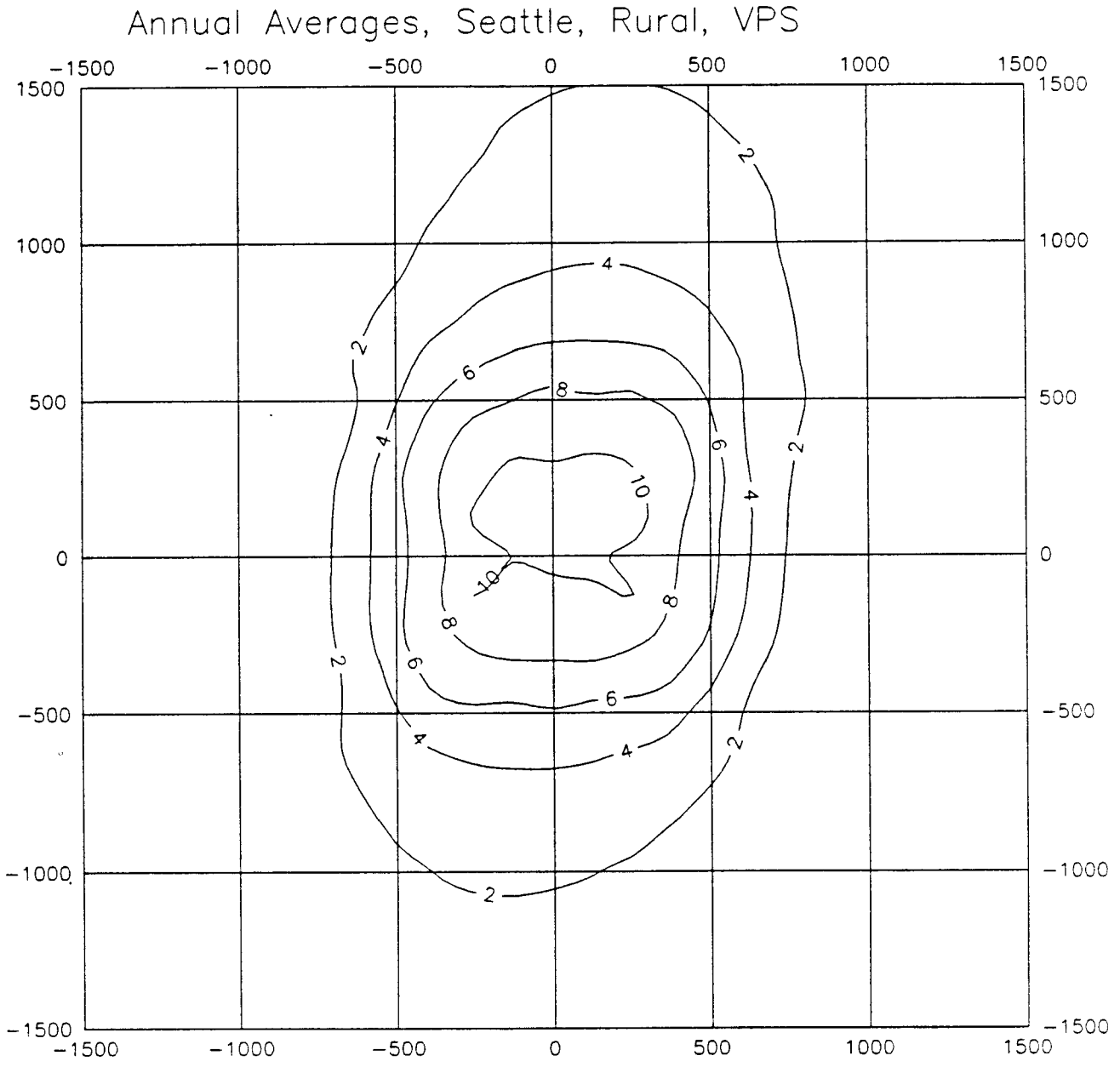

Figure 4.14. Contour Diagram of Annual Average Rural Concentrations ($\mu g/m^3$) from the Virtual Point Source Algorithm for the 1000 Meter Wide Ground Level Source with Close-in Receptors Using Seattle 1989 STAR Data.

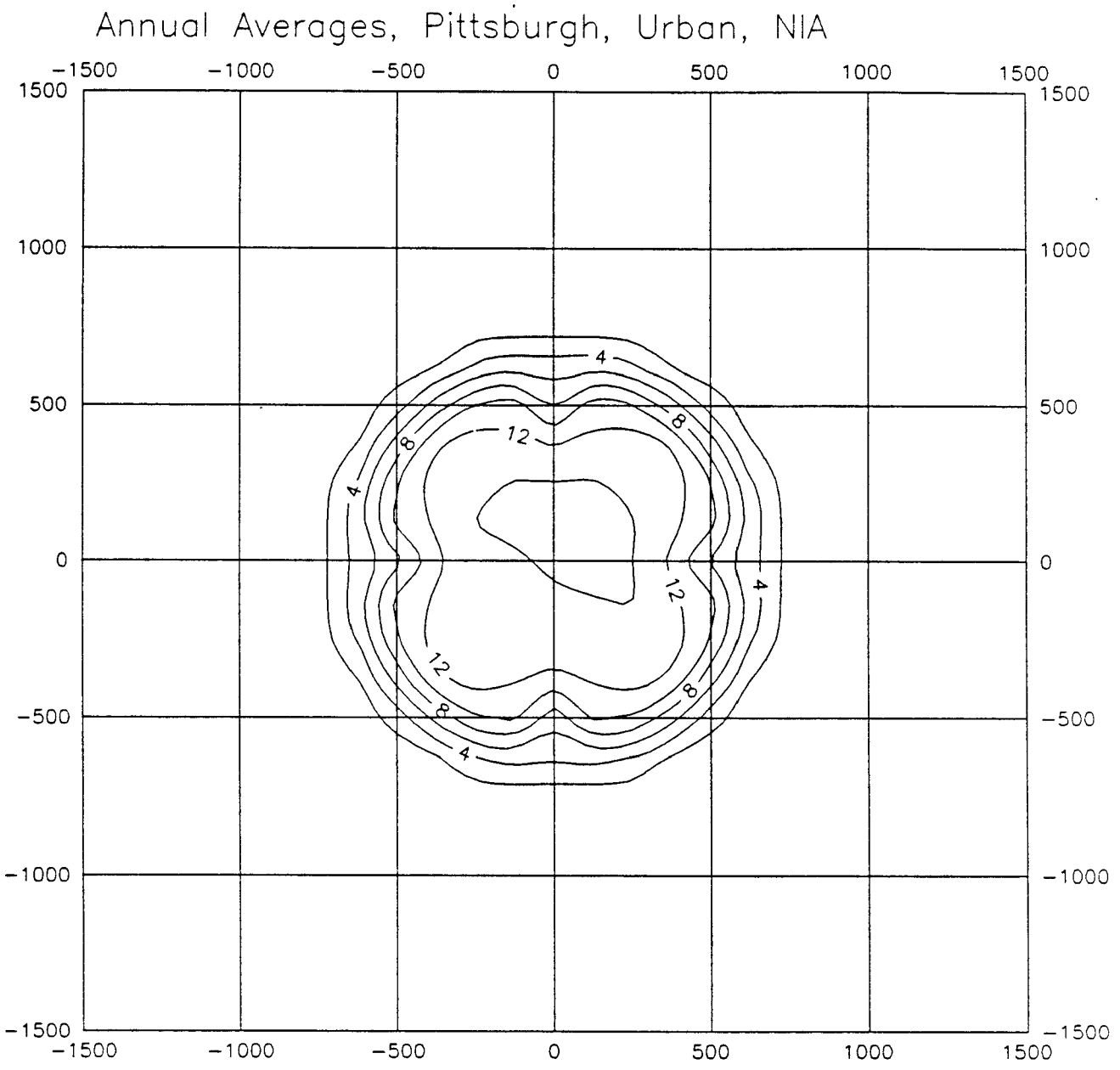

Figure 4.15. Contour Diagram of Annual Average Urban Concentrations($\mu g/m^3$) from the Numerical Integration Algorithm for the 1000 Meter Wide Ground Level Source with Close-in Receptors Using Pittsburgh 1989 STAR Data.

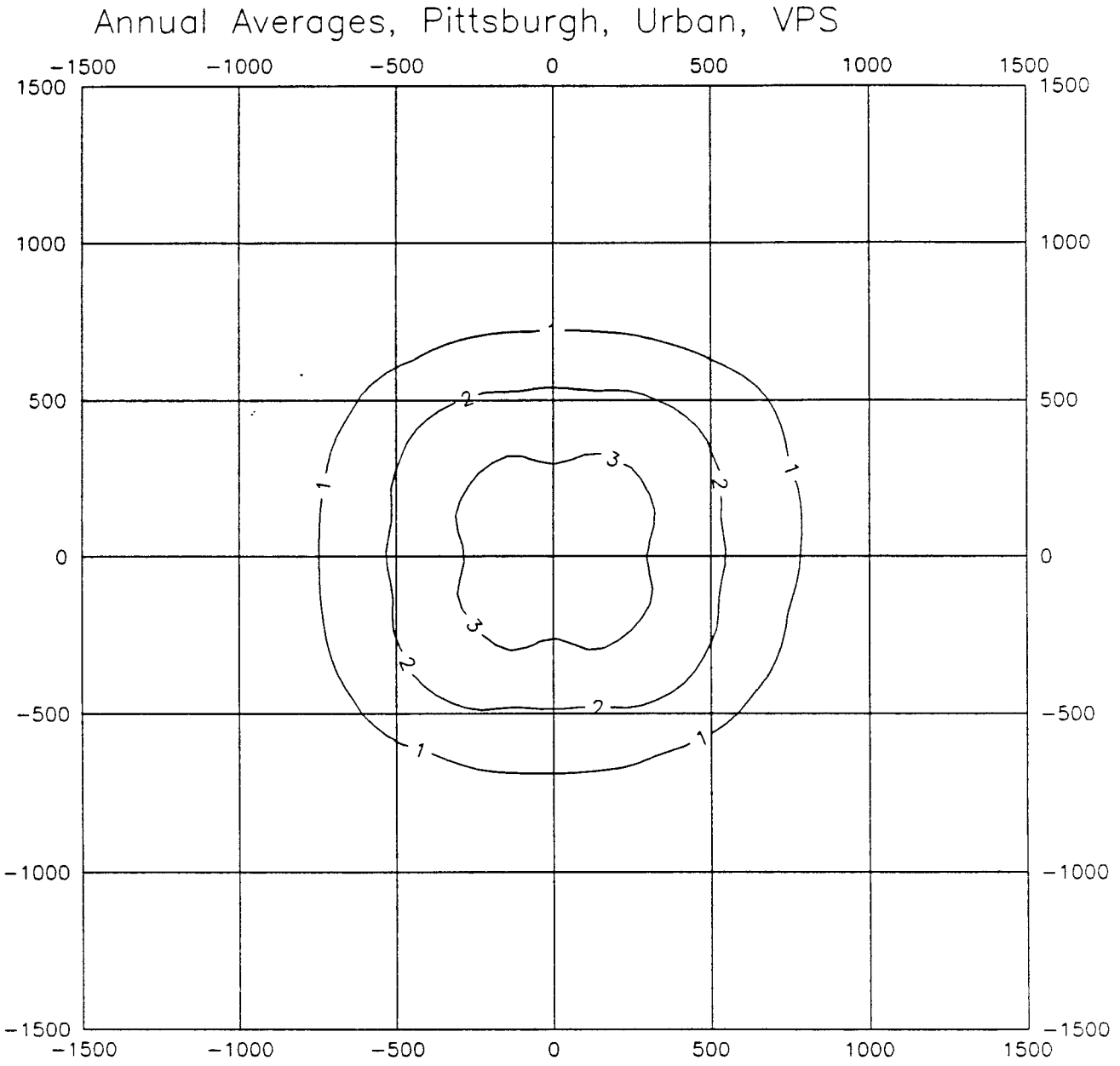

Figure 4.16. Contour Diagram of Annual Average Urban Concentrations($\mu g/m^3$) from the Virtual Point Source Algorithm for the 1000 Meter Wide Ground Level Source with Close-in Receptors Using Pittsburgh 1989 STAR Data.

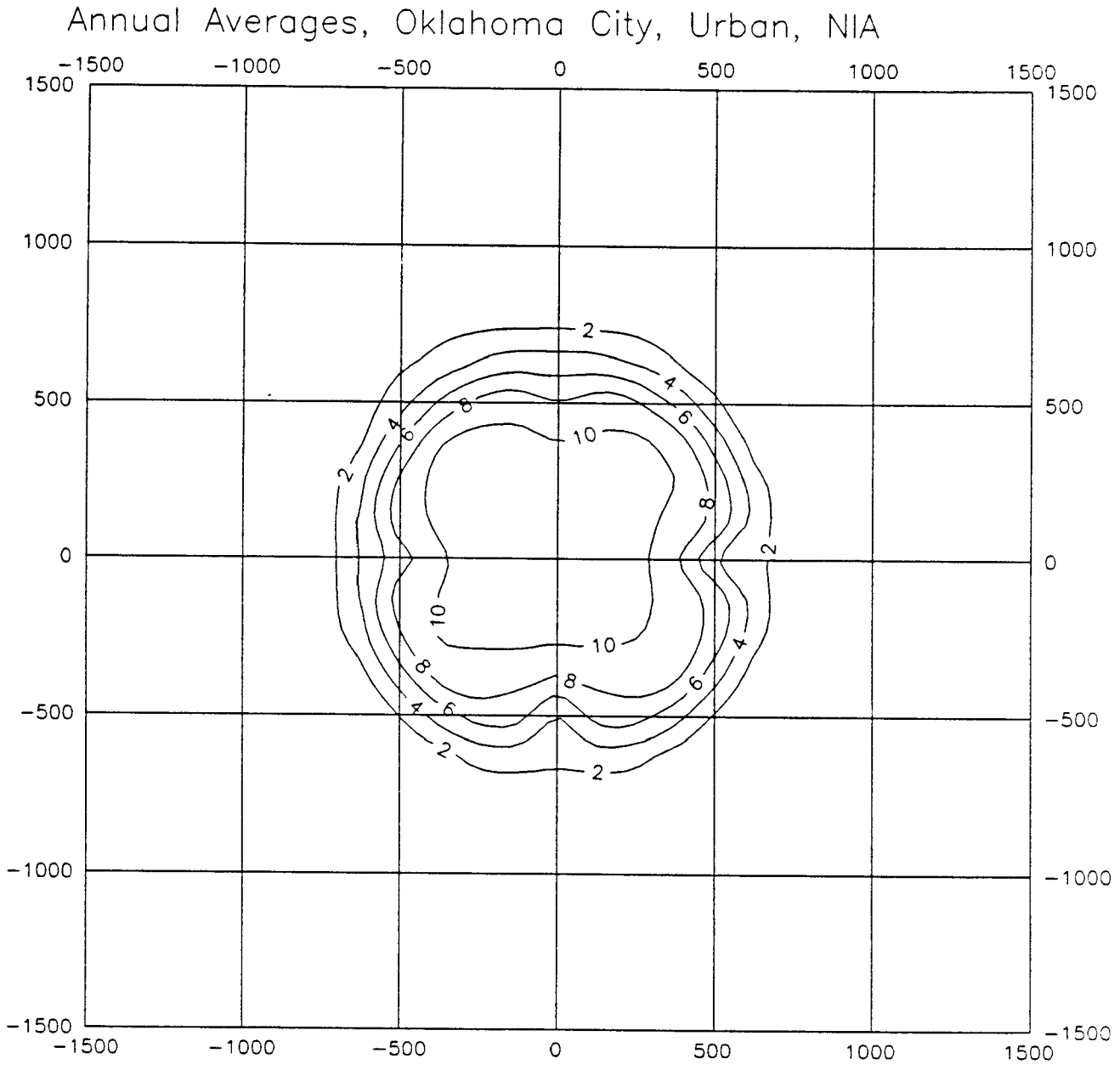

Figure 4.17. Contour Diagram of Annual Average Urban Concentrations($\mu g/m^3$) from the Numerical Integration Algorithm for the 1000 Meter Wide Ground Level Source with Close-in Receptors Using Oklahoma City 1989 STAR Data.

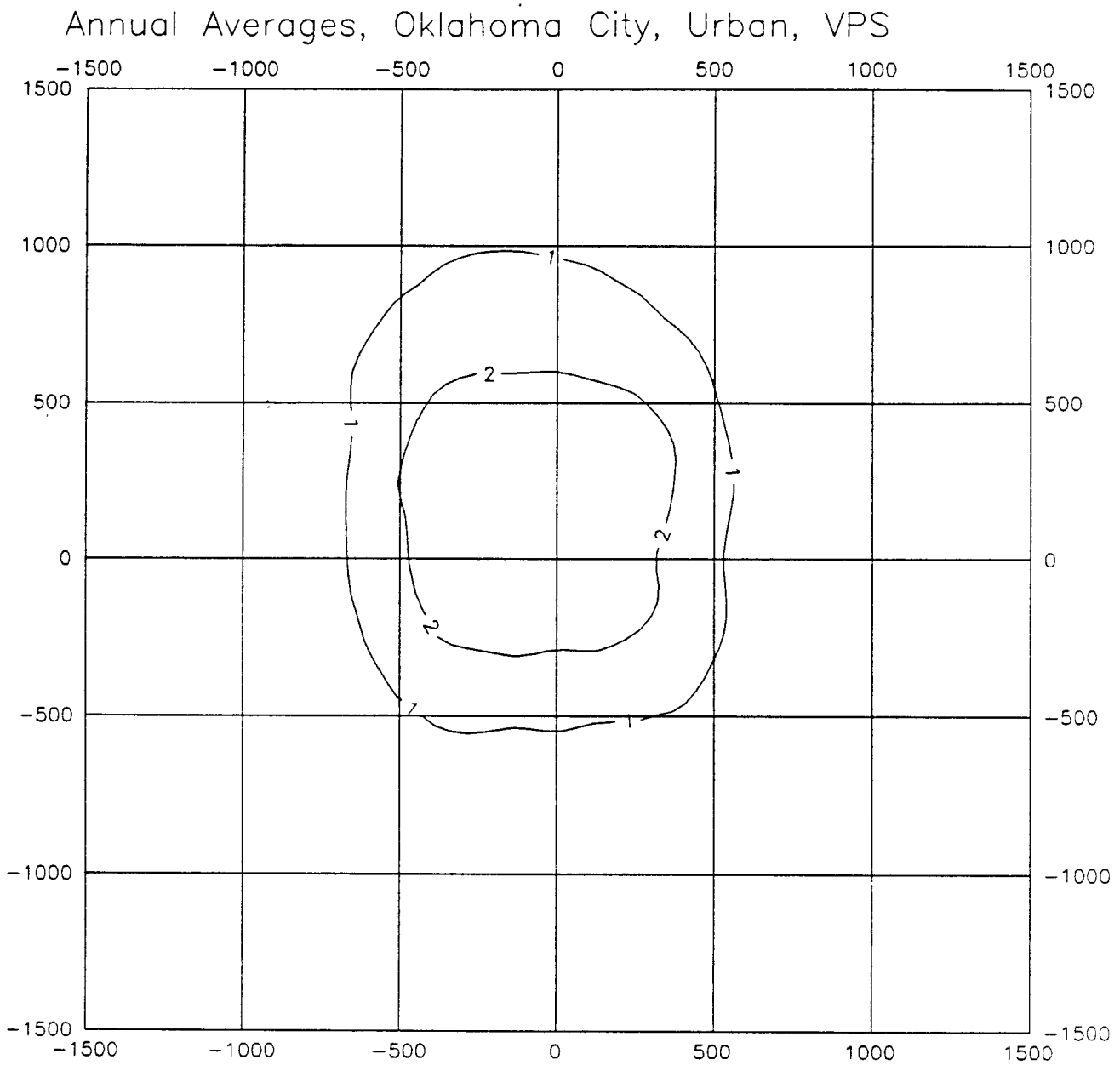

Figure 4.18. Contour Diagram of Annual Average Urban Concentrations($\mu g/m^3$) from the Virtual Point Source Algorithm for the 1000 Meter Wide Ground Level Source with Close-in Receptors Using Oklahoma City 1989 STAR Data.

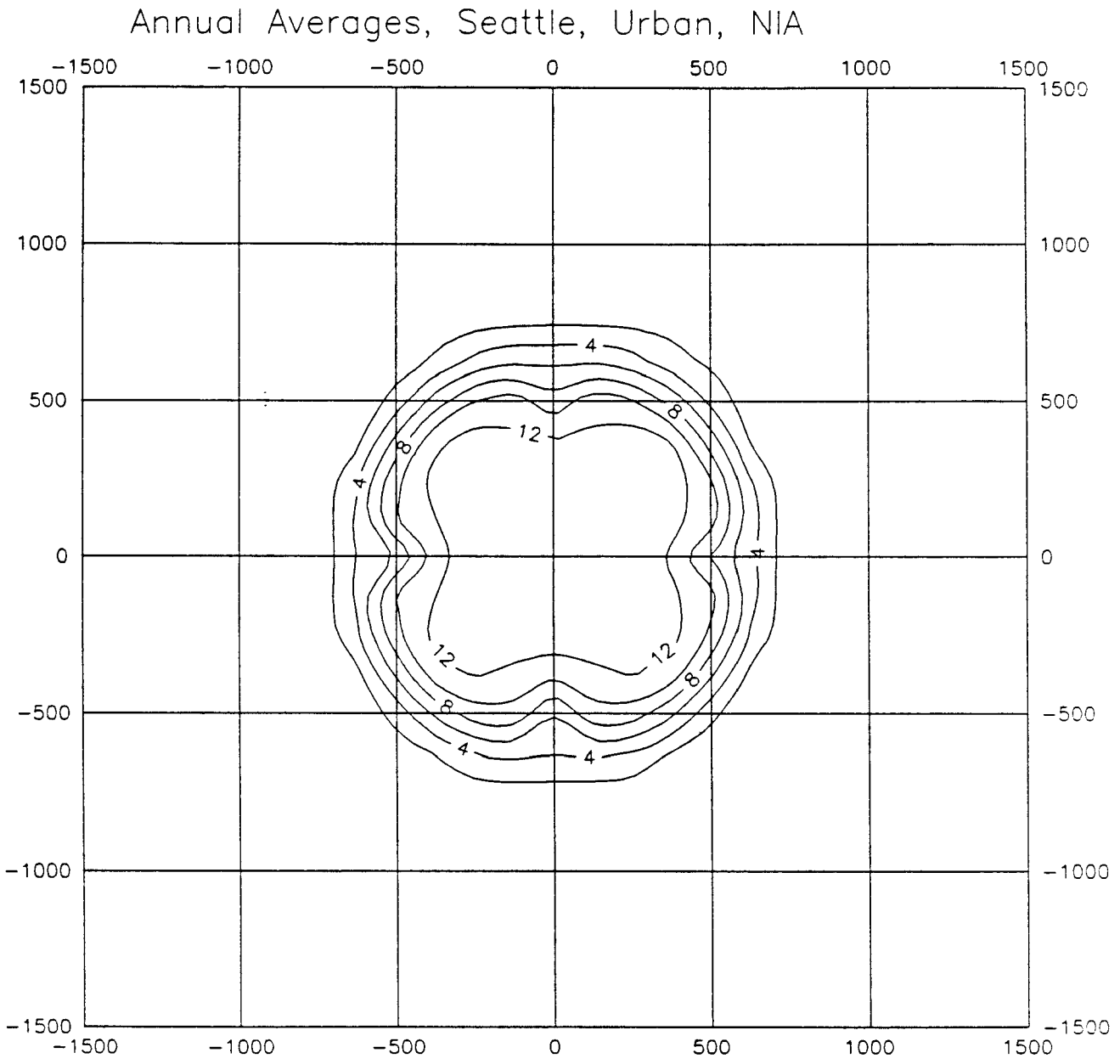

Figure 4.19. Contour Diagram of Annual Average Urban Concentrations($\mu g/m^3$) from the Numerical Integration Algorithm for the 1000 Meter Wide Ground Level Source with Close-in Receptors Using Seattle 1989 STAR Data.

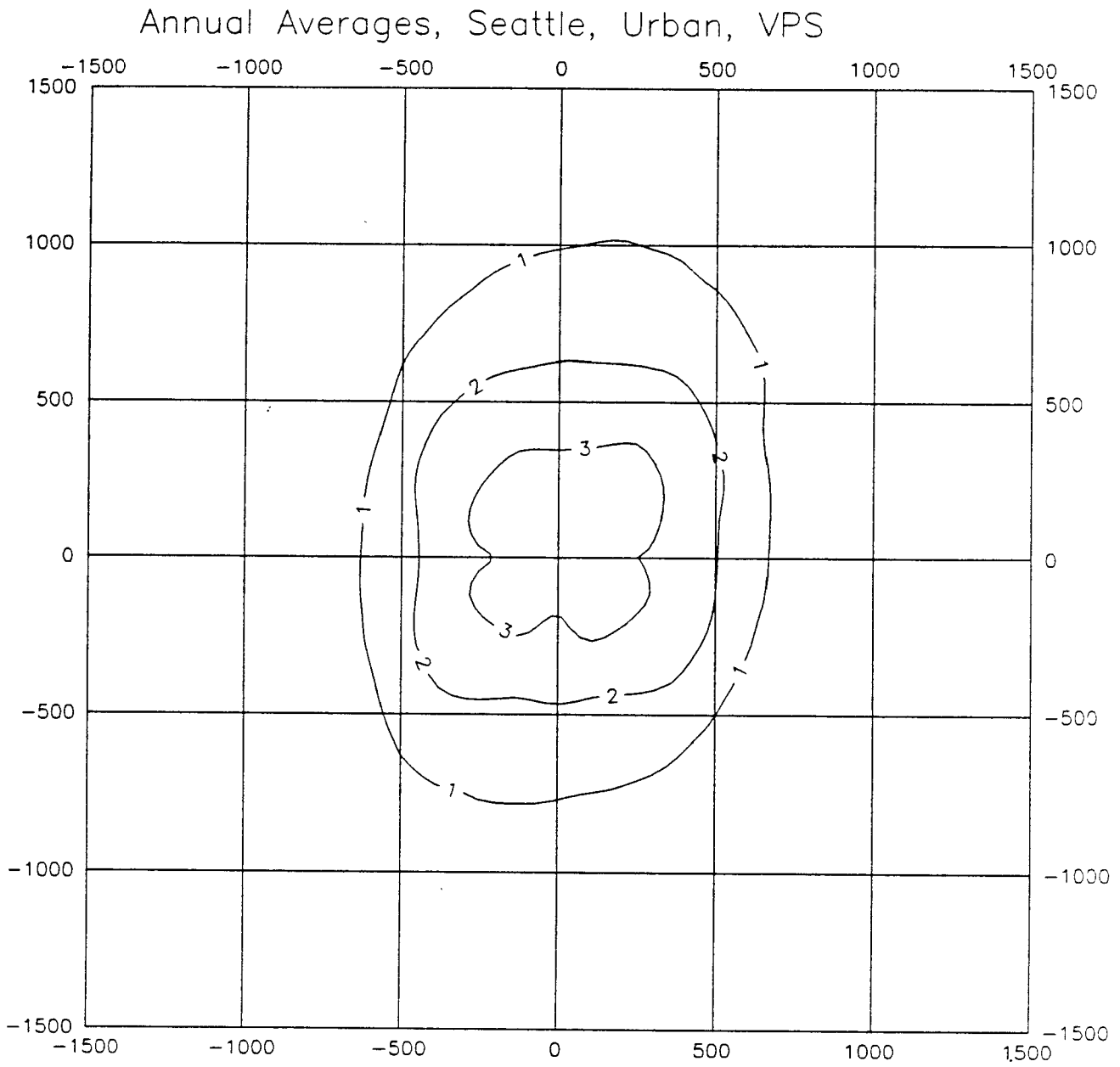

Figure 4.20. Contour Diagram of Annual Average Urban Concentrations($\mu g/m^3$) from the Virtual Point Source Algorithm for the 1000 Meter Wide Ground Level Source with Close-in Receptors Using Seattle 1989 STAR Data.

5. CONCLUSION

This report documents the development, testing and evaluation of a new numerical integration algorithm for modeling area sources for the ISCLT2 model. This algorithm, which is based on the numerical integration algorithm for area sources recently implemented in the ISCST2 model, allows users to handle the complex geometry of irregularly shaped area sources, and allows the calculation of the area source impact for receptors located within and nearby the area source. Detailed performance tests, statistical analyses and sensitivity analyses have been completed to assure the reliability and reasonableness of the modeling results. The algorithm has been compared with the currently used ISCLT2 virtual point source algorithm, as well as with the numerical integration area source algorithm for the ISCST2 model.

The results show that the new numerical integration ISCLT2 area source algorithm performs very well. Using idealized meteorological conditions, the new algorithm achieves very good comparison results when compared with the newly developed ISCST2 area source algorithm. For realistic meteorological data, the discrepancies between the prediction of this new algorithm and the prediction of its ISC2 short term counterpart are within about 10 percent for a typical area source. The differences between the long term and short term algorithms using actual meteorological data are because the ISC2 long term model uses STAR meteorological frequency distribution data, which is only a statistical summary of the hourly data, and does not contain the precise information on specific combinations of wind speed, wind direction, stability class and mixing height that typically control the design values for the short term model.

It is also concluded that the currently used ISCLT2 area source algorithm based on the virtual point source approach underestimates the concentration value by a factor of about 2 to 4, especially when the receptors are located inside or near the source. This is due mainly to the fact that the virtual point source algorithm does not properly treat the lateral distribution of the area source plume close to the source, and also because it cannot calculate the air quality impact inside the source unless the area is subdivided into very small sources.

An evaluation of convergence criteria for the algorithm shows that the algorithm normally converges for all combinations in the STAR summary by level 7, corresponding to a maximum of about 129 simulations per wind direction sector. It is concluded that for routine applications, computations out to level 10 (1025 simulations per sector) will provide acceptable accuracy without significantly compromising the run time performance of the algorithm. This convergence criterion based on a limit on the number of computations per sector, together with the 2 percent error tolerance check and the lower threshold cutoff of 1.0E-10, is recommended for use in the ISCLT2 model to obtain optimum overall performance of the new area source algorithm.

6. REFERENCES

Environmental Protection Agency, 1989. Review and Evaluation of Area Source Dispersion Algorithms for Emission Sources at Superfund Sites. EPA-450/4-89-020. U.S. Environmental Protection Agency, Research Triangle Park, North Carolina.

Environmental Protection Agency, 1992. User's Guide for the Industrial Source Complex (ISC2) Dispersion Models. EPA-450/4-92-008. U.S. Environmental Protection Agency, Research Triangle Park, North Carolina.

McGill, Robert, John W. Tukey, and Wayne A. Larsen, 1978. "Variations of Box Plots", The American Statistician 32:12-16.

Press, W.B. Flannery, S. Teukolsky, and W. Vetterling, 1986. Numerical Recipes, Cambridge University Press, New York.

Turner, D.B., 1970. Workbook of Atmospheric Dispersion Estimates, Revised, Sixth Printing, 1973. EPA Office of Air Programs Publication No. AP-26. U.S. Environmental Protection Agency, U.S. Government Printing Office, Washington, D.C.

TECHNICAL REPORT DATA
(Please read Instructions on reverse before completing)

1. REPORT NO.	2.	3. RECIPIENT'S ACCESSION NO.
EPA-454/R-92-016		

4. TITLE AND SUBTITLE	5. REPORT DATE
Development and Evaluation of a Revised Area Source Algorithm for the ISC2 Long Term Model	October 1992
	6. PERFORMING ORGANIZATION CODE
7. AUTHOR(S)	8. PERFORMING ORGANIZATION REPORT NO.
9. PERFORMING ORGANIZATION NAME AND ADDRESS Pacific Environmental Services 5001 South Miami Boulevard Post Office Box 12077 Research Triangle Park, NC 27709-2077	10. PROGRAM ELEMENT NO.
	11. CONTRACT/GRANT NO. WA No. I-131 EPA Contract No. 68 D00124
12. SPONSORING AGENCY NAME AND ADDRESS U.S. Environmental Protection Agency Office of Air Quality Planning and Standards Technical Support Division Research Triangle Park, NC 27711	13. TYPE OF REPORT AND PERIOD COVERED Final Report
	14. SPONSORING AGENCY CODE

15. SUPPLEMENTARY NOTES
EPA Work Assignment Manager: Jawad S. Touma

16. ABSTRACT

This report includes information on an improved algorithm for modeling dispersion from area sources, which has been developed based on a numerical integration of the point source concentration function. A sensitivity analysis is presented of the algorithm as implemented in the long-term version of the Industrial Source Complex (ISC2) model. For the performance tests, the new ISCLT2 numerical integration area source algorithm is challenged in various ways. First, quality assurance tests are conducted to examine the reasonableness of the results and the efficiency of the algorithm. These quality assurance tests include printing out the intermediate calculation results to perform a line-by-line check of the computer code of the new algorithm. Second, cases with simple area source characteristics (square arrea source or rectangular area source) and idealized meteorological conditions are used to examine the reliability and accuracy of the algorithm. Third, several tests are conducted to show the concentration distribution for various area source shapes. Fourth, tests are conducted to examine the effects of subdividing the area source and the effects of rotation of the area source on the simulated concentration values. Finally, several cases are examined using realistic meteorological conditions. This report is being released to establish a basis for reviews of the capabilities of this methodology and of the consequences resulting from use of this methodology in routine dispersion modeling of air pollutant impacts.

17. KEY WORDS AND DOCUMENT ANALYSIS

a. DESCRIPTORS	b. IDENTIFIERS/OPEN ENDED TERMS	c. COSATI Field/Group
Air Pollution Toxic Air Pollutants Air Quality Dispersion Models	Dispersion Modeling Meteorology Air Pollution Control	

18. DISTRIBUTION STATEMENT	19. SECURITY CLASS (Report)	21. NO. OF PAGES
Release Unlimited	Unclassified	
	20. SECURITY CLASS (Page) Unclassified	22. PRICE